

UNIVERSITÉ DE MONTRÉAL

DYNAMIC BEHAVIOR MODELING AND NONLINEARITY PRE-
COMPENSATION FOR BROADBAND TRANSMITTERS

TAIJUN LIU

DÉPARTEMENT DE GÉNIE ÉLECTRIQUE
ÉCOLE POLYTECHNIQUE DE MONTRÉAL

THÈSE PRÉSENTÉE EN VUE DE L'OBTENTION
DU DIPLÔME DE PHILOSOPHIAE DOCTOR (Ph.D.)
(GÉNIE ÉLECTRIQUE)

DÉCEMBRE 2005

© TAIJUN LIU, 2005



Library and
Archives Canada

Bibliothèque et
Archives Canada

Published Heritage
Branch

Direction du
Patrimoine de l'édition

395 Wellington Street
Ottawa ON K1A 0N4
Canada

395, rue Wellington
Ottawa ON K1A 0N4
Canada

Your file *Votre référence*
ISBN: 978-0-494-17006-9
Our file *Notre référence*
ISBN: 978-0-494-17006-9

NOTICE:

The author has granted a non-exclusive license allowing Library and Archives Canada to reproduce, publish, archive, preserve, conserve, communicate to the public by telecommunication or on the Internet, loan, distribute and sell theses worldwide, for commercial or non-commercial purposes, in microform, paper, electronic and/or any other formats.

The author retains copyright ownership and moral rights in this thesis. Neither the thesis nor substantial extracts from it may be printed or otherwise reproduced without the author's permission.

AVIS:

L'auteur a accordé une licence non exclusive permettant à la Bibliothèque et Archives Canada de reproduire, publier, archiver, sauvegarder, conserver, transmettre au public par télécommunication ou par l'Internet, prêter, distribuer et vendre des thèses partout dans le monde, à des fins commerciales ou autres, sur support microforme, papier, électronique et/ou autres formats.

L'auteur conserve la propriété du droit d'auteur et des droits moraux qui protègent cette thèse. Ni la thèse ni des extraits substantiels de celle-ci ne doivent être imprimés ou autrement reproduits sans son autorisation.

In compliance with the Canadian Privacy Act some supporting forms may have been removed from this thesis.

Conformément à la loi canadienne sur la protection de la vie privée, quelques formulaires secondaires ont été enlevés de cette thèse.

While these forms may be included in the document page count, their removal does not represent any loss of content from the thesis.

Bien que ces formulaires aient inclus dans la pagination, il n'y aura aucun contenu manquant.


Canada

UNIVERSITÉ DE MONTRÉAL
ÉCOLE POLYTECHNIQUE DE MONTRÉAL

Cette thèse intitulée :

DYNAMIC BEHAVIOR MODELING AND NONLINEARITY PRE-
COMPENSATION FOR BROADBAND TRANSMITTERS

présenté par : TAIJUN LIU

En vue de l'obtention du diplôme de : PHILOSOPHIAE DOCTOR (Ph. D.)

A été dûment accepté par le jury d'examen constitué de :

M. BOSISIO, Renato G., M. SC. A, président

M. TSIRONIS, Chisrtos, Ph. D., membre externe

M. MALHAMÉ, Roland P., Ph.D., membre

M. GHANNOUCHI, Fadhel M., Ph.D., membre et directeur de recherche

DEDICATION

To my parents and my brothers

To my wife Yan Ye

To my son Xudong Liu

ACKNOWLEDGEMENTS

The research work presented in this dissertation was completed during my staying at the Poly-Grames Research Center, Department of Electrical Engineering, École Polytechnique de Montréal, Université de Montréal, Montréal, Québec, Canada.

First of all, I would like to express my sincere gratitude to my advisor, Professor Fadhel M. Ghannouchi, for offering me the opportunity and financial support to pursue my Ph.D. study in such a challenge and exciting research field, for his fruitful advice and guidance throughout my thesis, and for his encouragement and stimulation which helped me to overcome a variety of difficulties to reach the final success.

I would like to thank my thesis committee members: Prof. Renato G. Bosisio, Prof. Roland P. Malhamé and Dr. Chirsotos Tsironis for taking time to serve on my committee and for their questions and comments to improve the quality of this dissertation. I am grateful for Prof. Ke Wu and Prof. Ammar Kouki for spending time to act as a member of my synthesis examination committee and for their precious suggestions.

I benefit a lot from Jules Gauthier, Steve Dube, Roch Brassard, René Archambault and Jean-Sebastien Décarie from Poly-Grames Research Center for providing technical and software support during power amplifier design, assembly and measurement process.

I also deeply appreciate my collaborator Dr. Slim Boumaiza for his beneficial discussion, valuable suggestions and technique support during measurement process.

Thanks also go to my colleagues Mohamed Helaoui, Jing Li, Ying Tian, Haykel Ben Naser, Hammi Oualid, Ping Yang, Yufei Wu, Bouchaib Hraïmel, Xiaoma Jiang, Hui Zhang, Yan Ding, Xinyu Xu, Yanyang Zhao, Wenxin Hou, Fang Xu, Duochuan Li for their generous helps when I meet problems.

A lot of thanks go to my parents and brothers for their unconditional support and understanding. Last but not least, I want to express my heartfelt thanks to my wife, Yan Ye, for her love, encouragement and support.

RÉSUMÉ

Le modèle du comportement dynamique d'un émetteur est un outil utile dans la simulation au niveau système pour les concepteurs de systèmes de communication puisque le modèle du comportement peut réduire considérablement la complexité et le temps alloué dans les procédures de conception et d'optimisation. En outre, le modèle du comportement peut fournir une approche rapide et efficace pour valider la performance des différents schémas de prédistorsion pendant le processus d'extraction de paramètres du dispositif de prédistorsion, et peut être utile pour déterminer la topologie du dispositif de prédistorsion et ainsi compenser la non-linéarité dynamique de l'émetteur à large bande. Dans cette thèse, nous rapportons un nouveau modèle à deux boîtes basées sur le modèle du comportement dynamique pour caractériser un émetteur à large bande et les dispositifs de prédistorsion correspondants pour pré-corriger la non-linéarité dynamique de l'émetteur. D'ailleurs, un réseau de neurones de délai de valeurs en temps réel est présenté afin de modéliser le comportement dynamique non linéaire d'un amplificateur de puissance de la troisième génération (3G) pour les stations de base.

Tout d'abord, un algorithme moyen en mouvement à pondération exponentielle dynamique est développé pour établir un modèle de Wiener non linéaire, basé sur table à correspondance (LUT), pour les émetteurs à large bande sans mémoire. Afin d'identifier précisément les effets de mémoire, un algorithme d'évaluation de temps de délai basé sur l'interpolation de Lagrange et le calcul de covariance croisée est développé pour aligner les vecteurs de données en bande de base d'entrée et de sortie capturée à l'avance.

D'ailleurs, pour évaluer l'exactitude et la robustesse des différents modèles de Wiener, on a proposé une nouvelle méthode de validation. Cette méthode est basée sur l'annulation de la croissance du spectre qui est provoquée par la non-linéarité statique, avec l'aide de cascader l'inverse du modèle sans mémoire complexe. Pour améliorer l'exactitude relativement limitée du modèle conventionnel de Wiener, un nouveau modèle augmenté de Wiener est proposé. L'efficacité du modèle augmenté de Wiener proposé et son procédé d'identification ont été évalués en utilisant un émetteur basé sur un amplificateur ACPR à base de GaAs FET de 60-watt conduit par un signal à deux porteuses WCDMA. La supériorité du modèle augmenté de Wiener au modèle conventionnel de Wiener est validée en comparant les spectres mesurés des deux comportements à celui de l'émetteur.

Ensuite, basé sur l'excellente performance du modèle augmenté de Wiener, on propose pour la première fois, un dispositif de prédistorsion augmentée de Hammerstein, basé sur la table de correspondance, pour améliorer plus loin la performance de précompensation du dispositif de prédistorsion traditionnelle de Hammerstein pour les émetteurs à large bande. Un prototype d'émetteur sans fil, qui inclut un amplificateur "push-pull" ex cent un puissance de 60-Watt opérant dans la bande L, est utilisé pour évaluer la performance du dispositif de prédistorsion nouvellement proposée. La performance de précompensation du dispositif de prédistorsion augmentée proposée en supprimant la croissance du spectre sera illustrée en comparant les spectres de sortie de l'émetteur linéarité par les différents dispositifs de prédistorsion à celui de l'émetteur sans prédistorsion.

Finalement, un nouveau réseau neurologique à temps de délai de valeurs en temps réel est également proposé pour construire un modèle de comportement dynamique pour les amplificateurs de puissance de station de la base 3G. Comparé aux modèles de base sur des réseaux de neurones précédemment proposés, une complexité sensiblement réduite et une durée de traitement plus courte dans l'analyse et les procédures d'apprentissage sont obtenues avec ce modèle d'un réseau neuronal à valeurs réelles à délai (RVTDNN). Après la formation du RVTDNN avec les données mesurées en bande de base, le modèle de la AP basée sur le comportement de RVTDNN est obtenu et différents signaux d'essai sont appliqués à ce modèle pour valider son exactitude et sa généralité. Les résultats de validation dans le domaine temporel, fréquentiel et de puissance sont présentés pour démontrer l'exactitude du modèle de RVTDNN en prévoyant les effets de mémoire.

ABSTRACT

The dynamic behavioral model of a transmitter is a useful tool in the system simulation for designers of communication systems since the behavioral model can greatly reduce complexity and time-consuming for design and optimization procedures. In addition, the behavioral model can provide a fast and effective approach to validate the performance of the different predistortion schemes during the predistorter parameter extraction process, and can be helpful for determining the topology of the predistorter for pre-compensating the dynamic nonlinearity of the broadband transmitter. In this thesis, a novel two-box model based dynamic behavioral model for characterizing a broadband transmitter and the corresponding predistorters for pre-correcting the dynamic nonlinearity of the transmitter is reported. Moreover, a real-valued time delay neural network is presented for modeling the dynamic nonlinear behavior of a 3G base-station power amplifier.

At first, a dynamic exponential weighted moving average algorithm is developed to establish a LUT-based nonlinear Wiener model for memoryless wideband transmitters. To improve the relatively limited accuracy of the conventional Wiener model, a new augmented Wiener model is proposed. The superiority of the augmented Wiener model to the conventional Wiener model is validated by comparing the measured spectra of the two behavioral with that of the practical transmitter.

Then, an augmented look-up-table-based Hammerstein predistorter is proposed for the first time to further improve the pre-compensation performance of the traditional

Hammerstein predistorter for the broadband transmitters. A wireless transmitter prototype, which includes an L-band push-pull GaAs FET 60-Watt peak-envelope-power amplifier, is utilized to evaluate the performance of the newly proposed predistorter. The pre-compensation performance of the proposed augmented predistorter in suppressing the spectrum regrowth will be illustrated by comparing the output spectra of the transmitter linearized by the different predistorters with that of the transmitter without predistortion.

Finally, a novel real-valued time delay neural network is also put forward to construct a dynamic behavior model for 3G base station power amplifiers (PA). Compared with the previously published neural network based PA models, a significantly reduced complexity and shorter processing time in the analysis and training procedures is obtained with this RVTDNN model. After training the RVTDNN with the measured baseband data, the RVTDNN behavioral model of the PA is obtained and different test signals are applied to this model to validate its accuracy and generality. The time-, frequency- and power-domain validation results are presented to demonstrate the accuracy of the RVTDNN model in predicting the memory effects.

CONDENSÉ EN FRANÇAIS

MODELISER LE COMPORTEMENT DYNAMIQUE ET LA PRECOMPENSATION DE NON-LINÉARITÉ POUR LES ÉMETTEURS À BANDE LARGE

0.1 INTRODUCTION

Les systèmes de communication sans fil à large bande moderne ont appliqué des conditions strictes aux émetteurs dus à l'utilisation de schémas de modulation de haute capacité, tels que l'accès multiple par répartition en code (CDMA), de l'accès multiple par répartition en code à large bande (WCDMA), de multiplexage fréquentiel orthogonal (OFDM), de l'interopérabilité mondiale pour l'accès en micro-onde (WiMAX) et, etc., pour tirer profit des ressources limitées précieuses de fréquence. Certaines des conditions sont contradictoires. Par exemple, la réalisation simultanée de linéarité supérieure et d'efficacité en puissance élevée est une condition de conflit et devient un grand défi pour les concepteurs. Il est bien connu que ces signaux modulés mentionnés ci-dessus général des enveloppes non constantes avec les rapports Crête sur Moyenne de puissance (PAPR) élevés, qui peuvent être aussi élevés que les 12 dB dans certains cas. En conséquence, l'amplificateur de puissance (PA) dans l'émetteur doit être conçu pour fonctionner près de sa région de saturation, afin de fournir une efficacité du système en puissance plus élevée, ou a une grande remontée de sa région non linéaire afin de

rencontrer la linéarité exigée. En conséquence, la PA finit avec une efficacité élevée et une mauvaise linéarité ou vice-versa. Par conséquent, pour répondre à l'exigence de linéarités en fonctionnant le PA dans sa région non linéaire, on doit corriger toutes les différentes sources de distorsion le long de la chaîne entière d'émetteur.

Pour cette raison, on a proposé différentes techniques de linéarisation telles que la rétroaction, post-compensation, et la prédistorsion, pour améliorer les linéarités de l'émetteur. Parmi les diverses techniques de linéarisation, la prédistorsion numérique de bande de base est l'une des techniques de linéarisation les plus prometteuses et les plus rentables dues à son exécution numérique qui offre une exactitude et une flexibilité significative.

Pour un système non linéaire de bande de base, un modèle du système non linéaire peut être obtenu en formant un réseau ou en extrayant les paramètres du modèle en utilisant l'entrée du système comme entrée désirée du modèle et la sortie du système comme sortie désirée du modèle directement. Un tel modèle s'appelle un modèle de comportement (ou le modèle "de boîte noire") du système non linéaire.

D'autre part, un modèle inverse du système non linéaire peut être facilement réalisé si nous prenons la sortie normalisée du système non linéaire comme entrée désirée du modèle tandis que l'entrée du système est prise comme sortie désirée du modèle. En fait, un tel modèle inverse est généralement référé comme dispositif de prédistorsion, qui est largement utilisé pour compenser la non-linéarité du système en le précédant au système non linéaire comme décrit ci-dessus.

Puisque le modèle de comportement réduit considérablement la complexité et le

temps alloué aux procédures de conception et d'optimisation, c'est un outil utile dans la simulation de système et aide beaucoup le concepteur des systèmes de communication, en particulier, des émetteurs et des amplificateurs de puissance. En outre, le modèle de comportement peut fournir une approche rapide et efficace pour valider la performance de différents schémas de prédistorsion durant le processus d'extraction de paramètre du dispositif de prédistorsion. Ce modèle de comportement est également utile pour déterminer la topologie du dispositif de prédistorsion. En d'autres termes, le modèle de comportement joue également un rôle important pour étudier les techniques de précompensation du système non linéaire. Par conséquent, cette dissertation se concentrera d'abord sur la modélisation comportementale de l'émetteur à bande large. Ensuite, basé sur le modèle comportemental, la topologie de prédistorsion est développée.

L'objectif de cette dissertation est de développer un modèle de comportement précis et stable de l'émetteur sans fil à bande large, et en outre d'obtenir une topologie dynamique efficace de précompensation de non-linéarité pour supprimer la croissance de spectre dans l'émetteur, qui est provoqué par les effets de mémoire et la non-linéarité de l'émetteur. Les efforts de recherches sont concentrés sur les sections suivantes :

- Modèle de comportement dynamique en utilisant un modèle de deux boîtes;
- Schémas de précompensation de la non-linéarité en utilisant un modèle de deux boîtes;
- Modèle de comportement dynamique en utilisant un réseau neuronal.

Puisque le modèle conventionnel de deux boîtes ne peut pas modéliser exactement les

effets de mémoire ou précompenser efficacement la non-linéarité dynamique dans l'émetteur dû à la limitation du filtre linéaire inclus, on propose un modèle augmenté de deux boîtes en cette dissertation. Dans ce modèle augmenté de deux boîtes, le filtre linéaire dans le modèle conventionnel de deux boîtes est remplacé par un filtre faiblement non linéaire. Au meilleur de notre connaissance, c'est la première fois qu'un tel modèle non linéaire de deux boîtes est présenté et mis en application pratique. Basé sur l'excellente performance du modèle augmenté de Wiener, on propose un dispositif de prédistorsion augmenté de Hammerstein pour précompenser la non-linéarité dynamique de l'émetteur sans fil à large bande. D'ailleurs, comme une nouvelle tentative, un réseau neuronal à valeurs réelles à délai (RVTDNN) est présenté en cette dissertation pour simuler la non-linéarité dynamique d'un amplificateur de puissance de la troisième génération (3G), qui est le plus important composant non linéaire dans l'émetteur. Avec ce réseau neuronal à valeurs réelles, une variété d'algorithmes de propagation en arrière peut être mise en application pour extraire les paramètres du modèle. De cette façon, l'algorithme complexe d'apprentissage pour le réseau neuronal complexe est évité et la vitesse d'apprentissage peut être en grande partie améliorée.

0.2 EXCLUSION DES NON LINÉARITÉS STATIQUES ET MODÉLISATION ET IDENTIFICATION EXACTES DES EFFETS DE MÉMOIRE DES ÉMETTEURS RF À LARGE BANDE

Un modèle non linéaire de Wiener se compose d'un filtre linéaire dynamique suivi d'un bloc non linéaire statique, est adopté pour construire un modèle de comportement d'un émetteur RF à large bande. La non-linéarité statique peut être caractérisée par les

tables de correspondance basées sur les courbes de AM/AM et de AM/PM de l'émetteur. Ces courbes peuvent être extraites directement à partir des données de mesure en bande de base au moyen d'un procédé de moyenne mobile. En conséquence, le problème complexe de non linéaire dynamique original est simplifié à un ensemble de problèmes dynamiques linéaires. De cette façon, l'identification du modèle non linéaire de Wiener devient plus facile que les solutions traditionnelles, où tous les paramètres linéaires et non linéaires du modèle de Wiener sont résolus concurremment au moyen d'algorithmes compliqués.

Pour extraire la non-linéarité statique de l'émetteur, une moyenne mobile exponentiellement pondérée est appliquée aux données dynamiques de AM/AM et de AM/PM pour enlever la dispersion. L'algorithme moyen mobile exponentiellement pondéré est basé sur l'équation suivante :

$$y(n) = \alpha y(n-1) + (1-\alpha)x(n) \quad (1)$$

Où α est le facteur de pondération avec une valeur entre 0 et 1. Considérez la dispersion significative dans les caractéristiques AM/AM et AM/PM du l'émetteur, un α fixe sur la gamme dynamique du signal d'entrée mènera à une qualité moyenne mobile faible. En fait, une grande valeur α produit des traces douces (aucune dispersion) mais incorrectes en raison de la propagation d'erreur moyenne. De même, une petite valeur finie par une courbe déchiquetée. Par conséquent, pour adapter une valeur α à la variation de AM/AM et de AM/PM, un arrangement dynamique de α est essentiel. Pour cette raison, la valeur α doit être exprimée en fonction de la puissance d'entrée, c.-à-d

$\alpha = F(|x(n)|^2)$. Les entrées de table de correspondance sont déterminées à partir des courbes de AM/AM et de AM/PM de l'émetteur obtenu en lissant les caractéristiques dynamiques en utilisant cette moyenne mobile exponentiellement pondérée. Ces entrées entourent les composants en phase G_i et en quadrature G_q de la compression complexe du gain correspondant à différentes valeurs de grandeur $x(n)$.

Le tracé des caractéristiques AM/AM et AM/PM que l'on considère $u(n)$ comme entrée et $x(n)$ comme sortie, indique le déplacement de la non linéarité. Par conséquent, le problème original compliqué modélisant la non linéaire est simplifié à un problème linéaire d'identification. Afin d'éviter l'instabilité potentielle d'un filtre de réponse d'impulsion infinie, un filtre FIR est adopté pour construire le modèle linéaire dynamique en cet article. L'identification des poids du filtre FIR peut être faite en utilisant l'algorithme des moindres carrés récursifs.

Les sources à effet de mémoire d'un émetteur RF sont habituellement attribuées aux effets thermiques et/ou de dispersion électrique. Dans le contexte d'un émetteur à large bande, les effets de mémoire électriques sont les sources dominantes de dispersion puisque la constante de temps thermique est trop grande comparée à l'inverse de la largeur de bande de signal. Vuolevi et autres, Ku et autres, et Remley et autres, ont attribué les effets de mémoire électriques à différentes sources comprenant : les effets de piégeage, l'ionisation d'impact, la réponse en fréquence du AP autour de la fréquence porteuse, aux conditions d'adaptation, aux fréquences harmoniques et aux conditions d'adaptation d'impédance à la fréquence d'enveloppe (conception de circuit de

polarisation). Les effets des deux dernières sources sont responsables des vecteurs supplémentaires de distorsion d'intermodulation d'ordre impair. En effet, les non-linéarités d'ordre pair après le mélange avec les fréquences porteuses mènent aux produits d'intermodulation d'ordre impair, qui sont dedans ou très près du canal principal.

Le filtre linéaire de FIR dans le modèle de Wiener tient compte de la réponse fréquentielle autour de la fréquence porteuse (distorsion linéaire) et pas des sources non linéaires de déformation d'ordre pair. En fait, les caractéristiques extraites de AM/AM et de AM/PM du modèle dynamique à effet de mémoire ne sont pas complètement symétriques autour de l'axe des abscisses. Ceci suggère que les non-linéarités faibles existent toujours même après extraction de la non-linéarité statique et forte à partir de données mesurées. C'est pourquoi, il n'est pas suffisant pour modéliser ces non-faibles linéarités avec un filtre linéaire comme il est normalement fait dans les modèles conventionnels de Wiener. Ceci explique également les possibilités relativement limitées du modèle conventionnel de Wiener pour prévoir la réponse de l'émetteur.

Par conséquent, on propose un nouveau modèle complet à effet de mémoire, où une nouvelle branche parallèle est ajoutée au filtre linéaire de FIR. Dans cette nouvelle branche parallèle, le signal d'entrée est multiplié par son amplitude et appliqué à un autre filtre de FIR. De cette façon, le filtre linéaire de FIR dans le modèle conventionnel de Wiener est remplacé par un filtre basé sur FIR de faible non linéaire dynamique. Les termes du second ordre sont introduits au modèle dynamique à effet de mémoire de façon à le rendre capable d'imiter plus exactement les effets de mémoire.

En utilisant le nouveau modèle incluant l'effet de mémoire, on propose un modèle augmenté de Wiener pour modéliser exactement les émetteurs RF à large bande. Ce modèle augmenté de Wiener est une cascade d'un modèle non linéaire faible dynamique et d'un modèle non linéaire statique fort. Le modèle non linéaire fort, basé sur des caractéristiques douces de AM/AM et de AM/PM des émetteurs, est normalement mis en application en employant des tables de correspondance. Le modèle non linéaire faible dynamique se compose du nouveau modèle incluant l'effet de mémoire, qui tient compte des propriétés dynamiques des émetteurs en présence du signal de communication modulé. Ce modèle augmenté de Wiener peut également être identifié avec le procédé d'extraction du modèle conventionnel de Wiener décrit ci-dessus en faisant quelques réarrangements.

L'efficacité du modèle augmenté proposé de Wiener et de sa procédure d'identification a été évaluée en utilisant un émetteur basé sur amplificateur "push-pull" de 60-watt PEP GaAs FET excitée par un signal WCDMA à deux porteuses. Les résultats de comparaison des spectres entre les différents modèles d'émetteur et le prototype d'émetteur indique que le modèle augmenté proposé d'émetteur de Wiener surpasse d'autres modèles en prévoyant la croissance de spectre provoquée par les effets de mémoire de l'émetteur à large bande.

0.3 DISPOSITIF DE PRE-DISTORSION HAMMERSTEIN AUGMENTÉ POUR LA LINÉARISATION DES ÉMETTEURS SANS FIL À BANDE LARGE

D'abord un dispositif de prédistorsion de Hammerstein est utilisé pour établir une fonction de prédistorsion pour un émetteur sans fil à bande large. En conséquence, le dispositif de prédistorsion est décomposé en sous-ensemble sans mémoire statique non linéaire et dynamique linéaire. Le sous-ensemble sans mémoire statique est prévu pour pré compenser la non-linéarité statique de l'émetteur tandis que le filtre dynamique linéaire est concentré sur la suppression la croissance de spectre provoquée par les effets de mémoire. Le dispositif de prédistorsion sans mémoire peut être mis en application en utilisant la table traditionnelle de correspondance (LUT). Cette LUT est construite en se basant sur les caractéristiques AM/AM et AM/PM de l'émetteur qui sont extraites directement à partir des données de mesure en bande de base au moyen d'un procédé moyen mobile comme expliqué ci-dessus. En conséquence, le problème dynamique complexe de prédistorsion est simplifié à un problème dynamique linéaire relativement facile. De cette façon, la résolution de prédistorsion de Hammerstein devient plus commode que les solutions traditionnelles, où tous les paramètres linéaires et non linéaires du modèle de Hammerstein sont résolus concurremment au moyen d'algorithmes élaborés.

L'identification du paramètre de Hammerstein est effectuée en utilisant un programme d'apprentissage en différé. Pour identifier les paramètres du dispositif de prédistorsion, la sortie de l'émetteur $z_{TX}(n)$ est normalisée par le gain linéaire

G_{linear} indiqué de l'émetteur et prise comme séquence d'apprentissage $u(n)$ à l'entrée du dispositif de prédistorsion, c.-à-d.,

$$u(n) = \frac{z_{TX}(n)}{G_{linear}} \quad (2)$$

L'entrée de l'émetteur $y_{TX}(n)$ est employée comme séquence d'apprentissage $y(n)$ de sortie du dispositif de prédistorsion, c.-à-d.,

$$y(n) = y_{TX}(n) \quad (3)$$

Alors la méthode pondérée exponentielle dynamique de la moyenne mobile (DEWMA) est appliquée aux séquences d'apprentissage $u(n)$ et $y(n)$ du dispositif de prédistorsion et afin d'enlever la dispersion des caractéristiques dynamiques AM/AM et AM/PM. Les courbes lissées extraites AM/AM et AM/PM sont alors employées pour construire la LUT du dispositif de prédistorsion. Ensuite, le groupe de données d'apprentissage intermédiaire $x(n)$ est déduit par l'intermédiaire de l'application des données d'apprentissage d'entrée $u(n)$ au LUT précédemment construit. Ici un filtre fini de réponse d'impulsion (FIR) est choisi, au lieu d'un filtre infini de la réponse d'impulsion (IIR), pour construire le filtre linéaire dynamique afin d'éviter l'instabilité potentielle d'un filtre IIR. L'identification des paramètres du filtre de FIR peut être effectuée en utilisant l'algorithme récursif des moindres carrés (RLS), où les valeurs déduites $x(n)$ et mesurées $u(n)$ sont prises comme signal d'entrée et signal désiré, respectivement.

Dans le dispositif de prédistorsion traditionnel de Hammerstein discuté ci-dessus, les effets de mémoire sont précompensés à l'aide d'un filtre linéaire FIR. Ce filtre linéaire corrigerait les effets électriques de mémoire attribués principalement à la réponse en fréquence non constante de l'émetteur autour de la fréquence porteuse. En conséquence, il ne précompense pas complètement les effets électriques de mémoire dus à la variation d'impédance des circuits polarisés et aux charges harmoniques des transistors de puissance. Pour cette raison, on propose un dispositif de prédistorsion augmenté de Hammerstein pour accroître les possibilités de correction dans le contexte des émetteurs sans fil à large bande. Ce dispositif de prédistorsion augmentée de Hammerstein est une cascade d'un sous-ensemble statique fortement non linéaire et d'un sous-ensemble faiblement non linéaire dynamique. Le sous-ensemble fortement non linéaire, qui est basé sur des caractéristiques AM/AM et AM/PM du dispositif de prédistorsion ramenées à une moyenne, peut être mis en application en utilisant les Tableaux de correspondance (LUT). Cependant, le sous-ensemble faiblement non linéaire dynamique se compose de nouveau filtre FIR dynamique qui annule la croissance du spectre produite par les sources dynamiques de déformation à la sortie de l'émetteur quand celui-ci est attaqué avec un signal modulé. Pour ce nouveau filtre FIR dynamique, une branche parallèle supplémentaire est ajoutée au filtre linéaire de FIR. Dans cette branche parallèle, le signal d'entrée $x(n)$ est multiplié par son amplitude $|x(n)|$ afin de produire des distorsions d'ordre pair qui seront appliquées à un deuxième filtre de FIR. En conséquence, le nouveau dispositif de prédistorsion inclut les sources de distorsions qui sont près de celles produites dans le vrai émetteur à linéariser. Ainsi, une performance

supérieure à celle obtenue avec un filtre linéaire simple de FIR est prévue. Ce dispositif de prédistorsion augmenté de Hammerstein peut également être identifié avec le procédé d'extraction des paramètres du dispositif de prédistorsion conventionnel de Hammerstein décrit ci-dessus en faisant quelques réarrangements.

Le dispositif de prédistorsion basé sur LUT de Hammerstein et le nouveau dispositif de prédistorsion augmenté basé sur LUT de Hammerstein sont examinés en utilisant un prototype d'émetteur basé sur amplificateur 60-Watt de "push-pull" excitée par des signaux 3GPP-FDD d'une seule porteuse et de trois porteuses. Le spectre de sortie linéarisé et les résultats de comparaison d'ACPR démontrent que le dispositif de prédistorsion proposée, augmenté basé sur LUT de Hammerstein, surpasse le dispositif de prédistorsion conventionnel, basé sur LUT de Hammerstein, en supprimant la croissance du spectre provoquée par les effets de mémoire de l'émetteur sans fil à bande large.

0.4 MODÉLISER LE COMPORTEMENT DYNAMIQUE DES AMPLIFICATEURS DE PUISSANCE 3G EMPLOYANT LES RÉSEAUX NEURONAUX À DÉLAI TEMPORELLE À VALEURS RÉELLES RÉSEAUX NEUROLOGIQUES

Dans les procédures artificielles conventionnelles de développement de modèle de réseau neuronal, les signaux mesurés d'entrée-sortie complexe sont d'abord convertis en représentation polaire (amplitude et phase) ou rectangulaire (les composants en phase ρ et en quadrature φ). Ensuite, deux réseaux neuronaux à valeurs réelles séparés et désaccouplés sont employés pour modéliser les variations de l'amplitude et de la phase

de la sortie (ou les composants I et Q de sortie) en fonction de l'amplitude de puissance d'entrée (ou les composants I et Q d'entrée). Les coefficients réels des deux réseaux sont identifiés pendant un procédé d'apprentissage en utilisant l'amplitude et la phase mesurées (ou I et Q composantes) de l'entrée et de la sortie. Cette topologie souffre des problèmes de convergence du procédé d'apprentissage puisque les deux réseaux sont formés séparément. En outre, Benvenuto et Ibnkahla ont proposé d'appliquer directement au signal complexe un réseau neuronal basé sur des valeurs complexes. Dans un tel cas, les poids et les fonctions d'activation du réseau sont complexes. Ce type de réseau neuronal rend nécessaire un algorithme complexe encombrant d'opérationnelle tel que l'algorithme complexe d'apprentissage de propagation en arrière. Ainsi, les deux topologies de réseaux neuronaux décrites ci-dessus mènent à un temps d'apprentissage prolongé et à des ressources élevées de calcul.

Dans ce chapitre, nous proposons un nouveau réseau neurologique à délai temporel réel (RVTDNN) pour construire un modèle à comportement dynamique approprié pour 3G PAs en état d'opération réelle. Contrairement aux méthodes présentées précédemment, cette approche emploie seulement un réseau neuronal à valeurs réelles au lieu de deux réseaux séparés. Le RVTDNN nouvellement proposé, qui se compose des deux couches, emploie des paramètres à valeurs réelles (des poids et des polarisations) avec des composants des signaux réels à l'entrée et à la sortie. Le modèle de RVTDNN utilise les deux composants du signal d'entrée afin de prévoir les deux composants correspondants du signal de sortie. Le RVTDNN proposé est basé sur le réseau neuronal à couplage vers l'avant (FFNN), avec l'addition de deux lignes de retard

tapées (TDLs) dans ses deux entrées en bande de base. Les TDLs sont employés afin de considérer l'histoire du signal d'entrée, qui est nécessaire pour modéliser l'effet de mémoire. Ainsi, les entrées de FFNN incluent non seulement la valeur courante du signal d'entrée mais également sa précédente. La profondeur de mémoire du Dispositif Sous Essai (DUT) sera réfléchi sur la longueur des piquages de TDL. En conséquence, la structure de TDL, incluse dans le RVTDNN, mène à modéliser des effets de mémoire à court terme présenté par l'amplificateur de puissance. Cependant, la mémoire à long terme est établie dans le RVTDNN par un apprentissage dirigé. Ce genre de mémoire à long terme peut être employé pour simuler les changements dynamiques lents, des caractéristiques non linéaires du AP, avec le temps. L'extraction des paramètres du modèle de RVTDNN, généralement dénoté comme le procédé d'apprentissage, est exécuté en raccordant les composants I et Q mesurée à l'entrée et à la sortie. En outre, le modèle de RVTDNN peut être converti en réseau neuronal a couplage vers l'avant commun (FFNN) ou Perceptron multicouche (MLP) avec $p+q+2$ entrées et deux sorties. Ainsi, le problème dynamique devient un problème statique et l'algorithme standard d'apprentissage à propagation en arrière peut être utilisé pour le former. Une fois que le RVTDNN est formé, tous les paramètres du modèle sont connus et il devient le modèle à comportement dynamique de l'amplificateur de puissance.

L'évaluation de la validation et de l'exactitude du modèle développé de RVTDNN dans le domaine temporel a montré un accord entre les données de sortie des modèles de comportement RVTDNN et celles mesurées pour les signaux 3G. La validation dans le domaine fréquentiel du modèle a également montré une bonne concordance entre le

spectre calculé à la sortie du PA en utilisant les formes d'onde prévues par le modèle RVTDNN et le spectre mesuré pour IS 95, signaux à une seule porteuse CDMA2000-SR3 et trois porteuses CDMA2000-SR3.

Les résultats de la simulation dynamique de AM/AM et de AM/PM précisent que le RVTDNN peut très bien expliquer les effets de mémoire (effets dépendant du temps) de la PA LDMOS. D'ailleurs, les caractéristiques dynamiques de AM/AM et de AM/PM suggèrent également que la faible valeur du signal exahertz le PA de LDMOS soit fortement affectée par les effets de mémoire pour les applications 3G. Les résultats satisfaisants de validation du signal IS95, qui a été appliqué à un modèle RVTDNN formé par un signal d'une seule porteuse CDMA2000-SR3, montrent que les modèles RVTDNN obtenus ont la bonne généralité pour les signaux semblables ayant des caractéristiques et des facteurs de crête statistiques proches. Dans ce cas, les modèles RVTDNN montrent qu'ils sont compatibles et peuvent être employés pour prévoir la réponse de la PA avec des signaux ayant une plus petite largeur de bande de modulation.

D'ailleurs, une RVTDNN à trois couches est également utilisée pour établir un modèle de comportement non linéaire dynamique, qui peut prévoir la réponse d'un amplificateur de puissance 3G à large bande avec une meilleure exactitude. Un autre amplificateur de puissance de 90-Watt LDMOS opérant à 2.110-2.170 GHz est utilisé comme dispositif sous essai. Les résultats d'essai dans le domaine temporel, de puissance et spectraux illustrent l'excellente exactitude de prévision du comportement dynamique de bande de base de l'amplificateur de puissance opérant avec un signal à deux porteuses 3GPP.

0.5 CONCLUSION

Cette dissertation a présenté un nouveau modèle de deux boîtes, où on a proposé pour la première fois un filtre dynamique faiblement non linéaire pour remplacer le filtre linéaire dans le modèle conventionnel de deux boîtes pour caractériser les effets de mémoire en émetteur à bande large. Ce nouveau modèle de deux boîtes peut être employé pour simuler ou pré compenser la non-linéarité dynamique de l'émetteur sans rien changer dans la topologie du modèle.

Les résultats de validation indiquent que le nouveau modèle proposé peut imiter l'émission hors bande provoquée par les effets de mémoire plus exactement que le modèle conventionnel de deux boîtes. La supériorité du nouveau dispositif de prédistorsion, basé sur le modèle de deux boîtes, par rapport au dispositif de prédistorsion conventionnelle, basée sur le modèle de deux boîtes, pour pré compenser la non-linéarité dynamique de l'émetteur est également démontrée par les résultats du spectre et par la comparaison du ACPR. D'ailleurs, ce nouveau modèle de deux boîtes et le dispositif de prédistorsion, basée sur lui, montrent une stabilité numérique meilleure que celle du modèle de mémoire polynomial et le dispositif de prédistorsion correspondant.

En outre, la dissertation a également illustré comment un nouveau réseau neuronal, à valeurs de délai temporel en temps réel, proposé peut être utilisé pour simuler la non-linéarité dynamique d'un amplificateur de puissance de station de base 3G. Les résultats de la validation dans le domaine temporel, fréquentiel et de puissance prouvent l'efficacité de ce nouveau modèle pour modéliser les effets de mémoire.

Les contributions principales de cette dissertation sont récapitulées comme suit :

- Un modèle de Wiener à comportement augmenté, avec sa procédure d'identification des paramètres, a été proposé ;
- On a proposé un dispositif de prédistorsion de Hammerstein augmenté basé sur la table de correspondance, ainsi que le procédé d'évaluation dispositif de prédistorsion ;
- On a développé une technique de modélisation robuste pour les émetteurs RF sans mémoire de la bande large, en utilisant un algorithme moyen mobile à pondération exponentielle dynamique ;
- On a présenté une méthode de validation du modèle basé sur un pré compensateur sans mémoire pour identifier facilement les possibilités des différents comportements des modèles pour prévoir les effets de mémoire ;
- On a proposé un nouveau réseau neuronal à valeurs de délai temporel en temps réel pour établir un modèle de comportement dynamique pour caractériser les comportements non linéaires en bande de base des amplificateurs de puissance de station de base 3G.

TABLE OF CONTENTS

| | |
|--|---------------|
| DEDICATION..... | IV |
| ACKNOWLEDGEMENTS..... | V |
| RÉSUMÉ..... | VII |
| ABSTRACT..... | X |
| CONDENSÉ EN FRANÇAIS..... | XII |
| 0.1 INTRODUCTION..... | XII |
| 0.2 EXCLUSION DES NON LINÉARITÉS STATIQUES ET MODÉLISATION ET IDENTIFICATION EXACTES DES EFFETS DE MÉMOIRE DES ÉMETTEURS RF À LARGE BANDE..... | XV |
| 0.3 DISPOSITIF DE PRE-DISTORSION HAMMERSTEIN AUGMENTÉ POUR LA LINÉARISATION DES ÉMETTEURS SANS FIL À BANDE LARGE..... | XX |
| 0.4 MODELER LE COMPORTEMENT DYNAMIQUE DES AMPLIFICATEURS DE PUISSANCE 3G EMPLOYANT LES RÉSEaux NEURONAUX A DÉLAI TEMPORELLE A VALEURS RÉELLES RÉSEaux NEUROLOGIQUES..... | XXIII |
| 0.5 CONCLUSION..... | XXVII |
| FIGURE LIST..... | XXXII |
| TABLE LIST..... | XXXVI |
| LIST OF SIGNS AND ABBREVIATION..... | XXXVII |
| | |
| CHAPTER 1 INTRODUCTION..... | 1 |
| 1.1 MOTIVATION..... | 2 |
| 1.2 BRIEF REVIEW OF THE MAIN BEHAVIOR MODELING AND THE CORRESPONDING NONLINEARITY PRE-COMPENSATION TECHNIQUES..... | 6 |
| 1.2.1 <i>Volterra series</i> | 7 |
| 1.2.2 <i>Memory polynomial</i> | 8 |
| 1.2.2 <i>Two-box model</i> | 9 |
| 1.3 OBJECTIVES AND OUTLINE OF THE DISSERTATION..... | 11 |
| 1.3.1 <i>Objectives</i> | 11 |

| | |
|---|-----------|
| 1.3.2 Outline..... | 12 |
| REFERENCES | 15 |
| | |
| CHAPTER 2 DE-EMBEDDING STATIC NONLINEARITIES AND ACCURATELY IDENTIFYING AND MODELING MEMORY EFFECTS IN WIDEBAND RF TRANSMITTERS..... | 17 |
| 2.1 INTRODUCTION..... | 17 |
| 2.2 WIDEBAND RF TRANSMITTER PROTOTYPE | 22 |
| 2.3 WIENER BEHAVIORAL MODEL CONSTRUCTION..... | 23 |
| 2.3.1 <i>Static Nonlinearity De-embedding with Dynamic Exponentially Weighted Moving Average</i> | 25 |
| 2.3.2 <i>Identification and Modeling of Memory Effects</i> | 28 |
| 2.3.2.1 Memory effect identification | 28 |
| 2.3.2.2 Modeling of the linear distortion | 28 |
| 2.4 INFLUENCE OF TIME DELAY ON MEMORY EFFECT IDENTIFICATION..... | 29 |
| 2.5 WIENER MODEL VALIDATION AND LIMITATION ASSESSMENT..... | 32 |
| 2.5.1 <i>Wiener Transmitter Model Validation Method</i> | 38 |
| 2.5.2 <i>Wiener Model Validation</i> | 38 |
| 2.6 AUGMENTED WIENER BEHAVIORAL MODEL..... | 41 |
| 2.6.1 <i>Inclusive Memory Effect Model</i> | 41 |
| 2.6.2 <i>Augmented Wiener Model Identification</i> | 46 |
| 2.7 EXPERIMENTAL SETUP AND NEWLY PROPOSED MODEL VALIDATION..... | 47 |
| 2.8 VALIDATION RESULTS AND DISCUSSION | 49 |
| 2.9 CONCLUSION | 51 |
| REFERENCES | 53 |
| | |
| CHAPTER 3 HAMMERSTEIN PREDISTORTER FOR LINEARIZATION OF BROADBAND WIRELESS TRANSMITTERS | 55 |
| 3.1 INTRODUCTION | 55 |
| 3.2 LUT-BASED HAMMERSTEIN PREDISTORTER AND IDENTIFICATION | 59 |
| 3.2.1 <i>LUT-Based Hammerstein Predistorter</i> | 59 |

| | |
|--|------------|
| 3.2.2 <i>Hammerstein Predistorter Identification</i> | 60 |
| 3.3 AUGMENTED HAMMERSTEIN PREDISTORTER | 66 |
| 3.4 VALIDATION EXPERIMENTAL SETUP | 69 |
| 3.5 VALIDATION RESULTS AND DISCUSSION | 71 |
| 3.5.1 <i>Hammerstein Predistorter</i> | 72 |
| 3.5.2 <i>Augmented Hammerstein Predistorter</i> | 75 |
| 3.6 CONCLUSION | 82 |
| REFERENCES | 84 |
| | |
| CHAPTER 4 DYNAMIC BEHAVIORAL MODELING OF 3G POWER AMPLIFIERS USING REAL-VALUED TIME DELAY NEURAL NETWORKS | 87 |
| 4.1 INTRODUCTION | 88 |
| 4.2 RVTDNN BEHAVIOR MODEL OF POWER AMPLIFIERS | 90 |
| 4.3 EXTRACTION OF RVTDNN BEHAVIORAL MODEL PARAMETERS | 95 |
| 4.4 MEASUREMENTS OF BASEBAND DATA OF A 3G PA | 97 |
| 4.5 RVTDNN MODEL: TRAINING AND VALIDATION RESULTS (I) | 99 |
| 4.5.1 <i>Training and validation of the RVTDNN Model with three-carrier CDMA2000-SR3 signal</i> | 101 |
| 4.5.2 <i>Dynamic AM/AM and AM/PM Curves for RVTDNN and RVFFNN Models</i> | 105 |
| 4.5.3 <i>Validation with IS95 and CDMA-2000-SR3 signals</i> | 109 |
| 4.6 RVTDNN MODEL: TRAINING AND VALIDATION RESULTS (II) | 111 |
| 4.7 CONCLUSION | 116 |
| REFERENCES | 118 |
| | |
| CHAPTER 5 CONCLUSIONS AND FUTUTRE WORKS | 121 |
| 5.1 CONTRIBUTIONS | 124 |
| 5.2 FUTURE WORKS | 125 |
| | |
| APPENDIX A PUBLICATION LIST | 127 |

FIGURE LIST

| | |
|---|----|
| Fig. 1-1. Principle diagram for adaptive baseband predistortion scheme. | 5 |
| Fig. 1-2. Memory polynomial model. | 9 |
| Fig. 1-3. Two-box nonlinear model. | 11 |
| Fig. 2-1 Wideband RF transmitter prototype. | 23 |
| Fig. 2-2 FLL600IQ-2 power amplifier line-up. | 23 |
| Fig. 2-3 Wiener transmitter model diagram from [8]. | 24 |
| Fig. 2-4. The smoothed AM/AM curve vs. the raw measurement AM/AM data of the transmitter prototype..... | 26 |
| Fig. 2-5. The AM/PM curve smoothed vs. the raw measurement AM/PM data of the transmitter prototype..... | 27 |
| Fig. 2-6 Dynamic AM/AM characteristics of the linear filter extracted from the measurement data of the transmitter prototype. | 30 |
| Fig. 2-7 Dynamic AM/PM characteristics of the linear filter extracted from the measurement data of the transmitter prototype. | 31 |
| Fig. 2-8 The simulated AM/AM characteristic comparison between the memoryless models with and without 0.63 ns delay. | 33 |
| Fig. 2-9 The simulated AM/PM characteristic comparison between the memoryless models with and without 0.63 ns delay. | 35 |
| Fig. 2-10 Measured transmitter AM/AM characteristic comparison with different time delays. | 36 |
| Fig. 2-11 Measured transmitter AM/PM characteristic comparison with different time delays. | 37 |
| Fig. 2-12 Cross-covariance calculation results with 15.8ns delay. | 37 |
| Fig. 2-13 Spectrum comparison among the spectra of memoryless model, 64-tap Wiener model and transmitter measurement. (a) Transmitter measurement. (b) Memoryless model. (c) Wiener model with a 64-tap FIR filter. (d) Spectrum differences between the memoryless transmitter model and the actual transmitter. | |

| | |
|---|----|
| (e) Spectrum differences between the 64-tap Wiener transmitter model and the actual transmitter. | 40 |
| Fig. 2-14 Spectrum comparison of different Wiener transmitter models and the transmitter prototype. (a) Transmitter measurement. (b) Wiener model with a 64-tap FIR filter. (c) Wiener model with a 10-tap FIR filter. (d) Wiener model with a 5-tap FIR filter. (e) Memoryless model. | 42 |
| Fig. 2-15 ACPR comparison of different Wiener transmitter models and the transmitter prototype. | 43 |
| Fig. 2-16 Dynamic memory effect model. | 45 |
| Fig. 2-17 Augmented Wiener transmitter model diagram. | 45 |
| Fig. 2-18 Wideband RF transmitter characterization platform. | 48 |
| Fig. 2-19 Spectrum comparison of different transmitter models and the transmitter prototype. (a) Transmitter measurement. (b) Augmented Wiener model with two 3-tap FIR filter. (c) Wiener model with a 64-tap FIR filter. (d) Memoryless model. | 50 |
| Fig. 2-20 ACPR comparison of different transmitter models and the transmitter prototype. | 50 |
| Fig. 3-1 Hammerstein predistorter diagram. | 60 |
| Fig. 3-2 An offline training scheme for Hammerstein predistorter identification. | 61 |
| Fig. 3-3 Predistorter AM/AM curve smoothed with DEWMA vs. the raw measurement AM/AM data. | 62 |
| Fig. 3-4 Predistorter AM/PM curve smoothed with DEWMA vs. the raw measurement AM/AM data. | 63 |
| Fig. 3-5 Dynamic AM/AM characteristics of the linear filter extracted from the measurement data. | 64 |
| Fig. 3-6 Dynamic AM/PM characteristics of the linear filter extracted from the measurement data. | 64 |
| Fig. 3-7 Augmented Hammerstein predistorter diagram. | 67 |
| Fig. 3-8 Experimental set-up for verifying digital predistorters. | 71 |

- Fig. 3-9 Spectrum comparison of the transmitter with different Hammerstein predistorters. (a) Without predistorter. (b) With memoryless predistorter. (c) Hammerstein predistorter with a 10-tap FIR filter. (d) Hammerstein predistorter with a 64-tap FIR filter. (e) Hammerstein predistorter with a 128-tap FIR filter. 74
- Fig. 3-10 ACPR comparison of the transmitter with different Hammerstein predistorter. (a) Without predistorter. (b) With memoryless predistorter. (c) Hammerstein predistorter with a 10-tap FIR filter. (d) Hammerstein predistorter with a 64-tap FIR filter. (e) Hammerstein predistorter with a 128-tap FIR filter. 75
- Fig. 3-11 Spectrum comparison of different predistorters for one-carrier WCDMA signal. (a) Without predistorter. (b) Memoryless predistorter. (c) Hammerstein predistorter with a 128-tap FIR filter. (d) Augmented Hammerstein predistorter with two twenty-tap FIR filter. 77
- Fig. 3-12 ACPR comparison of different predistorters for one-carrier WCDMA signal. (a) Without predistorter. (b) Memoryless predistorter. (c) Hammerstein predistorter with a 128-tap FIR filter. (d) Augmented Hammerstein predistorter with two twenty-tap FIR filter. 78
- Fig. 3-13 Spectrum comparison of different predistorters for one-carrier WCDMA signal. (a) Without predistorter. (b) Memoryless predistorter. (c) Hammerstein predistorter with a 128-tap FIR filter. (d) Augmented Hammerstein predistorter with two twenty-tap FIR filter. 79
- Fig. 3-14 Spectrum comparison of different predistorters for three-carrier WCDMA signal. (a) Without predistorter. (b) Memoryless predistorter. (c) Hammerstein predistorter with a 128-tap FIR filter. (d) Augmented Hammerstein predistorter with two ten-tap FIR filter. 80
- Fig. 3-15 Spectrum comparison of different predistorters for one-carrier WCDMA signal. (a) Without predistorter. (b) Memoryless predistorter. (c) Hammerstein predistorter with a 128-tap FIR filter. (d) Augmented Hammerstein predistorter with two twenty-tap FIR filter. 81
- Fig. 3-16 ACPR comparison of different predistorters for three-carrier WCDMA signal. (a) Without predistorter. (b) Memoryless predistorter. (c) Hammerstein predistorter with a 128-tap FIR filter. (d) Augmented Hammerstein predistorter with two ten-tap FIR filter. 82
- Fig. 4-1 Complex signal processing models of the conventional real-valued neural network. 91
- Fig. 4-2 Complex signal processing models of the complex-valued neural network. 93

| | | |
|-----------|---|-----|
| Fig. 4-3 | Block diagram of new two-layers RVTDNN PA behavioral model..... | 93 |
| Fig. 4-4 | An accurate complex behavioral test-bed block diagram..... | 98 |
| Fig. 4-5 | Envelope waveforms of the three-carrier CDMA2000 signal. (a) Normalized input and output signals magnitude vs. time. (b) Zoom-in of the input and output waveforms. | 101 |
| Fig. 4-6 | A typical convergence curve of the training process..... | 103 |
| Fig. 4-7 | Validation results of I component in time domain. | 103 |
| Fig. 4-8 | Validation results of Q component in time domain..... | 104 |
| Fig. 4-9 | PSD comparison between the RVTDNN behavioral model and the measurement data of the three-carrier CDMA2000 signal..... | 104 |
| Fig. 4-10 | Dynamic AM/AM and AM/PM characteristic comparison between the RVFFNN behavioral model and the measurement data. (a) Dynamic AM/AM characteristics. (b) Dynamic AM/PM characteristics..... | 107 |
| Fig. 4-11 | Dynamic AM/AM and AM/PM characteristic comparison between the RVTDNN behavioral model and the measurement data. (a) Dynamic AM/AM characteristics. (b) Dynamic AM/PM characteristics..... | 108 |
| Fig. 4-12 | PSD comparison between the RVTDNN behavioral model and the measurement data of the one-carrier CDMA2000 signal..... | 110 |
| Fig. 4-13 | PSD comparison between the RVTDNN behavioral model and the measurement data of IS95 signal..... | 111 |
| Fig. 4-14 | Spectrum comparison of the test results..... | 114 |
| Fig. 4-15 | I component (in-phase) comparison of the test results..... | 114 |
| Fig. 4-16 | Q component (quadrature) comparison of the test results..... | 115 |
| Fig. 4-17 | AM/AM characteristics comparison of the test results | 115 |
| Fig. 4-18 | AM/PM characteristics comparison of the test results..... | 116 |

TABLE LIST

| | |
|--|-----|
| Table 4-1 Training and Validation Signal Characteristics..... | 100 |
| Table 4-2 Comparison of Training Performances for RVFFNN and RVTDNN..... | 106 |

LIST OF SIGNS AND ABBREVIATION

| | |
|----------|---|
| 3G | Third Generation |
| 3GPP | Third Generation Partnership Projects |
| 3GPP-FDD | Generation-Partnership-Projects Frequency-Division-Duplex |
| ACPR | Adjacent Channel Power Ratio |
| ADC | Analog to Digital Converter |
| ADS | Advanced Designed System |
| AM/AM | Amplitude-Modulation /Amplitude-Modulation |
| AM/PM | Amplitude-Modulation /Phase-Modulation |
| ANN | Artificial Neural Network |
| ARMA | Auto-Regressive Moving Average |
| CAD | Computer-Aided Design |
| CCPDF | Complementary Cumulative Probability Density Function |
| CDMA | Code Division Multiple Access |
| DAC | Digital to Analog Converter |
| DEWMA | Dynamic Exponential Weighted Moving Average |
| DSP | Digital Signal Processor |
| DUT | Device-Under-Test |
| ESG | Electronic Signal Generator |

| | |
|--------|--|
| FET | Field Effect Transistor |
| FFNN | FeedForward Neural Network |
| FIR | Finite Impulse Response |
| FPGA | Field Programmable Gate Array |
| HPA | High Power Amplifier |
| IF | Intermediate Frequency |
| IIR | Infinite Impulse Response |
| IMD3 | Third order inter-modulation |
| IMD5 | Fifth order inter-modulation |
| LDMOS | Later Double-diffused MOS |
| LUT | Look Up Table |
| MLP | Multi-Layer Perceptron |
| OFDM | Orthogonal Frequency-Division Multiplexing |
| PA | Power Amplifier |
| PC | Personal Computer |
| PEP | Peak-Envelope-Power |
| PSD | Power Spectral Density |
| QAM | Quadrature Amplitude Modulation |
| RF | Radio Frequency |
| RVFFNN | Real-Valued FeedForward Neural Network |

| | |
|--------|---|
| RVTDNN | Real-Valued Time-Delay Neural Network |
| TDL | Tapped Delay Line |
| TDNN | Time Delay Neural Network |
| VNA | Vector Network Analyzer |
| VSA | Vector Signal Analyzer |
| WCDMA | Wideband Code Division Multiple Access |
| WiMAX | Worldwide Interoperability for Microwave Access |

CHAPTER 1

INTRODUCTION

1.1 MOTIVATION

Modern wideband wireless communication systems applied strict requirements to the transmitters due to the utilization of the high capacity modulation schemes, such as Code Division Multiple Access (CDMA), Wideband Code Division Multiple Access (WCDMA), Orthogonal Frequency Division Multiplexing (OFDM), Worldwide Interoperability for Microwave Access (WiMax) and etc, to take advantage of the precious limited frequency resources. For these wireless systems, the transmitters are required to have ultra-high linearity as well as high efficiency. The ultra-high linearity of the transmitter is essential since the nonlinearity existing in the power amplifier will cause the out-of-band emission, which will interference the adjacent channels, and also produce additional code-errors for the channels themselves. Moreover, the RF signals modulated using one of the above high capacity modulation schemes are not the constant envelope any more. The Peak-to-Average Ratio (PAR) could be as high as 10 dB. In this way, in order to transmit the peak signals without clipping, the power amplifier of the transmitter has to be back-off at least 10 dB. However, such a back-off value cannot satisfy the linearity requirements of the transmitter yet since the peak power still will drive the PA to nearby its saturated area. To avoid that, a much larger back-off value is needed to satisfy the linearity requirements for such a highly varying envelope signal. In

addition, with a statistical analysis to a WCDMA signal, it is found that the modulated signal is under a small signal condition for most of the time. In other words, the PA operates in small signal conditions for most of the time. Consequently, the PA will exhibit extremely low power efficiency. In such a case, in order to provide enough large linear output power to satisfy the requirements of the practical wireless network design, the PA must have very high saturated output power. It is well-known that the high power transistors are expensive. In this way, the cost of the transmitter will increase dramatically. Moreover, such a design will cause serious heat dissipation problem since the PA operates under a condition with high output power and low efficiency. As a result, the reliability of the system will be reduced and the system operation cost will largely increase.

In addition, if we don't take additional linearization measures, the power amplifier (PA), which is the most power consuming component in the transmitter, should operate in class A with back-off so as to meet the linearity requirements of the system. In this way, the power efficiency of the transmitter will be further decreased. To improve the efficiency of the transmitter, the PA should be designed to work in a constantly driven mode such as class AB, class B, or switching mode such as class D, class E etc. Of course, the PA will have a poor linearity and a strong spectrum regrowth when it operates in such kinds of operating modes. In other words, high power efficiency and high linearity are two conflicting requirements for power amplifier design. Consequently, in order to employ these high efficiency PAs in the wideband transmitter, the additional linearization techniques have to be applied to these PAs to suppress the spectrum regrowth so as to

meet the high linearity requirements of the wideband transmitter.

There are varieties of linearization techniques that were proposed and have been widely used to improve the linearity of the transmitters. The most common linearization techniques can be roughly categorized into four types: feedback, feedforward, LINC, and predistortion.

Among these linearization techniques, predistortion is the most promising technique that can improve the linearity of the PA and keep that the PA still works under high efficiency conditions at the same time. Predistortion is conceptually the simplest form among the variety of linearization techniques for linearizing an RF transmitter or an RF power amplifier (PA). It is a technique in which the inverse nonlinearities of the known amplitude and phase nonlinearities of a transmitter or a PA are cascaded in front of the transmitter or the PA to compensate for its nonlinearities so as to eliminate its original nonlinear distortion. The predistortion can be implemented in RF, IF or baseband with the digital technique or the analog technique. On the one hand, based on the inverse nonlinearities of the nonlinear system, which are extracted and implemented with analog technique or digital technique, the predistortion technique can be divided into the analog predistortion and the digital predistortion. On the other hand, depending whether the predistortion is implemented in RF, IF or baseband, the predistortion can be categorized as RF/IF predistortion or baseband predistortion. In addition, the digital predistortion can be further classified as the RF/envelope digital predistorter and the baseband digital predistorter. It should be noted that generally the RF predistortion is suitable for pre-correcting the nonlinearity of the PA while the baseband predistortion technique is

independent on the type of the power amplifier and can pre-compensate for the nonlinearity of the whole transmitter, including the digital-to-analog converter, the modulator, the up-converter and the PA. Moreover, the baseband predistortion can fully take advantage of the modern digital signal processing techniques to provide a more accurate and flexible pre-compensation scheme, and can be implemented in a large scale integrated circuit with other baseband function block to form a system on chip.

Therefore, among the variety of predistortion schemes, the adaptive baseband predistortion [1], shown in Fig. 1-1, is getting more and more attentions of the researchers in both academic and industry fields all over the world in recent years. In this pre-compensation scheme, all of the nonlinearities in the transmitter, including the quadrature modulator and the power amplifier, can be pre-compensated by the digital predistorter in baseband. The baseband predistortion predicts the needed correction using past knowledge about the characteristics of the nonlinearity of the transmitter rather than using feedback from the current signal. In this way, the loop delay limitations associated with Cartesian feedback [2] is avoided so that a much wider bandwidth can be obtained with the baseband predistortion. In this particular technique, the feedback from the power amplifier output is demodulated by a quadrature demodulator and then digitally sampled with an A/D converter. The output of the A/D converter is fed into the predistortion estimator, which is implemented in a digital signal processor (DSP). The predistortion estimator will extract the parameters of the predistorter from the feedback baseband signals I_{out} and Q_{out} (samples of the equivalent baseband output of the transmitter), and

the baseband input signals I_{pd} and Q_{pd} of the A/D converter (the output of the predistorter). Finally, the parameters of the predistorter in the main path are updated with the parameters solved in the predistortion estimator.

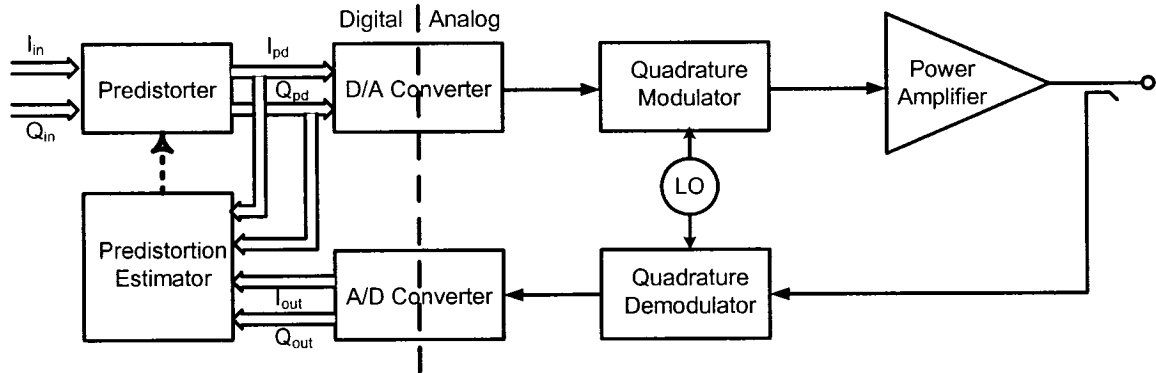


Fig. 1-1. Principle diagram for adaptive baseband predistortion scheme.

In fact, generally speaking, for a baseband nonlinear system, a forward model of the nonlinear system can be obtained by training a network or extracting the model parameters using the input of the system as the desired input of the model and the output of the system as the desired output of the model directly. Generally, such a model is called a behavioral model (or “black box” model) of the nonlinear system. On the other hand, a reverse model of the nonlinear system can be easily achieved if we take the normalized output of the nonlinear system as the desired input of the model while the input of the system is taken as the desired output of the model. In fact, such an inverse model is generally referred as a predistorter, which is widely used to pre-compensate the nonlinearity of the system by preceding it to the nonlinear system as described above.

Since the behavioral model provides greatly reduced complexity and time-consumption for design and optimization procedures, it is a useful tool in the system simulation and provides great help for the designer of communication systems, in particular, transmitters and power amplifiers. In addition, the behavioral model can provide a fast and effective approach to validate the performance of the different predistortion schemes during the predistorter parameter extraction process. This behavioral model is also helpful for determining the topology of the predistorter. In other words, the behavioral model also plays an important role for studying the pre-compensation techniques of the nonlinear system. Therefore, this dissertation will concentrate on the behavior modeling of the broadband transmitter at first. Then, based on the behavioral model, the predistortion topology is developed.

1.2 BRIEF REVIEW OF THE MAIN BEHAVIOR MODELING AND THE CORRESPONDING NONLINEARITY PRE-COMPENSATION TECHNIQUES

The most popular behavioral model and nonlinearity pre-compensation technique is look-up table (LUT). For this technique, two LUTs are constructed from the measured AM/AM and AM/PM data for the nonlinear system [1]-[6]. Then, these LUTs are used to represent the nonlinear system or to pre-compensate the nonlinearity of the nonlinear system. This is a simple and effective way to characterize or pre-correct the nonlinearity of the nonlinear system, but it is only limited to memoryless or quasi-memoryless nonlinear system, where the output of the system is fully determined by the current input

of the system. However, for the wideband wireless communication systems, the output of the system depends on not only the current input of the system, but also the previous input of the system. Such a nonlinear system is referred as a nonlinear system with memory. For a nonlinear system with memory, the simple LUT cannot well characterize its dynamic nonlinearity and a predistorter based on LUT cannot effectively suppress the out-of-band emission caused by its dynamic nonlinearity [7].

In order to accurately characterize and effectively pre-correct the dynamic nonlinearity of the system with memory, a variety of schemes have been proposed in the last few years. In the following sub-section, several most popular baseband behavior modeling and pre-compensation techniques such as Volterra series, memory polynomial and two-box model, which can characterize and pre-correct both of the memory effects and the nonlinearity, will be summarized.

1.2.1. Volterra series

A nonlinear system with memory can be expressed by a Volterra series, which is a generalization of the Taylor series, as follows [8]:

$$y(n) = \sum_{i=1}^P y_p(n) \quad (1.1)$$

Where

$$y_p(n) = \sum_{i_1=-\infty}^{\infty} \cdots \sum_{i_p=-\infty}^{\infty} h_{i_1, i_2, \dots, i_p} \prod_{j=i_1}^{i_p} x(n-j) \quad (1.2)$$

Where $x(n)$ is the system input, $y(n)$ is the system response and $y_p(n)$ is the p-th order component of the system response. The coefficient h_{i_1, i_2, \dots, i_p} is referred as p-th order Volterra kernel, which is used to characterize the nonlinear system. When the order of the model increases above third order, it becomes very complicated to extract these coefficient values. In addition, in such a case, the convergence speed becomes very slow when trying to model strong nonlinearities. Therefore, the Volterra series is generally limited to describe weakly nonlinear systems, where all higher order terms are negligible in the system representation and the first two or three order terms can represent the system in a satisfactory accuracy.

1.2.2. Memory polynomial

To more accurately mimic the memory effects, a memory polynomial dynamic nonlinear model [9], as shown in Fig. 1-2, is utilized to characterize both of the memory effects and the static memoryless nonlinearity in the transmitter. This is a time delay line based multi-branch polynomial model. The memory depth is determined by the number of the taps of the time delay line. The output $x(n)$ can be expressed as follows:

$$x(n) = \sum_{i=0}^{m-1} u(n-i) \left(\sum_{j=0}^{p-1} a_j |u(n-j)|^j \right) \quad (1.3)$$

Where m stands for the tap number and p is the order of the polynomial. This memory polynomial model can be identified by applying the measured input and output data of the nonlinear system as the desired input and output data of the model. Its corresponding pre-compensator can be directly obtained by using the normalized measurement output of the transmitter as the desired input of the model and the measurement input of the transmitter as the desired output of the model to extract the model parameters. This memory polynomial model can accurately characterize the dynamic nonlinearity of the transmitter and provide an excellent nonlinearity pre-compensation performance, but it may suffer from potentially instability problems while involving a strongly nonlinear problem [10].

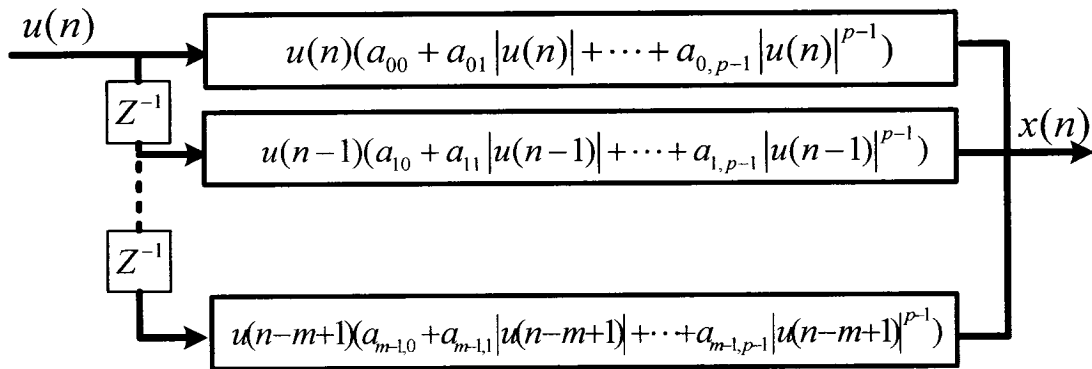


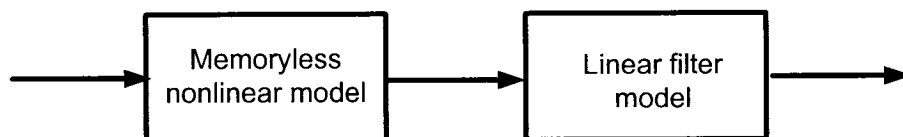
Fig. 1-2. Memory polynomial model.

1.2.3. Two-box model

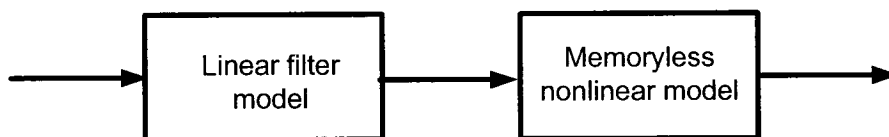
As pointed out above, a conventional memoryless nonlinear pre-compensator cannot

effectively suppress the out-of-band emission of the transmitter due to the memory effects [7]. Consequently, a linear filter has been utilized to characterize the memory effects of the transmitter. This linear filter can be preceded or followed by a memoryless nonlinear block to construct a so-called Hammerstein dynamic nonlinear system or Wiener dynamic nonlinear system, as shown in Fig. 1-3 [11]-[13]. Since this model consists of a nonlinear block and a linear block, it is also directly referred as a two-box model. For the two-box model, the memoryless nonlinear model can be anyone of the traditional nonlinear models such as LUT, polynomial, Bessel function and etc. The linear filter can be a Finite Impulse Response (FIR) filter, an Infinite Impulse Response (IIR) filter or an Auto-Regressive Moving Average (ARMA) filter. Consider the potential instability for the IIR and ARMA filters, FIR filter is the most popular linear filter used in this configuration. It is well-known that such a linear filter acts as an adequate equalizer to compensate for device frequency response variations. Therefore, the linear filter could be a good candidate to characterize or compensate for the memory effects caused by the frequency response of the transmitter around the carrier frequency. For the memory effect components attributed to the other sources such as trapping effect, impact ionization, impedance matching conditions at harmonic frequencies and the envelope frequency (bias circuit design) [14]-[16], such a simple linear filter cannot handle them. In other words, the linear filter can only partially mimic or suppress the spectrum regrowth caused by the memory effects. It should be noted that if a nonlinear system can be well characterized by a Wiener model, the corresponding nonlinearity pre-compensator should be a Hammerstein system. In other words, if a Hammerstein model can accurately model a

nonlinear system, the corresponding nonlinearity pre-compensator should be a Wiener system.



(a) Hammerstein dynamic nonlinear model



(b) Wiener dynamic nonlinear model

Fig. 1-3. Two-box nonlinear model.

1.3 OBJECTIVES AND OUTLINE OF THE DISSERTATION

1.3.1 Objectives

The objective of this dissertation is to develop an accurate and stable behavioral model of the broadband wireless transmitter, and furthermore to obtain an effective dynamic nonlinearity pre-compensation topology to suppress the spectrum regrowth in the transmitter, which is caused by the memory effects and the nonlinearity of the transmitter.

The research efforts are concentrated on the following areas:

- Dynamic behavioral model using a two-box model;

- Nonlinearity pre-compensation scheme using a two-box model;
- Dynamic behavioral model using a neural network.

As discussed early, the conventional two-box model cannot accurately model the memory effects or effectively pre-compensate for the dynamic nonlinearity in the transmitter due to the limitation of the linear filter included. To solve this problem, an augmented two-box model is proposed in this dissertation. In this augmented two-box model, the linear filter in the conventional two-box model is replaced by a weakly nonlinear filter. Based on the excellent performance of the augmented Wiener model, an augmented Hammerstein predistorter is proposed to pre-compensate the dynamic nonlinearity of the wideband wireless transmitter.

Moreover, as a new attempt, a real-valued time-delay neural network (RVTDNN) is presented in this dissertation to simulate the dynamic nonlinearity of a 3G power amplifier, which is a most important nonlinear component in the transmitter. With this real-valued neural network, a variety of the back-propagation algorithms can be implemented to extract the model parameters. In this way, the complicate complex training algorithm for the complex neural network is avoided and the training speed can be improved.

1.3.2. Outline

The remainder of the dissertation is organized as follows:

In Chapter 2, a dynamic exponential weighted moving average algorithm is developed to establish a LUT-based nonlinear Wiener model for memoryless wideband transmitters.

To improve the relatively limited accuracy of the conventional Wiener model, a new augmented Wiener model is proposed. The superiority of the augmented Wiener model on the conventional Wiener model is validated by comparing the measured spectra of the two behavior with that of the practical transmitter.

Based on the excellent modeling accuracy of the proposed augmented Wiener model in Chapter 2, an augmented look-up-table-based Hammerstein predistorter is to further improve the pre-compensation performance of the traditional Hammerstein predistorter for the broadband transmitters in Chapter 3. A wireless transmitter prototype, which includes an L-band push-pull GaAs FET 60-Watt peak-envelope-power amplifier, is utilized to evaluate the performance of the newly proposed predistorter. The pre-compensation performance of the proposed augmented predistorter in suppressing the spectrum regrowth will be illustrated by comparing the output spectra of the transmitter linearized by the different predistorters with that of the transmitter without predistortion.

In the subsequent Chapter 4, a novel real-valued time delay neural network (RVTDNN) is put forward to construct a dynamic behavior model for 3G base station power amplifiers (PA). Compared with the previously published neural network based PA models, a significantly reduced complexity and shorter processing time in the analysis and training procedures is obtained with this RVTDNN model. After training the RVTDNN with the measured baseband data, the RVTDNN behavioral model of the PA is obtained and different test signals are applied to this model to validate its accuracy and generality. The time-, frequency- and power-domain validation results are presented to demonstrate the accuracy of the RVTDNN model in predicting the memory effects.

Finally, Chapter 5 summaries the main contributions of this dissertation and gives suggestions for further research work.

REFERENCES

- [1] Jeckeln, E., "An L Band Adaptive Digital Predistorter for Power Amplifiers using Direct IQ Modem," *IEEE MTT-S Digest*, May 1998, pp. 719-722.
- [2] J. K. Cavers, "A linearizing predistorter with fast adaptation," in *40th IEEE Vehicular Technology Conf.*, pp.41-47, 1990.
- [3] S. Boumaiza, J. Li, and F.M. Ghannouchi, "Adaptive digital/RF predistortion using a nonuniform LUT indexing function with built-in dependence on the amplifier nonlinearity," *IEEE Trans. Microwave Theory Tech.*, vol. 52, pp. 2670-2677, Dec. 2004.
- [4] J. K. Cavers, "Optimum indexing in predistorting amplifier linearizers," in *Proc. IEEE 47th Vehicular Tech. Conf.*, vol. 2, pp. 676-680, May 1997.
- [5] Q. Ren and I. Wolff, "Improvement of digital mapping predistorters for linearising transmitters," in *Proc. IEEE MTT-S Int. Microwave Symp. Dig.*, vol. 3, pp. 1691-1694, June 1997.
- [6] K. J. Muhonen, M. Kavehrad, and R. Krishnamoorthy, "Look-up table techniques for adaptive digital predistortion: a development and comparison," *IEEE Trans. Vehicular Tech.*, vol. 49, pp. 1995-2002, Sept. 2000.
- [7] J. S. Kenney, W. Woo, L. Ding, R. Raich, H. Ku, and G. T. Zhou, "The impact of memory effects on predistortion linearization of RF power amplifiers," in *Proc. 8th Intl. Symposium on Microwave and Optic Technology*, pp. 189-193, June 2001.
- [8] M. Tummla, M. T. Donovan, B. E. Watkins, R. North, "Volterra series based modeling and compensation of nonlinearities in high power amplifiers," in *1997 IEEE Int. Conf. on Acoustics, Speech, and Signal Processing*, vol.3, pp. 2417-2420, April 1997.
- [9] J. Kim and K. Konstantinou, "Digital predistortion of wideband signals based on power amplifier model with memory," *Electronics Letters*, vol. 37, pp.1417-1418, Nov. 2001.
- [10] R. Raich, H. Qian, and G. T. Zhou, "Orthogonal polynomials for power amplifier modeling and predistorter design," *IEEE Trans. Vehicular Tech.*, vol. 53, pp. 1468-1479, Sept. 2004.
- [11] M. Schetzen, *The Volterra and Wiener Theories Nonlinear Systems*, New York: Wiley, 1980.

- [12] C. J. Clark, G. Chrisikos, M.S. Muha, A.A. Moulthrop, and C.P. Silva, "Time-domain envelope measurement technique with application to wideband power amplifier modeling", *IEEE Trans. Microwave Theory Tech.*, vol.46, pp. 2531-2540, Dec. 1998.
- [13] P. Crama and Yves Rolain, "Broadband measurement and identification of a Wiener-Hammerstein model for an RF amplifier", *ARFTG Conference Digest*, vol.60, pp.49-57, Dec. 2002.
- [14] J. H. K. Vuolevi, T. Rahkonen, and J. P. A. Manninen, "Measurement technique for characterizing memory effects in RF power amplifiers," *IEEE Trans. Microwave Theory Tech.*, vol. 49, pp. 1383-1389, Aug. 2001.
- [15] H. Ku and J. S. Kenney, "Behavioral modeling of nonlinear RF power amplifiers considering memory effects," *IEEE Trans. Microwave Theory Tech.*, vol. 51, no. 12, pp. 2495-2504, Dec. 2003.
- [16] K. A. Remley, M. M. P. Schreurs, D. F. Williams, and J. Wood, "Extended NVNA bandwidth for long-term memory measurements," in *2004 IEEE MTT-S Int. Microwave Symp. Dig.*, Fort Worth, TX, Jun. 6-11, 2004, pp. 1739-1742.

CHAPTER 2

DE-EMBEDDING STATIC NONLINEARITIES AND ACCURATELY IDENTIFYING AND MODELING MEMORY EFFECTS IN WIDEBAND RF TRANSMITTERS

In this chapter, a robust modeling technique for memoryless wideband radio frequency transmitters using a dynamic exponential weighted moving average algorithm is developed and tested. To improve the relatively limited accuracy of the conventional Wiener model in predicting the response of dynamic nonlinear transmitters, a new augmented Wiener model is proposed along with its parameter-identification procedure. The accuracy of the augmented Wiener model is compared with that of the conventional Wiener model by using an L-band 60-watt peak-envelope-power GaAs field-effect-transistor push-pull amplifier based transmitter, which is driven by a two-carrier wideband code-division multiple access signal.

2.1 INTRODUCTION

The design of the radio frequency (RF) front-end of third generation (3G) and beyond wireless communications transceivers is currently an extremely complicated task since it involves numerous criteria that are usually inconsistent. Although the main objective remains ensuring a good quality of signal at the receiver side, the optimization of the channel capacity (bit/Hz) is also a challenging assignment. This is particularly relevant in the context of wideband and highly varying envelope signals, as in the cases of multi-

carrier code-division multiple access and orthogonal frequency-division multiplexing, where the coexistence of linear and nonlinear distortion sources in the RF transmitter chains compromises their performances in terms of error vector magnitude and adjacent channel power ratio. The minimization of the effects of such distortion sources relies primarily on accurate modeling of the RF transmitters.

In the literature, one can distinguish several topologies that were applied to the modeling of dynamic nonlinear systems. For example, Schetzen [1] utilized Volterra series to model nonlinear power amplifiers with memory effects. However, the use of such series-based models is restricted to weak nonlinear systems. Since the models require a high-order kernel which, in turn, yields high computational complexity, difficulties are often encountered during the model identification procedure when systems are driven by wideband signals. Although the truncated Volterra series model is considered a good means of resolving the computational complexity [2], this model suffers from the difficulty of real-time implementation. Liu et al. [3] proposed a real-valued time-delay neural network to establish a dynamic behavioral model of 3G power amplifiers. Although this new architecture largely simplifies the model topology, it undergoes a relatively slow convergence of the back-propagation algorithm, which was employed to extract the model parameters.

Silva et al. presented a nonlinearity filter structure to model a wideband power amplifier, and applied a polyspectral technique for its identification [4], [5]. The principal part of such a model consists of either a filter-nonlinearity or a nonlinearity-filter in parallel with another linear filter. The authors mentioned the superiority of this model

over a conventional two-box Wiener model (linear + nonlinear) in predicting the response of traveling wave tube amplifiers. Despite the closed form expressions used in the identification of the model parameters, the required measurement data are difficult to collect in an adaptive context. Indeed, it requires a vector network analyzer (VNA) for determining the memoryless part of the model and the frequency transfer function of one of the linear filters. In addition, the memoryless characteristics of the power amplifier under a modulated signal with a high peak-to-average differ from the measured characteristics under a continuous wave signal [6].

Clark et al. in [7] reported a two-box model approach – a Wiener system [1] that consists of a two-block structure. The first block represents a linear auto-regressive moving average filter that accounts for the memory effects, and the second block denotes a conventional Bessel series model that is used to represent the memoryless nonlinearity. Such a topology can easily deal with strong nonlinearity, but the identification procedure suggested by the authors is difficult to implement under real field conditions, since it requires an initial estimation of the auto-regressive moving average filter coefficients through a frequency domain measurement under a small signal condition using a VNA. Alternatively, Crama et al. in [8] proposed a method that estimates the Wiener and Hammerstein structures based on a frequency domain identification procedure using special multi-sine signals. However, the accuracy of the identification method is greatly compromised by the phase difference between the two channels used to sample the input and the output of the device-under-test. Although a relative calibration can be applied with the assumption that one of the two channels is perfect, the identified model suffers

from a lack of accuracy due to the residual phase error.

Ku et al. [9] presented a parallel Wiener system that established a behavioral model for RF power amplifiers with memory. The model parameters are extracted using two-tone inter-modulation distortion measurements with different tone frequency spacings and power levels. The authors claimed that this model is able to predict accurately adjacent channel power ratio (ACPR) levels close to the carrier frequency for high-power amplifiers. Recently, Jantunen et al. [10] developed a nonlinear model with memory based on the Hammerstein structure (static nonlinearity + linear filter) to predict the behavior of a power amplifier for a fourth generation mobile communications system. They employed a polynomial model for the nonlinearity and a finite impulse response filter with a bulk delay for the linear component. However, the model is extracted based on single-tone measurement data instead of realistic modulated signal data. Even though a satisfactory result was reported for the single-tone test signal, its performance under modulated signals is unknown.

The common difficulty for the previous models is in the identification procedure of the parameters of their different modules. The above-mentioned models and procedures encounter high complexity and/or low accuracy. In most cases, they are not appropriate for implementation in adaptive communications systems.

In this chapter, a new augmented Wiener model that is capable of accurately modeling wideband RF transmitters in a 3G context, as well as its related identification procedure, is presented. The remainder of this chapter is organized as follows. Section II briefly depicts the wideband RF transmitter prototype used in this work. Section III explains the

newly proposed procedure and method to de-embed the strong nonlinearity from the transmitter response and to identify and quantify accurately the memory effects originally exhibited by the transmitter [11]. Then, the identification procedure and the algorithm needed to identify the parameters of the Wiener nonlinear system chosen to model wideband RF transmitters are explained in detail. In Section IV, an accurate time-delay estimation procedure, which is needed for modeling purposes in the context of broadband transmitters, is presented to align precisely the I and Q streams at the input and output of the transmitters. Section V introduces and verifies an elaborate validation method, in terms of annulling the spectrum regrowth caused by the static nonlinearity, so as to validate the performance of the Wiener models in the prediction of memory effects. In Section VI, a new comprehensive memory effect model is proposed. This model is able to account for linear distortion (frequency response near the carrier) and weak nonlinear distortion due to baseband frequency response, harmonic loading conditions, and trap effects that might occur in semiconductor devices. Based on this new memory effect model, an augmented Wiener model is established and found to be much more accurate than the conventional Wiener model in predicting ACPR levels of a wideband 60-watt peak-envelope-power (PEP) GaAs field-effect-transistor (FET) push-pull amplifier based transmitter driven by multi-carrier wideband code-division multiple access (WCDMA) signals. Section VII gives the description of the test-bed used in the experimental validation of the different models involved in this chapter. Finally, Section VIII is dedicated to the validation of the proposed augmented Wiener model and to the discussion of the measurement results.

2.2 WIDEBAND RF TRANSMITTER PROTOTYPE

As shown in Fig. 2-1, the wideband RF transmitter prototype consists of two digital-to-analog converters (DAC), an RF vector modulator and a power amplifier. The last amplification stage of the power amplifier built for this work, in the band of 1930–1990 MHz, is based on a 60-watt PEP push-pull FET transistor (FLL600IQ-2) from Eudyna Devices USA [12]. As shown in Fig. 2-2, a driver amplifier, based on an MRF19045 LDMOS transistor and an MHL19936 gain block both from Freescale Semiconductor, is used as the driver stage. The whole line-up has 53 dB gain and 45 dBm saturated power. Furthermore, an electronic signal generator (ESG: Agilent E4438C) is utilized in this work to emulate the rest of the transmitter. Hence, both the ESG and the power amplifier (PA) constitute the transmitter prototype.

It should be pointed out that the power amplifier (last stage) used in this work is based on an FLL600IQ-2 FET transistor, which is of a dual transistor push-pull configuration. This transistor is designed for use in personal-communications-services/networks base station amplifiers instead of the third generation partnership projects (3GPP) base station amplifier. Therefore, the frequency response is relatively poor for 3GPP applications, especially around the center frequency of 1.96GHz, as can be seen in its datasheet [12]. Moreover, it should be noted that all of the measured transmitter data in the following sections were captured using this transmitter prototype. These data will generally be referred to as transmitter measurements or raw measurement data in the figures of the subsequent sections. Since the output of the memoryless transmitter model only depends on the magnitude of the current input signal, this model is represented by the transmitter

amplitude-modulation / amplitude-modulation (AM/AM) and amplitude-modulation / phase-modulation (AM/PM) look-up table model in this work.

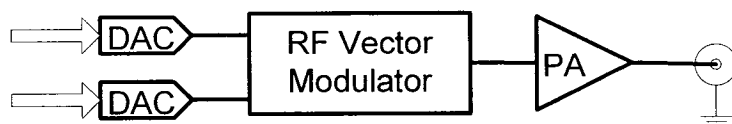


Fig. 2-1 Wideband RF transmitter prototype.

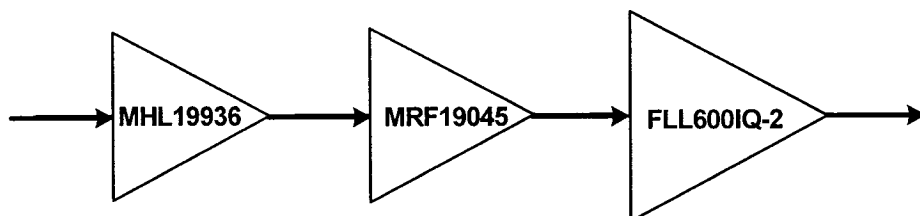


Fig. 2-2 FLL600IQ-2 power amplifier line-up.

2.3 WIENER BEHAVIORAL MODEL CONSTRUCTION

A Wiener nonlinear model, shown in Fig. 2-3, consisting of a dynamic linear filter followed by a static nonlinear block, is adopted to construct a behavioral model of a wideband RF transmitter. The static nonlinearity can be characterized by the look-up tables based on the AM/AM and AM/PM curves of the transmitter. These curves can be extracted directly from the baseband measurement data by means of a moving average procedure, as explained below. Accordingly, the complex original dynamic nonlinear

problem is simplified to a set of linear dynamic problems. In this way, identifying the Wiener nonlinear model becomes easier than the traditional solutions [13], [14], where all of the linear and nonlinear parameters of the Wiener model are resolved concurrently by means of complicated algorithms.

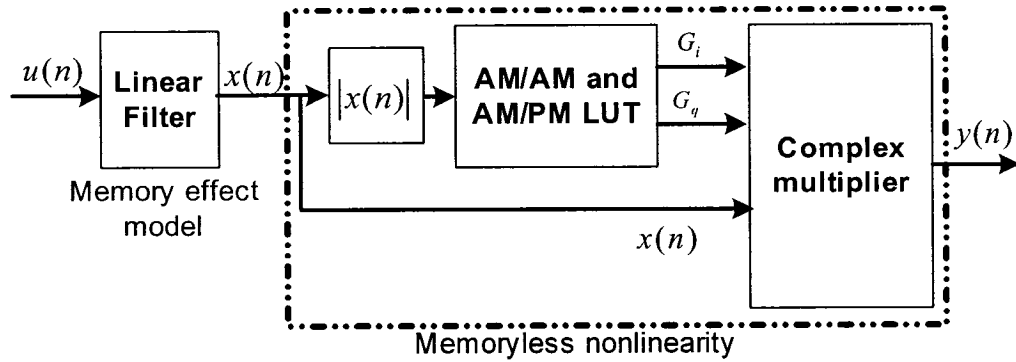


Fig. 2-3 Wiener transmitter model diagram from [8].

Assuming that the linear filter in Fig. 2-3 is a finite impulse response (FIR) filter, then the input and output signals of the two blocks in Fig. 2-3 can be related as follows:

$$x(n) = \sum_{i=0}^{M-1} a_i u(n-i) \quad (1)$$

$$y(n) = (G_i + jG_q)x(n) = Gx(n) \quad (2)$$

where $G = G_i + jG_q$ denotes the memoryless complex gain of the transmitter that depends

only on the instantaneous magnitude of $x(n)$, M stands for the taps of the FIR filter, and a_i are the FIR filter coefficients.

According to (1) and (2), the knowledge of the static nonlinear part of the transmitter model turns the identification of the coefficients a_i of the FIR filter into a simple task. Contrary to previous papers in the literature, the memoryless behavior of the transmitter is represented by a tabulated model (AM/AM and AM/PM) in this work. It allows us to alleviate the burden of the identification procedure of the analytical model's parameters, such as the high-order (even and odd) polynomial function's coefficients [15] and the Bessel series model's coefficients [7], particularly when the power amplifier (PA) operates in Class AB. Therefore, this modeling approach is robust, and it is independent of the PA technology and its operation class.

2.3.1 Static Nonlinearity De-embedding with Dynamic Exponentially Weighted Moving Average

Given the instantaneous measurements of the in-phase and quadrature input and output waveforms of the transmitter, the dynamic AM/AM and AM/PM characteristics are firstly plotted. These plots are assessed under a two-carrier WCDMA signal, which is synthesized according to 3GPP test model 3 with a separation of 5 MHz [16]. Fig. 2-4 and Fig. 2-5 give evidence of the significant dispersion of the AM/AM and AM/PM curves of the current transmitter and consequently confirm the presence of important memory effects. As a result, the construction of the corresponding model, which is capable of predicting transmitter behavior, necessitates the identification of the

parameters of the two blocks shown in Fig. 2-3. To extract the transmitter static nonlinearity, an exponentially weighted moving average is applied to the dynamic AM/AM and AM/PM data to remove the dispersion. The exponentially weighted moving average algorithm is based on the following equation:

$$y(n) = \alpha y(n-1) + (1-\alpha)x(n) \quad (3)$$

where α is the weight factor with a value between 0 and 1.

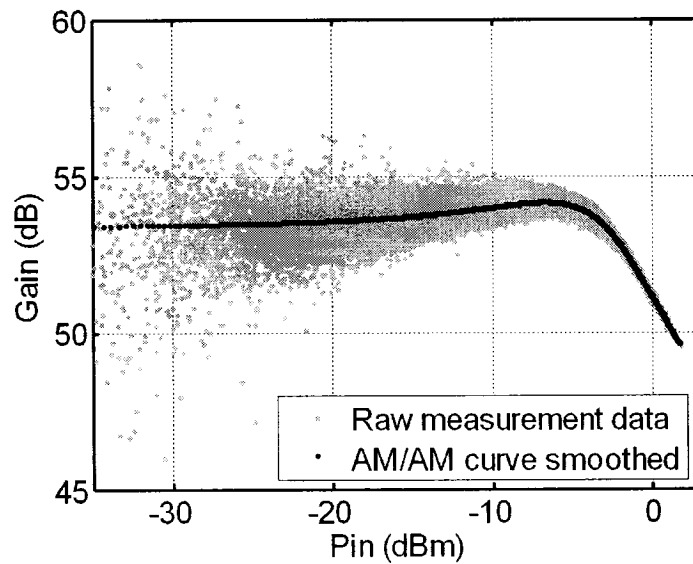


Fig. 2-4. The smoothed AM/AM curve vs. the raw measurement AM/AM data of the transmitter prototype.

Considering the significant dispersion in the AM/AM and AM/PM characteristics of the transmitter, a fixed α over the input signal dynamic range will lead to a poor moving

average quality. In fact, a large value of α will produce smooth (no dispersion) but incorrect traces because of the average error propagation. Similarly, a small value of α ends with a jagged curve. Consequently, to adapt a α 's value to the AM/AM and AM/PM variation, a dynamic setting of α is essential. For that reason, the α 's value must be expressed as a function of the input power, i.e. $\alpha = F(|x(n)|^2)$.

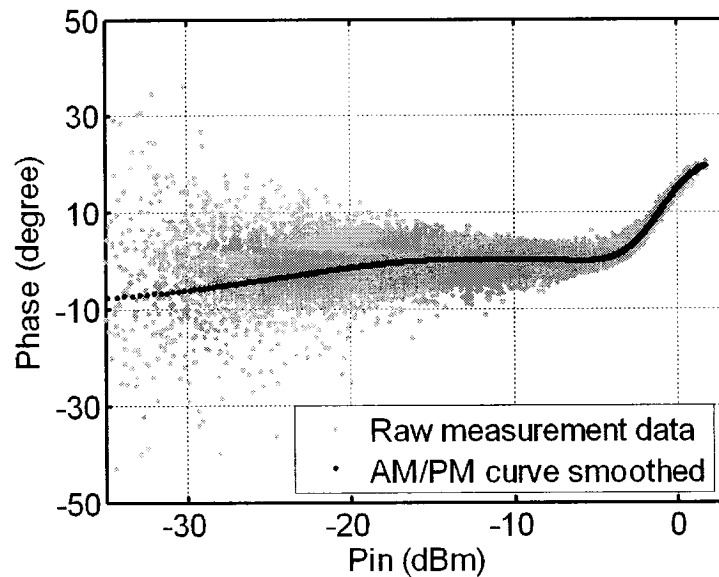


Fig. 2-5. The AM/PM curve smoothed vs. the raw measurement AM/PM data of the transmitter prototype.

The look-up table entries are determined from the AM/AM and AM/PM curves of the transmitter obtained by smoothing the dynamic characteristics using this exponentially weighted moving average. These entries encompass the in-phase G_i and the quadrature G_q components of the complex compression gain corresponding to different

magnitude values of $x(n)$.

2.3.2 Identification and Modeling of Memory Effects

2.3.2.1 Memory effect identification

The identification of the static nonlinear model on the basis of the dynamic characteristics of the transmitter allows us to fulfill the measured variables listed in Fig. 2-3. Indeed, the identification of the memory effect model necessitates the time records of $u(n)$ and $x(n)$, but transmitter characterization does not provide access directly to $x(n)$. In this way, the memoryless block initially identified will be utilized to deduce the time record of $x(n)$ on the basis of the output time record $y(n)$. Therefore, an inverse function of the static nonlinear model is numerically constructed and applied to the measured output signal $y(n)$ in order to get the dynamic linear filter output signal $x(n)$.

2.3.2.2 Modeling of the linear distortion

The plot of the AM/AM and AM/PM characteristics while considering $u(n)$ as input and $x(n)$ as output, as given in Fig. 2-6 and Fig. 2-7, indicates the removal of the nonlinearity. Therefore, the complicated original nonlinear modeling problem is simplified to a linear identification problem. In order to avoid the potential instability of an infinite impulse response filter, a FIR filter is adopted to construct the dynamic linear model in this chapter.

If both lengths of the training sequences $u(n)$ and $x(n)$ are N , then (1) can be rewritten

in matrix format as follows:

$$X = AW \quad (4)$$

where

$$X = [x(M), x(M+1), \dots, x(N)]^T \quad (5)$$

$$W = [a_0, a_1, \dots, a_{M-1}]^T \quad (6)$$

$$A = [U(M) \quad U(M+1) \quad \dots \quad U(N)]^T \quad (7)$$

$$U = [u(n) \quad u(n-1) \quad \dots \quad u(n-M+1)] \quad (8)$$

$$n = M, M+1, \dots, N$$

Therefore, the identification of FIR filter weights can be made using the recursive least-squares algorithm [17]. Here, the measured $u(n)$ and the deduced $x(n)$ are taken as the input signal and the desired signal, respectively. The detailed recursive least-squares algorithm statement is given as follows.

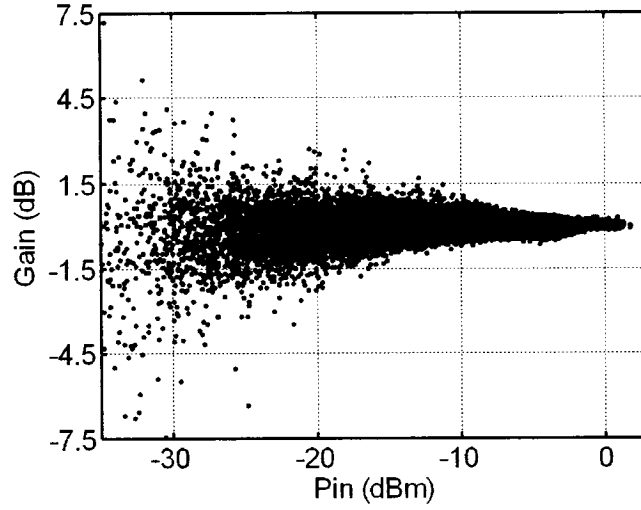


Fig. 2-6 Dynamic AM/AM characteristics of the linear filter extracted from the measurement data of the transmitter prototype.

At first, $F(n)$, $K(n)$ and $P(n)$ are calculated in terms of following equations:

$$F(n) = P(n-1)U(n) \quad (9)$$

$$K(n) = \frac{F(n)}{\lambda + U^H(n)F(n)} \quad (10)$$

$$P(n) = \frac{1}{\lambda} (P(n-1) - K(n)U^H(n)P(n-1)) \quad (11)$$

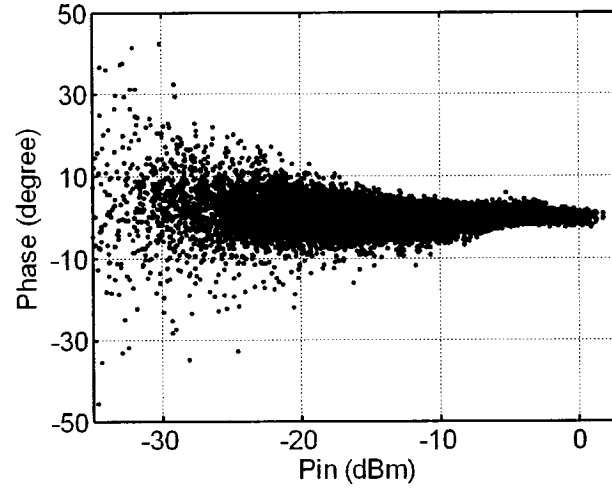


Fig. 2-7 Dynamic AM/PM characteristics of the linear filter extracted from the measurement data of the transmitter prototype.

where $P(n)$ is a $M \times M$ matrix. Both $F(n)$ and $K(n)$ are $M \times 1$ matrices. λ is a scalar and denotes the forgetting factor. Then the output $x_1(n)$ of the filter at the current instant is

$$x_1(n) = W^H(n-1)U(n) \quad (12)$$

Thus, the output error of the dynamic filter at the current instant is

$$e(n) = x(n) - x_1(n) \quad (13)$$

Finally, the weights of the dynamic filter are updated by:

$$W(n) = W(n-1) + K(n)e^*(n) \quad (14)$$

The recursive least-squares algorithm is initialized by setting

$$W(0) = 0 \quad (15)$$

$$P(0) = \delta^{-1}I$$

where δ is a small positive constant, and I is the $M \times M$ identity matrix.

2.4 INFLUENCE OF TIME DELAY ON MEMORY EFFECT IDENTIFICATION

The time delay that exists between the input and the output baseband data waveforms of the transmitter has to be accurately estimated so as to align input and output I - Q streams prior to identifying the transmitter behavioral model. In fact, the time-delay estimation becomes more critical when wideband transmitters are concerned, since any time-delay misalignment induces an extra dispersion of AM/AM and AM/PM characteristics of the transmitter. To illustrate the contribution of time delay to the dispersion of AM/AM and AM/PM characteristics of the transmitter, a 0.63 ns delay under a 61.44 MSPS sample rate condition was added while capturing the output of a memoryless transmitter model, which was constructed by the transmitter AM/AM and

AM/PM look-up table. The AM/AM and AM/PM characteristics of the memoryless models with and without a 0.63 ns delay are shown in Fig. 2-8 and 9, respectively. One can clearly observe the dispersion attributed to the time-delay offset. A similar experiment was also carried out to further demonstrate the influence of the time-delay mismatch on memory effect identification. As shown in Fig. 2-10 and 11, a 3.0 ns time delay causes strong additional dispersion and scattering in the AM/AM and AM/PM curves. Therefore, inaccurate time-delay estimation and misalignment will conceal the genuine memory effects.

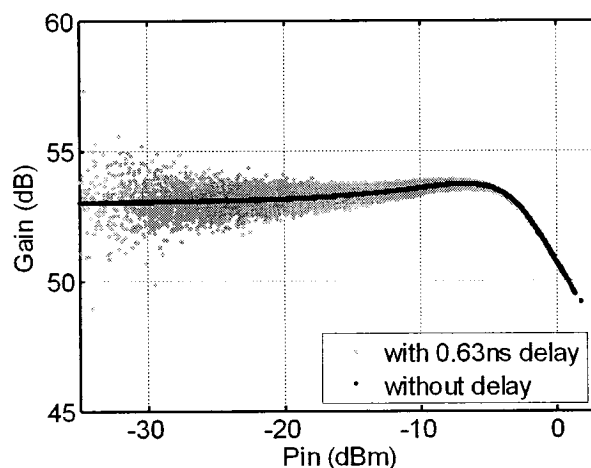


Fig. 2-8 The simulated AM/AM characteristic comparison between the memoryless models with and without 0.63 ns delay.

To accurately estimate the time delay between the input sequence $u(n)$ and the output sequence $y(n)$, a cross-covariance of $u(n)$ and $y(n)$ is calculated as follows [18]:

$$C_{xy}(m) = \begin{cases} \sum_{n=0}^{N-m-1} (u(n+m) - \bar{u})(y^*(n) - \bar{y}^*) & m \geq 0 \\ \sum_{n=0}^{N+m-1} (u^*(n-m) - \bar{u}^*)(y(n) - \bar{y}) & m < 0 \end{cases} \quad (16)$$

where, N is the length of the sequence. \bar{u} and \bar{y} represent the average values of $u(n)$ and $y(n)$ respectively, which are given by:

$$\bar{u} = \frac{1}{N} \sum_{i=0}^{N-1} u(i) \quad (17)$$

$$\bar{y} = \frac{1}{N} \sum_{i=0}^{N-1} y(i) \quad (18)$$

Therefore, the time delay can be determined by:

$$\tau = m_{\max} \times \frac{1}{f_s} \quad (19)$$

where, f_s denotes the sampling rate and m_{\max} is the index of the maximum covariance.

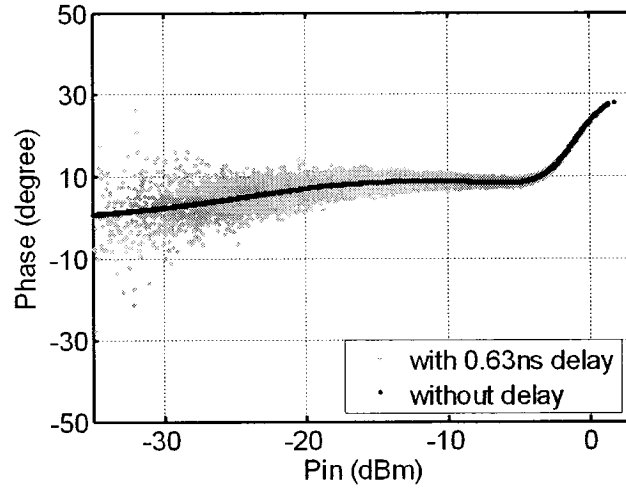


Fig. 2-9 The simulated AM/PM characteristic comparison between the memoryless models with and without 0.63 ns delay.

According to (20), the time-delay estimation accuracy is mainly determined by the sample rate f_s . For example, when the sample rate f_s equals 61.44 MSPS, the time resolution is 16.3 ns. However, in practical situations, the time delay of a PA is generally lower than 15 ns. Thus, the resolution is even larger than the time delay caused by the PA. Consequently, this sample rate cannot meet the requirement of time-delay estimation and should be increased. Indeed, the sample rate fully depends on the speed of the analog-to-digital converters (ADC) of the feedback path. One possible solution to circumvent this limitation is to update the hardware. Nevertheless, this solution is not always possible due to the currently available ADC speed, as well as related expenses. An alternative solution is to use digital signal processing (DSP) techniques. The Lagrange interpolation [19] has, therefore, been adopted in this work to increase the sample rate by 20-30 times. Finally, a higher resolution can be obtained and a satisfactory time-delay estimation achieved. The

cross-covariance calculation results with a 26-times interpolation for a two-carrier WCDMA signal are shown in Fig. 2-12. It is clear that the maximum cross-covariance can be found easily and accurately.

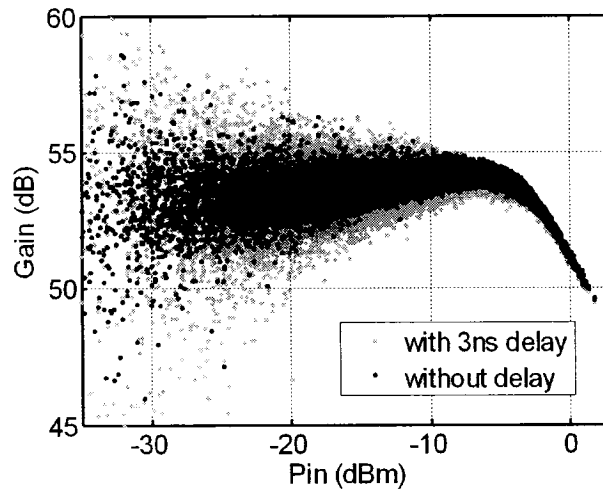


Fig. 2-10 Measured transmitter AM/AM characteristic comparison with different time delays.

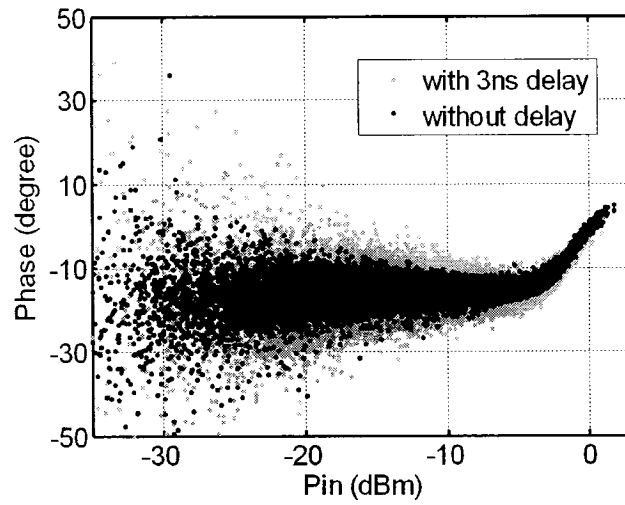


Fig. 2-11 Measured transmitter AM/PM characteristic comparison with different time delays.

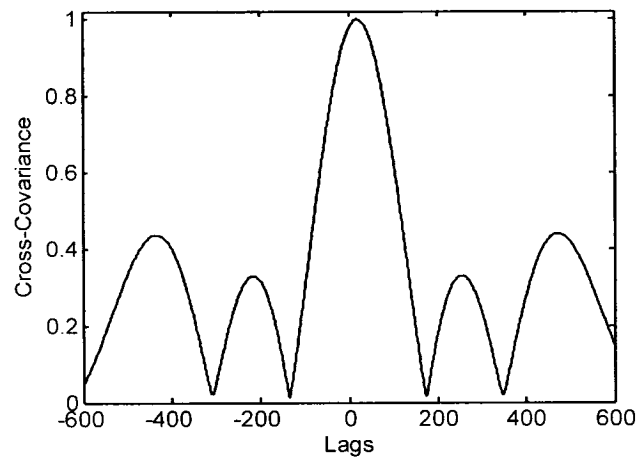


Fig. 2-12 Cross-covariance calculation results with 15.8ns delay.

It should be pointed out that this time-delay estimation method will use more resources and take longer processing times, while having a higher rate interpolation under long

time-delay conditions. To overcome this shortcoming, a two-step strategy is adopted for practical implementation. In the first stage, coarse time-delay estimation is performed without interpolation. In the second stage, fine time-delay estimation is carried out by having a higher interpolation rate on a very short data sequence.

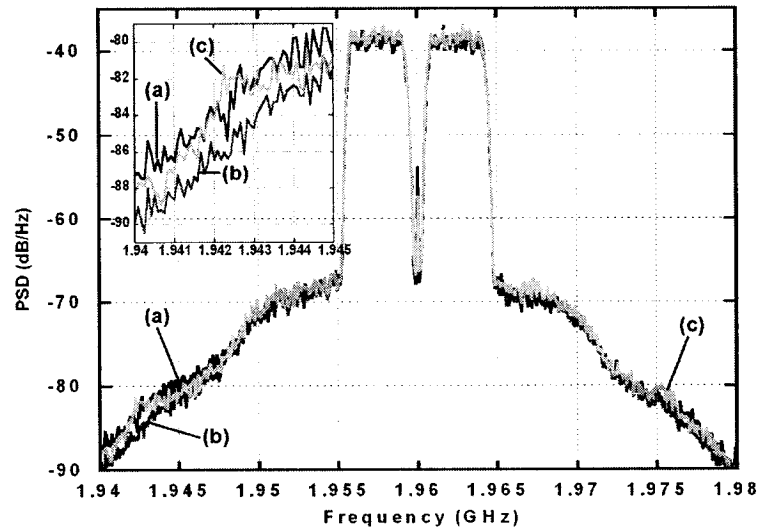
2.5 WIENER MODEL VALIDATION AND LIMITATION ASSESSMENT

2.5.1 Wiener Transmitter Model Validation Method

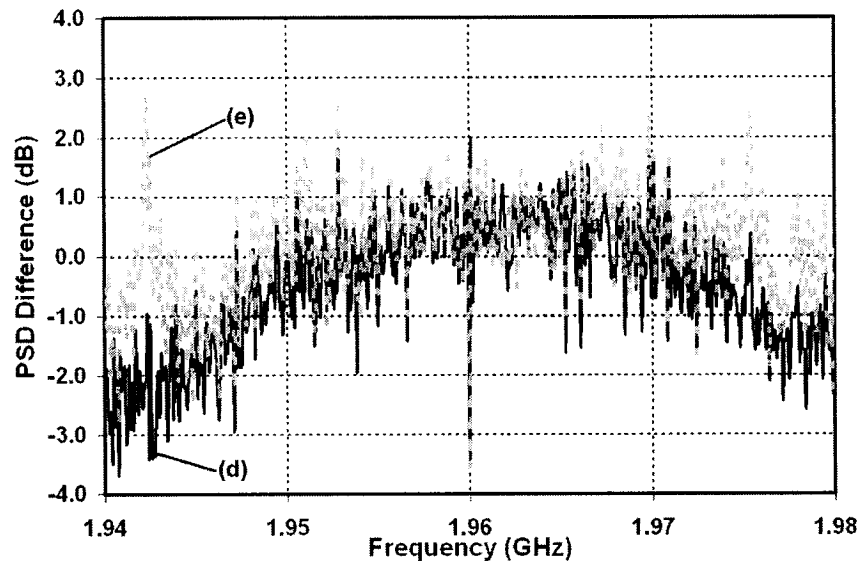
The validation of the Wiener model, which is identified using the procedure explained above, was initially carried out through a comparison of the output spectra obtained from the actual transmitter-under-test, the memoryless transmitter model and the Wiener transmitter model, where a two-carrier WCDMA signal was applied directly to the two transmitter models and to the transmitter prototype. According to Fig. 2-13 (A), the Wiener transmitter model with a 64-tap FIR filter produced an output spectrum that seemed to be close to the measured one. However, to further investigate this matter, the spectrum differences between the two transmitter models and the actual transmitter are illustrated in Fig. 2-13 (B). From this figure, one cannot assert that the Wiener transmitter model performs better than the memoryless transmitter model.

At first glance, such a result seems ambiguous. In fact, the strong static nonlinearity of the transmitter dominates most parts of the emergence of the out-of-band spectrum emission at the transmitter and the model outputs. Consequently, the spectrum regrowth caused by the memory effects is obscured by the spectrum emission produced by the

static strong nonlinearity. The contribution of the memory effects in the spectrum regrowth acts as a kind of perturbation; therefore, with such a validation approach, it is very difficult to distinguish the influence of the memory effects on the spectrum regrowth. For that reason, a more appropriate approach has to be applied in order to prove the superiority of the Wiener model over the memoryless behavioral model in mimicking the memory effects of wideband transmitters.



(A) Spectrum comparison



(B) Spectrum difference

Fig. 2-13 Spectrum comparison among the spectra of memoryless model, 64-tap Wiener model and transmitter measurement. (a) Transmitter measurement. (b) Memoryless model. (c) Wiener model with a 64-tap FIR filter. (d) Spectrum differences between the memoryless transmitter model and the actual transmitter. (e) Spectrum differences between the 64-tap Wiener transmitter model and the actual transmitter.

As mentioned earlier, the Wiener model consists of a dynamic linear block and a static nonlinear block. Thus, a pre-compensation of the static nonlinearity of the transmitter by applying its inverse function permits the decoupling of the out-of-band emission, which is caused by the memory effects, and the spectrum regrowth resulting from the memoryless nonlinearity. In this way, the spectrum regrowth produced by the static nonlinearity is numerically removed from the output spectrum of the transmitter. As a result, the output spectrum observed in the spectrum analyzer is strongly dominated by the memory effects of the wideband RF transmitter.

With this new model validation method, the output spectrum of the transmitter

memoryless model will be almost free of spectrum regrowth. However, the Wiener model and the transmitter prototype output spectrum will include a spectrum regrowth which can be attributed to the memory effects.

2.5.2 *Wiener Model Validation*

For the purpose of the validation of the Wiener transmitter model, a 1024-entry look-up table and FIR filters with different numbers of taps were constructed by using the in-phase and quadrature components of the input and output signals of the transmitter. As mentioned earlier, the look-up table was constructed first, by using the proposed static nonlinearity de-embedding procedure with Matlab[®] software. Then, the recursive least-squares algorithm was applied to determine the weights of the FIR filter. The constructed Wiener model was implemented in Agilent advanced design system (ADS) for validation purposes. It is worth noting that, in order to check the generality of the Wiener model, a frame of WCDMA signal different from that used in the model identification step was applied during the validation phase.

Fig. 2-14 illustrates the capacity of the Wiener models to predict the output spectrum of the transmitter. Here the transmitter and the Wiener models were cascaded with the inverse of the static nonlinearity block. Compared with the measurement spectrum, the Wiener model with 64-tap FIR filter allows for better prediction of the output spectrum of the transmitter than the Wiener models using five- or ten-tap FIR filters. Furthermore, ACPRs for the different Wiener models and the transmitter prototype output were assessed at several frequency offsets (-15MHz, -10MHz, -5MHz, 5MHz, 10MHz and

15MHz) from the center frequency within 3.84MHz bandwidth as shown in Fig. 2-15. ACPR results also demonstrated that the Wiener model with 64-tap FIR filter produced the best results among the three different Wiener models. However, a relatively large difference between the spectrum of the 64-tap Wiener model and the spectrum of the transmitter prototype still existed, especially with the out-of-band spectrum components nearby the two main channels. Therefore, one can conclude that the Wiener model cannot accurately predict the memory effects of the actual wideband transmitter used in 3G applications.

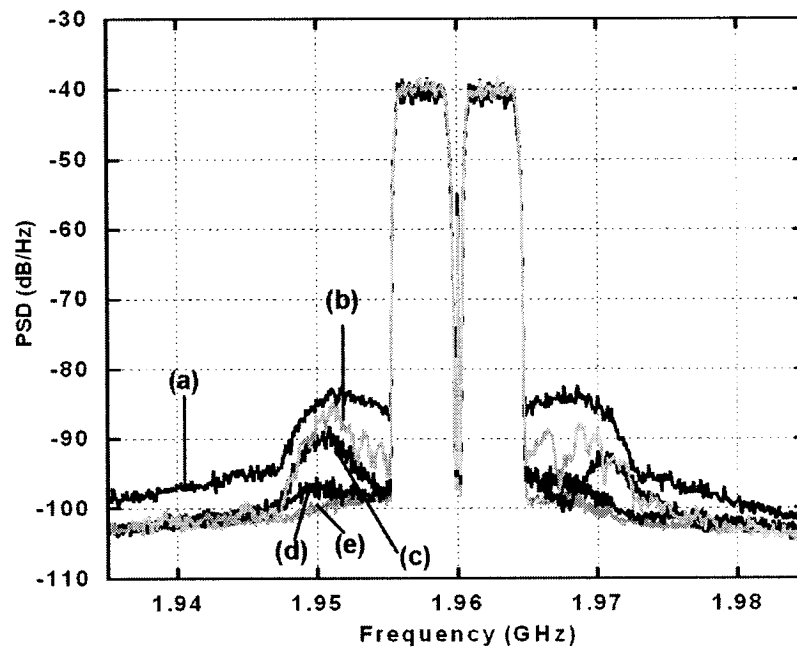


Fig. 2-14 Spectrum comparison of different Wiener transmitter models and the transmitter prototype. (a) Transmitter measurement. (b) Wiener model with a 64-tap FIR filter. (c) Wiener model with a 10-tap FIR filter. (d) Wiener model with a 5-tap FIR filter. (e) Memoryless model.

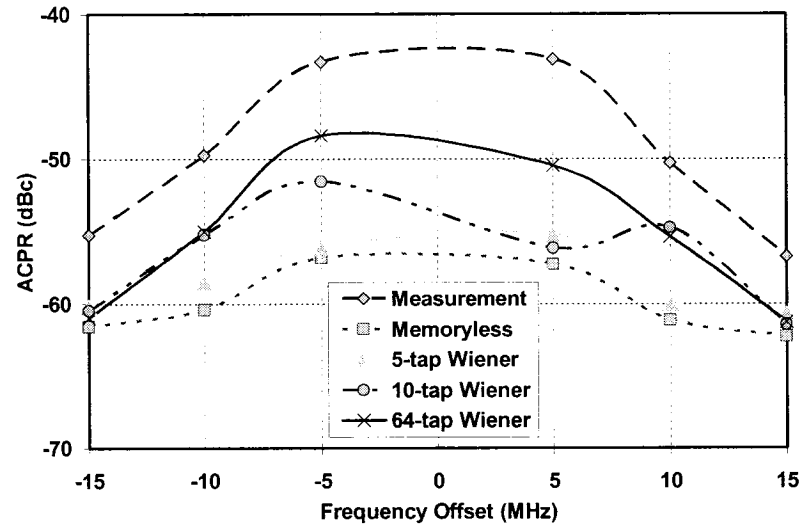


Fig. 2-15 ACPR comparison of different Wiener transmitter models and the transmitter prototype.

2.6 AUGMENTED WIENER BEHAVIORAL MODEL

2.6.1 Inclusive Memory Effect Model

The memory effect sources of an RF transmitter are usually attributed to thermal and/or electrical dispersion effects. In the context of a wideband transmitter, electrical memory effects are the dominant sources of dispersion since the thermal time constant is too large compared to the inverse of the signal bandwidth [20]. Vuolevi *et al.* [21], Ku *et al.* [22] and Remley *et al.* [23] attributed the electrical memory effects to different sources including: trapping effects, impact ionization, the frequency response of the PA

around the carrier frequency, matching conditions at harmonic frequencies and the impedance matching conditions at the envelope frequency (bias circuit design). The effects of the last two sources are responsible for extra odd-order inter-modulation distortion vectors. Indeed, even-order nonlinearities after remixing with the carrier frequencies lead to odd-order inter-modulation products, which are in or very close to the main channel.

The linear FIR filter in the Wiener model, as presented previously, takes into account the frequency response around the carrier frequency (linear distortion) and not the nonlinear even-order distortion sources. In fact, the extracted AM/AM and AM/PM characteristics of the dynamic memory effect model, as shown in Fig. 2-6 and Fig. 2-7, are not completely symmetric around the X-axis. This suggests that weak nonlinearities still exist even after de-embedding static and strong nonlinearity from the measured data. For this reason, it is not sufficient to model these weak nonlinearities with a linear filter as is normally done in conventional Wiener models. This also explains the relatively limited capability of the conventional Wiener model to predict the response of the transmitter.

Consequently, a new comprehensive memory effect model is proposed. As shown in Fig. 2-16, one can see that a new parallel branch is added to the linear FIR filter. In this new parallel branch, the input signal $u(n)$ is multiplied by its magnitude $|u(n)|$ and applied to another FIR filter. In this way, the linear FIR filter in the conventional Wiener model, as described in the previous section, is replaced by a weak nonlinear dynamic FIR-based filter. The second-order terms are introduced to the dynamic memory effect model in such

a way as to make it able to mimic memory effects more accurately.

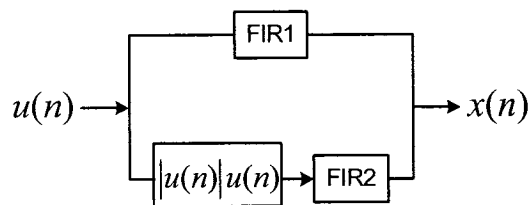


Fig. 2-16 Dynamic memory effect model.

Using the new inclusive memory effect model, an augmented Wiener model, as given by Fig. 2-17, is proposed to model wideband RF transmitters accurately. This augmented Wiener model is a cascade of a dynamic weak nonlinear model and a strong nonlinear static model. The strong nonlinear model, based on the smoothed AM/AM and AM/PM characteristics of the transmitters, is normally implemented by using look-up tables. The dynamic weak nonlinear model is composed of the new inclusive memory effect model, which takes into account the dynamic properties of the transmitters in the presence of the modulated communications signal.

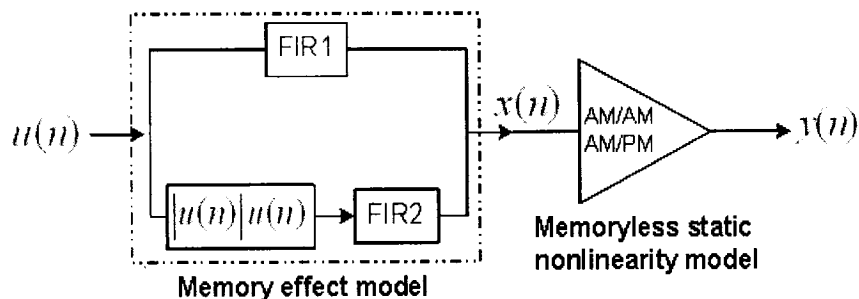


Fig. 2-17 Augmented Wiener transmitter model diagram.

2.6.2 Augmented Wiener Model Identification

Assuming that the two FIR filters have M_1 and M_2 taps respectively, the input signal $u(n)$ and the output signal $x(n)$ of the dynamic filter block in Fig. 2-17 can be written as follows:

$$x(n) = \sum_{i=0}^{M_1-1} a_i u(n-i) + \sum_{i=0}^{M_2-1} b_i |u(n-i)| u(n-i) \quad (20)$$

where M_1 and M_2 stand for the memory depth of the model. (20) can also be used for the identification of the augmented Wiener model. After removing the strong static nonlinearity using (20), the identification of the coefficients a_i and b_i of the nonlinear filter can be simplified. Let

$$v(n-i) = |u(n-i)| u(n-i) \quad (21)$$

Then, (21) can be rewritten as

$$x(n) = \sum_{i=0}^{M_1-1} a_i u(n-i) + \sum_{i=0}^{M_2-1} b_i v(n-i) \quad (22)$$

Consequently, (23) can be solved with recursive least-squares algorithm, if (6) and (8)

are modified as follows:

$$W = [a_0, a_1, \dots, a_{M_1-1}, b_0, b_1, \dots, b_{M_2-1}]^T \quad (23)$$

$$U = \begin{bmatrix} u(n), & u(n-1), & \dots, & u(n-M_1+1), \\ v(n), & v(n-1), & \dots, & v(n-M_2+1) \end{bmatrix} \quad (24)$$

$$n = M, M+1, \dots, N$$

$$M = \max(M_1, M_2)$$

where M is the larger one of M_1 and M_2 . Since only the first- and second-order terms of the input signals are included in this new model, the algorithm has good numerical stability.

2.7 EXPERIMENTAL SETUP AND NEWLY PROPOSED MODEL VALIDATION

The wideband RF transmitter characterization platform used in this work is shown in Fig. 2-18. A personal computer (PC) was utilized as the host digital signal processor (DSP) to synthesize the test signal and to capture the feedback signal. The I/Q signal source was initially synthesized using Agilent ADS and the arbitrary waveform generator in the ESG. The test signal had two neighboring WCDMA carriers (carrier spacing 5MHz), which were configured according to 3GPP test model 3 with 32 code channels [16]. The test signal synthesized using the ADS 3GPP library had a crest factor of 7.96

dB. The dynamic link between ADS and the ESG was utilized for dynamically uploading the test signal from the host DSP to the I/Q arbitrary waveform generator of the ESG. Then, the signal was modulated and up-converted to an RF carrier in the ESG, and the RF output of the ESG was fed to the PA.

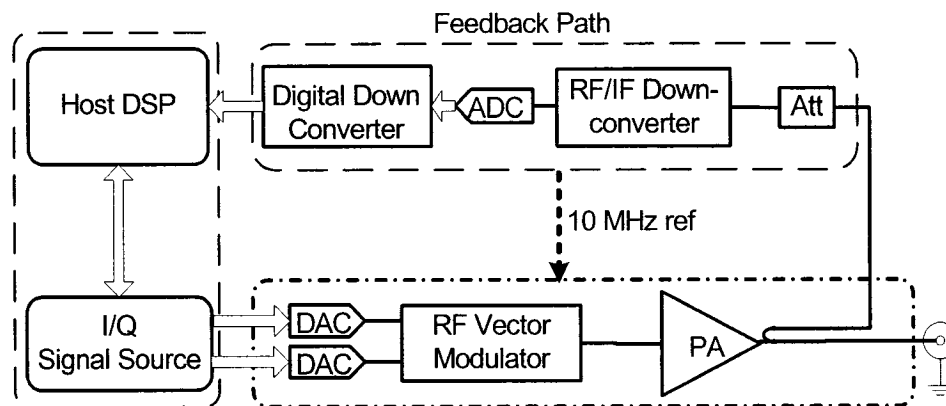


Fig. 2-18 Wideband RF transmitter characterization platform.

Having the baseband input waveform directly recorded in the host DSP during the signal synthesis step, the baseband waveform at the output of the transmitter was captured by a RF receiver. This receiver consisted of a RF/IF down-converter, a high-speed ADC, a digital down-converter and the host DSP, as shown in Fig. 2-18. In this work, the receiver prototype was physically formed by a spectrum analyzer (Agilent E4446A), a vector signal analyzer (VSA: Agilent 89611A) and a PC. The Agilent E4446A spectrum analyzer, which was fed with the output RF signal of the PA, translated the RF signal to a 70 MHz intermediate frequency (IF). Then, the IF signal was digitized by means of the high-speed digitizer module (Agilent 1439C) and was down-converted to baseband I and

Q signals. Finally, the baseband I and Q data were sent to the PC through a high-speed IEEE1394 interface for further processing. The delay calibration function of the vector signal analyzer was employed to compensate for the time delay caused by the group delay of the transmitter and the output waveform acquisition subsystem.

2.8 VALIDATION RESULTS AND DISCUSSION

As suggested earlier, the validation of the newly proposed model was carried out by preceding the transmitter with its memoryless nonlinear inverse function. Thus, one can concentrate on the capability of the new model in predicting memory effects. For that reason, the identification of the augmented Wiener model parameters was firstly performed according to the method explained in Section VI. A 1024-entry look-up table was constructed, and two three-tap FIR filters were subsequently identified. To illustrate the improved accuracy of this new model, the results obtained previously with the 64-tap Wiener model and the memoryless transmitter model were used as references in the validation process. Both the spectrum comparison results shown in Fig. 2-19 and the ACPR comparison results shown in Fig. 2-20 indicate that the augmented Wiener model can predict the memory effects of the transmitter more accurately than the conventional Wiener model. As expected, the memoryless transmitter model cannot predict the memory effects of the wideband transmitter at all.

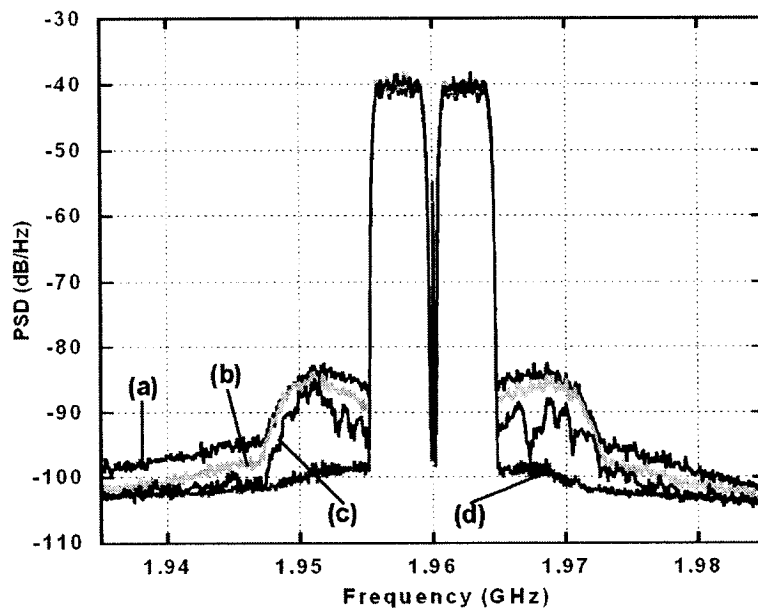


Fig. 2-19 Spectrum comparison of different transmitter models and the transmitter prototype. (a) Transmitter measurement. (b) Augmented Wiener model with two 3-tap FIR filter. (c) Wiener model with a 64-tap FIR filter. (d) Memoryless model.

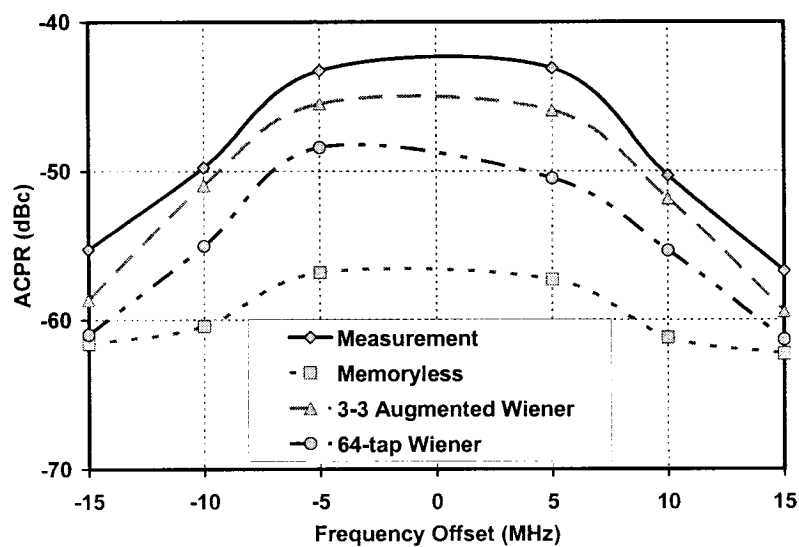


Fig. 2-20 ACPR comparison of different transmitter models and the transmitter prototype.

2.9 CONCLUSION

In this chapter, a non-analytical modeling technique for the memoryless static nonlinear behaviors of RF transmitters, based on a dynamic exponential weighted moving average algorithm, was developed and validated. This technique is inherently so robust that it can be used for any type of RF transmitters exhibiting any complex gain shape variations. In order to deduce an intermediate set of data that could be used in the identification of the dynamic (memory effects) sub-model of the Wiener model, the resulting memoryless AM/AM and AM/PM characteristics were utilized to de-embed the raw measurement data. Subsequently, to identify the memory effects accurately, a time-delay estimation algorithm based on Lagrange interpolation and cross-covariance calculation was developed to align the input and output raw baseband data captured beforehand.

Moreover, to evaluate the accuracy and robustness of the different Wiener models, a novel validation method was proposed. This method is based on annulling the spectrum regrowth that is caused by the static nonlinearity, with the help of cascading the inverse of the complex memoryless model. To improve the relatively limited accuracy of the conventional Wiener model, an augmented Wiener model has been proposed, where the linear FIR filter is replaced with a weak nonlinear filter structure. To the best of the authors' knowledge, this is the first time such a nonlinear model has been presented and implemented in practical applications. Finally, the effectiveness of the proposed augmented Wiener model and its identification procedure was assessed using a 60-watt PEP GaAs FET push-pull amplifier based transmitter driven by a two-carrier WCDMA

signal. The spectrum comparison results between the different transmitter models and the transmitter prototype reveal that the proposed augmented Wiener transmitter model outperforms other models in predicting the spectrum regrowth caused by the memory effects of the wideband transmitter.

REFERENCES

- [1] M. Schetzen, *The Volterra and Wiener Theories Nonlinear Systems*, New York: Wiley, 1980.
- [2] A. Zhu, M. Wren, and T. J. Brazil, "An Efficient Volterra-Based Behavioral Model for Wideband RF Power Amplifiers," in *2003 IEEE MTT-S Int. Microwave Symp. Dig.*, Philadelphia, PA, Jun. 8-13, 2003, pp. 787-790.
- [3] T. Liu, S. Boumaiza, and F. M. Ghannouchi, "Dynamic behavioral modeling of 3G power amplifiers using real-valued time-delay neural networks," *IEEE Trans. Microw. Theory Tech.*, vol. 52, no. 3, pp. 1025-1033, Mar. 2004.
- [4] C. P. Silva, A. A. Moulthrop, M. S. Muha, "Introduction to polyspectral modeling and compensation techniques for wideband communications systems," in *58th ARFTG Conf. Dig.*, San Diego, CA, Nov. 29-30, 2001, pp. 1-15.
- [5] C. P. Silva, A. A. Moulthrop, M. S. Muha, "Polyspectral techniques for nonlinear system modeling and distortion compensation," in *2002 3rd IEEE Int. Vacuum Electronics Conf. Dig.*, Monterey, CA, Apr. 23-25, 2002, pp. 314-315.
- [6] S. Boumaiza and F. M. Ghannouchi, "Realistic power-amplifiers characterization with application to baseband digital predistortion for 3G base stations," *IEEE Trans. Microw. Theory Tech.*, vol. 50, pp. 3016-3021, Dec. 2002.
- [7] C. J. Clark, G. Chrisikos, M. S. Muha, A. A. Moulthrop, and C. P. Silva, "Time-domain envelope measurement technique with application to wideband power amplifier modeling," *IEEE Trans. Microw. Theory Tech.*, vol. 46, no.12, pp. 2531-2540, Dec. 1998.
- [8] P. Crama and Y. Rolain, "Broadband measurement and identification of a Wiener-Hammerstein model for an RF amplifier," in *60th ARFTG Conf. Dig.*, Washington, D.C., Dec. 5-6, 2002, pp. 49-57.
- [9] H. Ku, M. D. McKinley, and J.S. Kenney, "Quantifying memory effects in RF power amplifiers," *IEEE Trans. Microw. Theory Tech.*, vol. 50, no. 12, pp. 2843-2849, Dec. 2002.
- [10] P. Jantunen, G. Gamez, and T. Laakso, "Measurements and modelling of nonlinear power amplifiers," in *Proc. of the 6th Nordic Signal Processing Symp.*, Meripuisto, Espoo, Finland, Jun. 9-11, 2004, pp. 328-331.
- [11] T. Liu, S. Boumaiza, M. Helaloui, H. Ben Nasr and F. M. Ghannouchi, "Behavior modeling procedure of wideband RF transmitters exhibiting memory effects," in *2005 IEEE MTT-S Int. Microwave Symp. Dig.*, Long Beach, CA, Jun. 12-17, 2005.

- [12] FLL600IQ-2 L-band high power GaAs FET datasheet, Eudyna Devices USA Inc., 2004, <http://www.us.eudyna.com/products/MWpdf/FLL600IQ-2.pdf>.
- [13] S. L. Lacy and D. S. Bernstein, "Identification of FIR Wiener systems with unknown, noninvertible, polynomial nonlinearities," in *Proc. of the 2002 American Control Conf.*, Anchorage, AK, May 2002, pp. 893-898.
- [14] P. Celka, N. J. Bershad, and J. M. Vesin, "Stochastic gradient identification of polynomial Wiener systems: analysis and application," *IEEE Trans. Signal Processing*, vol. 49, no.2, pp. 301-313, Feb. 2001.
- [15] L. Ding and G. T. Zhou, "Effects of even-order nonlinear terms on power amplifier modeling and predistortion linearization," *IEEE Trans. Vehicular Tech.*, vol. 53, no. 1, pp. 156-162, Jan. 2004.
- [16] 3GPP specifications: TS 25.104 v4.5.0, TS 25.141 v4.5.0, 2002, ftp://ftp.3gpp.org/specs/2002-06/Rel-4/25_series/.
- [17] S. Haykin, *Adaptive filter theory*, 3rd Edition, Prentice Hall, 1996.
- [18] S. J. Orfanidis, *Optimum Signal Processing: An Introduction*, 2nd Edition, Prentice-Hall, 1996.
- [19] R. S eroul, *Programming for Mathematicians*, Berlin: Springer-Verlag, 2000.
- [20] S. Boumaiza and F. M. Ghannouchi, "Thermal memory effects modeling and compensation in RF power amplifiers and predistortion linearizers," *IEEE Trans. Microw. Theory Tech.*, vol. 51, no. 12, pp. 2427-2433, Dec. 2003.
- [21] J. H. K. Vuolevi, T. Rahkonen, and J. P. A. Manninen, "Measurement technique for characterizing memory effects in RF power amplifiers," *IEEE Trans. Microw. Theory Tech.*, vol. 49, no. 12, pp. 1383-1389, Dec. 2001.
- [22] H. Ku and J. S. Kenney, "Behavioral modeling of nonlinear RF power amplifiers considering memory effects," *IEEE Trans. Microw. Theory Tech.*, vol. 51, no. 12, pp. 2495-2504, Dec. 2003.
- [23] K. A. Remley, M. M. P. Schreurs, D. F. Williams, and J. Wood, "Extended NVNA bandwidth for long-term memory measurements," in *2004 IEEE MTT-S Int. Microwave Symp. Dig.*, Fort Worth, TX, Jun. 6-11, 2004, pp. 1739-1742.

CHAPTER 3

AUGMENTED HAMMERSTEIN PREDISTORTER FOR LINEARIZATION OF BROADBAND WIRELESS TRANSMITTERS

In this chapter, an augmented look-up-table-based Hammerstein predistorter is proposed for the first time in order to further improve the pre-correction capability of the traditional Hammerstein predistorter in the context of broadband high power wireless transmitters. As the predistorter scheme consists of two separate modules, its parameters are determined in two steps: (i) static predistorter identification, and then (ii) dynamic part identification. The performance assessment of the newly proposed predistorter is carried out on a wireless transmitter prototype, which includes an L-band push-pull GaAs FET 60-Watt peak-envelope-power amplifier. Moreover, one-carrier and three-carrier 3GPP-FDD signals are used as test signals to verify the robustness of this novel predistorter under different bandwidth signals. The linearized transmitter prototype output spectrum demonstrate noticeable superiority of the proposed augmented predistorter in suppressing the spectrum regrowth caused by the memory effects in comparison to the traditional Hammerstein predistorter.

3.1 INTRODUCTION

High efficiency wideband transmitter design for modern high speed wireless communication systems, such as Worldwide Interoperability for Microwave Access

(WiMAX), 3rd Generation (3G) and beyond systems and etc., is a tricky task since it involves numerous inconsistent requirements. Particularly, in such contexts, accomplishing simultaneously high linearity and high power efficiency is a great challenge. In fact, to efficiently utilize the precious limited spectrum resources, several complicated modulation schemes have been widely used in the modern wideband wireless communication systems. These modulated signals lead to a non-constant envelope with large Peak-to-Average Power Ratios (PAPRs), which can be as high as 12 dB in some cases. Consequently, the power amplifier (PA) in the transmitter has to be designed either to operate near its saturated area so as to provide higher system power efficiency or at large back-off from its nonlinear region in order to meet the required linearity. Accordingly, the PA ends with either high efficiency with bad linearity or vice-versa. Therefore, to satisfy the linearity requirement while operating the PA at its nonlinear area one has to correct for the different sources of distortion all along the entire transmitter chain.

For this reason, different linearization techniques such as feedback [1], feed-forward [2], and predistortion [3], [4], have been proposed to improve the linearity of the transmitter. Among the various linearization techniques, digital baseband predistortion is one of the most promising and cost effective linearization techniques due to its digital implementation that offers a significant accuracy and flexibility.

Consider its simplicity and relative ease of implementation, look-up-table (LUT) is by far the most adopted means for the construction of the inverse of the Amplitude-Modulation /Amplitude-Modulation (AM/AM) and Amplitude-Modulation /Phase-

Modulation (AM/PM) characteristic curves of the transmitter or PA [5]-[8]. However, such type of predistorters is only valid for memoryless nonlinear cases such as the traditional narrow band wireless communication systems. For wideband transmitter/PA context, the memory effects exhibited by the transmitter/PA limit significantly the ability of the memoryless predistorter to suppress the spectrum regrowth [9]. These electrical memory effects are mainly attributed to the non-constant frequency response of the transmitter around the carrier frequency, the impedance variation of bias circuits at baseband as well as the harmonic loading in the PA power stage [10]-[12]. Therefore, different predistorter architectures, which are intended to compensate for the nonlinearity as well as the memory effects, have been reported in the literature. For example, a memory polynomial model was proposed in [13], or utilized in [14]-[16], to address these effects. However, such a memory polynomial based predistorter suffers from a numerical instability when higher order polynomial terms are included since a matrix inversion is needed for the determination of the polynomial coefficients [17]. Alternatively, Raich *et al.* [17] employed the orthogonal polynomials to alleviate the numerical instability problem associated with the traditional polynomials.

Two-box based predistorters, which are called Hammerstein or Wiener predistorter according to the cascading order of the nonlinear block and the linear block, are another type of common predistorter architectures in the literature. For example, a Hammerstein predistorter, which is a cascade of a memoryless nonlinear block followed by a linear filter, was utilized to compensate for the nonlinearity as well as the memory effects of a PA [18], [19]. Recently, Wang and Ilow [20] demonstrated the compensation

performance using a Wiener predistorter to linearize the high power amplifier (HPA) with memory effects in an Orthogonal Frequency-Division Multiplexing (OFDM) transmitter while considering the HPA as a Hammerstein nonlinear system. In these two examples, the memoryless nonlinearity is represented by a complex high-order memoryless polynomial. In addition, the identification of the coefficients of the memoryless nonlinear block and the taps of the linear filter are concurrently resolved by means of complicated algorithms that are applied either in time domain [18], [19] or in frequency domain [20].

In this chapter, a LUT-based Hammerstein predistorter is initially developed to compensate for the nonlinearity and the memory effects that occur in a broadband wireless transmitter. To further improve the compensation performance of the predistorter, an augmented Hammerstein predistorter is proposed. The remainder of this chapter is organized as follows. The section II elucidates the details of the LUT-based Hammerstein predistorter and its corresponding identification procedure. Then, in section III, a new augmented Hammerstein predistorter is proposed in order to improve the correction performance for the nonlinearity and the memory effects in the context of the broadband wireless transmitter. Section IV describes the test bed used in the experimental validation of different predistorters involved in this chapter. Finally, in section V, the validation results of the Hammerstein predistorter and the augmented Hammerstein predistorter with different configurations under one-carrier and three-carrier the 3rd – Generation-Partnership-Projects Frequency-Division-Duplex (3GPP-FDD) signals are illustrated and discussed using an L-band 60-Watt GaAs FET push-pull PA based transmitter.

3.2 LUT-BASED HAMMERSTEIN PREDISTORTER AND IDENTIFICATION

3.2.1 *LUT-Based Hammerstein Predistorter*

A Hammerstein predistorter, as illustrated in Fig. 3-1, is utilized to build a predistortion function for a broadband wireless transmitter. Accordingly, the predistorter is decomposed into a nonlinear static memoryless subsystem and a linear dynamic one. The static memoryless subsystem is intended to pre-compensate for the static nonlinearity of the transmitter while the linear dynamic filter is focused on suppressing the spectrum regrowth caused by the memory effects. The memoryless predistortion can be implemented using the traditional look-up table (LUT). This LUT is constructed based on the AM/AM and AM/PM characteristics of the transmitter that are extracted directly from the baseband measurement data by means of a moving average procedure as explained in [21]. Consequently, the complex dynamic predistortion problem is simplified to a relatively easy linear dynamic problem. In this way, resolving the Hammerstein predistortion becomes more convenient than the traditional solutions [18]-[20], where all of the linear and nonlinear parameters of the Hammerstein model are resolved concurrently by means of elaborate algorithms.

The identification of the static memoryless predistorter on the basis of raw measured baseband data, $u(n)$ and $y(n)$, permits the extraction of the non-measurable variable, $x(n)$ shown in Fig. 3-1, which is required in the identification of the linear filter subsystem. For this reason, the input signal $u(n)$ of the predistorter is applied to the

memoryless predistorter subsystem so as to get the dynamic linear filter input signal $x(n)$.

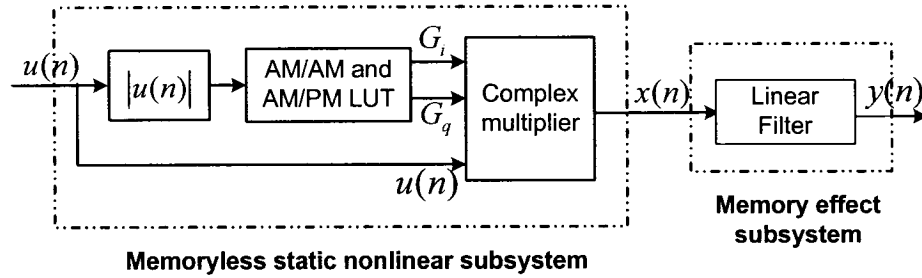


Fig. 3-1 Hammerstein predistorter diagram.

The input and output signals of the two blocks in Fig. 3-1 can be related as follows:

$$x(n) = \left[G_i(|u(n)|) + jG_q(|u(n)|) \right] u(n) = G(|u(n)|)u(n) \quad (1)$$

$$y(n) = f(x(n)) \quad (2)$$

Where $G(|u(n)|) = G_i(|u(n)|) + jG_q(|u(n)|)$ refers to the memoryless complex gain of the predistorter that depends only on the instantaneous magnitude of $u(n)$; $f(x)$ is a linear transfer function of the linear filter.

3.2.2 Hammerstein Predistorter Identification

Hammerstein parameter identification is performed using an offline training scheme as shown in Fig. 3-2. To identify the parameters of the predistorter, the output $z_{TX}(n)$ of the

transmitter is normalized by the designated linear gain G_{linear} of the transmitter and taken as the input training sequence $u(n)$ of the predistorter, i.e.,

$$u(n) = \frac{z_{TX}(n)}{G_{linear}} \quad (3)$$

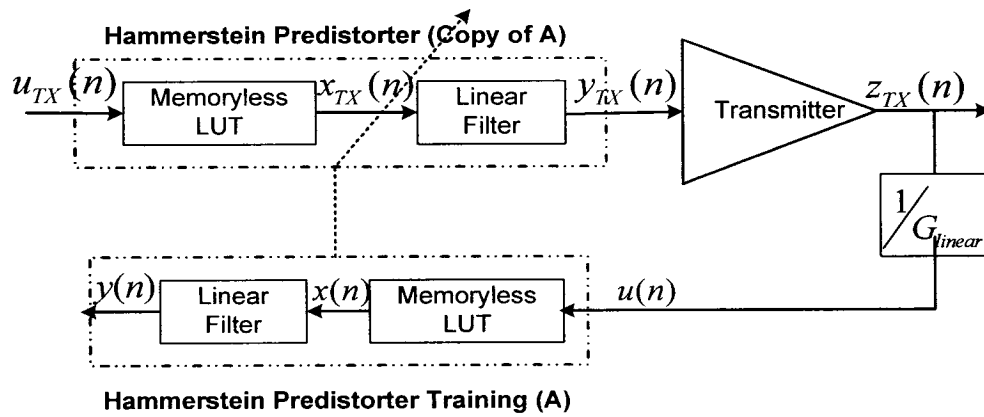


Fig. 3-2 An offline training scheme for Hammerstein predistorter identification.

The input $y_{TX}(n)$ of the transmitter is used as the output training sequence $y(n)$ of the predistorter, i.e.,

$$y(n) = y_{TX}(n) \quad (4)$$

Then the dynamic exponential weighted moving average (DEWMA) method [21] is applied to the predistorter training sequences $u(n)$ and $y(n)$ in order to remove the dispersion of the dynamic AM/AM and AM/PM characteristics. The extracted smoothed AM/AM and AM/PM curves are then used to construct the LUT of the predistorter. Fig. 3-3 and Fig. 3-4 show typical extracted AM/AM and AM/PM curves, which are based on the measurement data when the transmitter is driven with a three-carrier 3GPP-FDD signal. This latter is synthesized according to 3GPP test-model-3 with a carrier separation of 5 MHz each other [24].

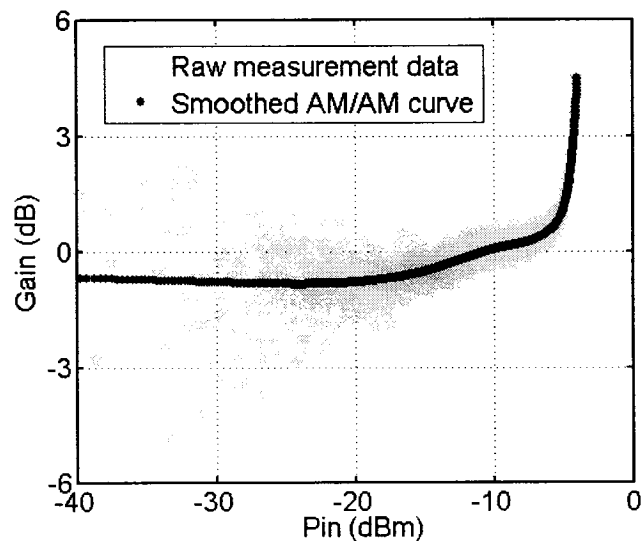


Fig. 3-3 Predistorter AM/AM curve smoothed with DEWMA vs. the raw measurement AM/AM data.

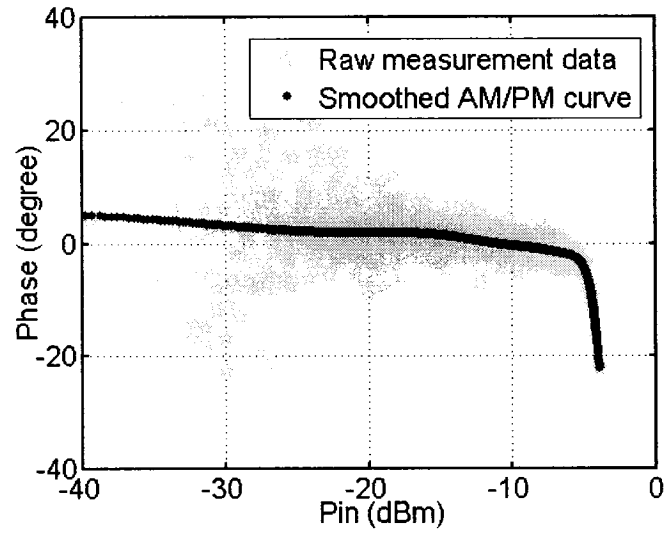


Fig. 3-4 Predistorter AM/PM curve smoothed with DEWMA vs. the raw measurement AM/AM data.

After that, the intermediate training data set $x(n)$ is deduced via the application of the input training data $u(n)$ to the previously constructed LUT. Based on the data set $x(n)$ and $y(n)$, the AM/AM and AM/PM characteristics of the memory effect subsystem in Fig. 3-1 are traced and shown in Fig. 3-5 and Fig. 3-6. The two figures illustrate the removal of the strong static nonlinearity.

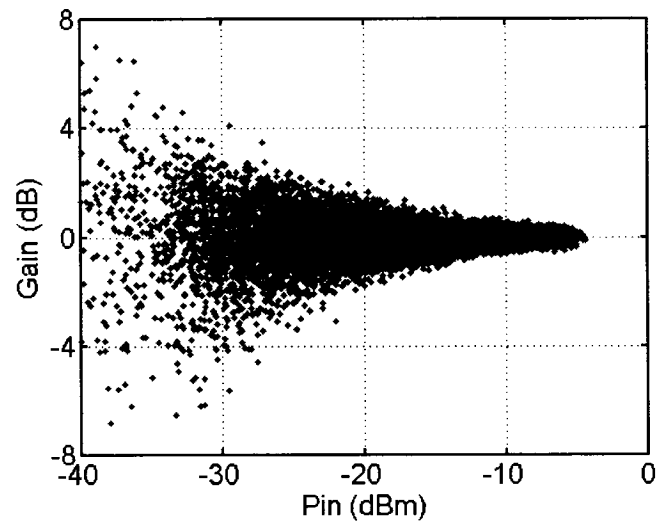


Fig. 3-5 Dynamic AM/AM characteristics of the linear filter extracted from the measurement data.

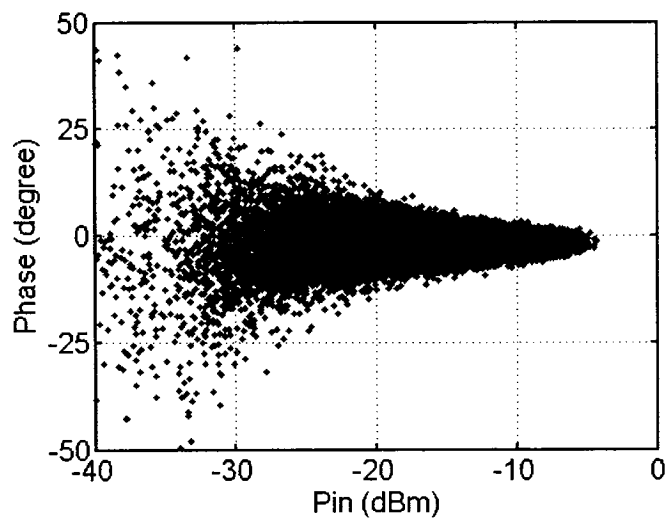


Fig. 3-6 Dynamic AM/PM characteristics of the linear filter extracted from the measurement data.

Here a Finite Impulse Response (FIR) filter is chosen, instead of an Infinite Impulse Response (IIR) filter, to build the dynamic linear filter in order to avoid the potential instability of an IIR filter. Thus, (2) can be expressed as:

$$y(n) = \sum_{i=0}^{M-1} a_i x(n-i) \quad (5)$$

Where M stands for the number of the FIR filter taps, and a_i denotes the coefficients of the FIR filter taps. Then again, (5) can be rewritten in matrix format as follows:

$$\mathbf{Y} = \mathbf{A}\mathbf{W} \quad (6)$$

where

$$\mathbf{Y} = [y(M), y(M+1), \dots, y(N)]^T \quad (7)$$

$$\mathbf{W} = [a_0, a_1, \dots, a_{M-1}]^T \quad (8)$$

$$\mathbf{A} = [\mathbf{X}(M) \quad \mathbf{X}(M+1) \quad \dots \quad \mathbf{X}(N)]^T \quad (9)$$

$$\mathbf{X} = [x(n) \quad x(n-1) \quad \dots \quad x(n-M+1)] \quad (10)$$

$$n = M, M+1, \dots, N$$

The FIR filter parameter identification can be performed using the Recursive Least-

Squares (RLS) algorithm [25], where the deduced $x(n)$ and the measured $u(n)$ are taken as the input signal and the desired signal, respectively.

Once the memoryless LUT and the linear filter parameters are identified, the offline training procedure is ended and the Hammerstein predistorter parameters are updated accordingly.

3.3 AUGMENTED HAMMERSTEIN PREDISTORTER

As discussed in the previous section, the memory effects are pre-compensated by means of a linear FIR filter in the traditional Hammerstein predistorter. This linear filter would correct for the electrical memory effects attributed mainly to the non-constant frequency response of the transmitter around the carrier frequency. Consequently, it failed to completely pre-compensate for the electrical memory effects due to the impedance variation of the bias circuits and harmonic loading of the power transistors. For that reason, an augmented Hammerstein predistorter, as given by Fig. 3-7, is proposed to enhance the correction capability in the context of broadband wireless transmitters. This augmented Hammerstein predistorter is a cascade of a strong nonlinear static subsystem and a dynamic weak nonlinear subsystem. The strong nonlinear subsystem, which is based on averaged AM/AM and AM/PM characteristics of the predistorter, can be implemented using Look-Up Tables (LUT). However, the dynamic weak nonlinear subsystem is composed of a new dynamic FIR-based filter, which is responsible for annulling the spectrum regrowth produced by the dynamic distortion sources at the transmitter output when the transmitter is driven with a modulated signal. For this new

dynamic FIR-based filter, an extra parallel branch is added to the linear FIR filter. In this parallel branch, the input signal $x(n)$ is multiplied by its magnitude $|x(n)|$ in order to generate even-order distortions that will be applied to a second FIR filter. Accordingly, the new predistorter includes distortions sources that are close to those encountered in the real transmitter to be linearized. Thus, a superior performance to that obtained with a simple linear FIR filter is anticipated.

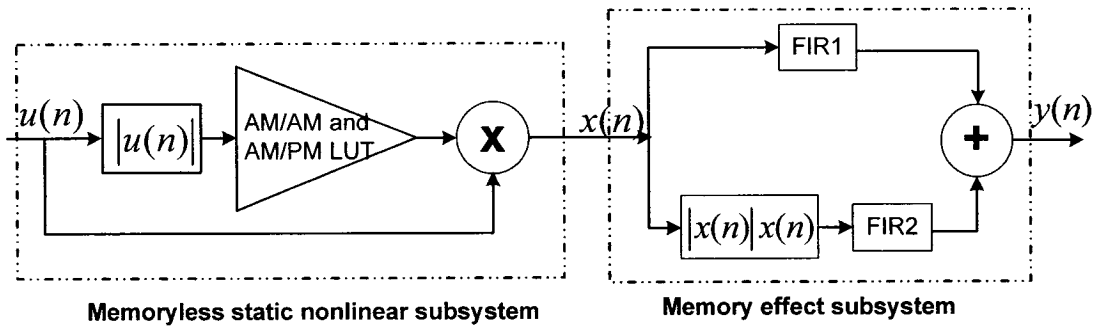


Fig. 3-7 Augmented Hammerstein predistorter diagram.

Assuming that the two FIR filters in the dynamic FIR-based filter have M_1 and M_2 taps respectively, the input signal $x(n)$ and the output signal $y(n)$ of this predistorter, given in Fig. 3-7, can be correlated as follows:

$$y(n) = \sum_{i=0}^{M_1-1} a_i x(n-i) + \sum_{i=0}^{M_2-1} b_i |x(n-i)| x(n-i) \quad (11)$$

Where M_1 and M_2 denote the memory depth of the predistorter. a_i and b_i represent the tap coefficients of the two FIR filters - FIR1 and FIR2, respectively.

The memoryless static nonlinear module in the augmented Hammerstein predistorter can also be expressed by (1). Based on the training sequence $u(n)$ and $x(n)$, the moving average procedure proposed in [21] can be utilized to extract the AM/AM and AM/PM LUT to construct a memoryless predistorter. After removing the strong static nonlinearity using the obtained LUT, the identification of the coefficients a_i and b_i can be largely simplified. Let

$$v(n-i) = |x(n-i)|x(n-i) \quad (12)$$

(11) can be rewritten as

$$y(n) = \sum_{i=0}^{M_1-1} a_i x(n-i) + \sum_{i=0}^{M_2-1} b_i v(n-i) \quad (13)$$

Consequently, (13) can be resolved with RLS algorithm if (8) and (10) are modified as follows:

$$\mathbf{W} = [a_0, a_1, \dots, a_{M_1-1}, b_0, b_1, \dots, b_{M_2-1}]^T \quad (14)$$

$$\mathbf{X} = [x(n), x(n-1), \dots, x(n-M_1+1), \\ v(n), v(n-1), \dots, v(n-M_2+1)] \quad (15)$$

$$n = M, M+1, \dots, N$$

$$M = \max(M_1, M_2)$$

Where M is the largest value of M_1 and M_2 . Since only the first and the second order terms of the input signals are involved in this new predistorter scheme, the RLS algorithm exhibits good numerical stabilities.

3.4 VALIDATION EXPERIMENTAL SETUP

The experimental set-up used to evaluate the compensation performance of the different predistorter schemes, namely conventional Hammerstein and augmented one, is shown in Fig. 3-8. The broadband wireless transmitter prototype includes a radio frequency (RF) vector modulator, two digital to analog converter (DAC) and a RF PA at the frequency band of 1930–1990 MHz. The RF PA is a cascade of three stages. The first stage contains a 12-Watt linear LDMOS power amplifier MHL-19936 with 29 dB gain from Freescale Semiconductor. The second stage is based on a Freescale MRF19045 LDMOS transistor. The final stage comprises a 60-Watt peak-envelop-power push-pull FET transistor (FLL600IQ-2) from Fujitsu. The whole line-up of the RF PA has 53 dB

gain and 45 dBm saturated power. Moreover, the RF vector modulator and two digital to analog converters (DAC) are emulated with an Electronic Signal Generator (ESG: Agilent E4438C). Therefore, the transmitter prototype is physically constructed with the ESG and the power amplifier.

The host DSP is implemented with a personal computer (PC), where the I/Q signal is initially synthesized using the 3GPP library in Agilent Advanced Design System (ADS). In this work, the I/Q test signals have one 3GPP-FDD carrier and three neighboring 3GPP-FDD carriers (carrier spacing 5MHz for every two neighboring carriers), which are configured according to 3GPP test-model-3 with 32 code channels [24]. The baseband I/Q signal is firstly pre-processed by the predistortion function and then downloaded to the I/Q arbitrary waveform generator of the ESG via the GPIB interface with the help of the dynamic link existing between ADS and the ESG. After that, the predistorted baseband signal is modulated to an RF carrier in ESG and fed to the PA. In this way, the ADS in the host DSP, the ESG, and the power amplifier work together to form a baseband linearized transmitter prototype. The baseband data at the output of the transmitter is captured by an RF receiver. As shown in Fig. 3-8, this receiver consists of a RF/IF down-converter, a high-speed analog to digital converter, a digital down-converter, and the host DSP. In this work, the receiver prototype is physically constructed by a spectrum analyzer (PSA, Agilent E4446A), a Vector Signal Analyzer (VSA, Agilent 89611A) and a PC. The spectrum analyzer PSA serves as down-converter, which transforms the RF signal to a 70 MHz intermediate frequency (IF). The IF signal is then digitized by means of the high speed digitizer module Agilent-1439C and digitally down-

converted to baseband I and Q signals. After that, the VSA software in the PC captures the baseband I and Q data via the high-speed IEEE1394 interface.

The captured baseband data at the input and output of the prototype transmitter are processed in Matlab[®] so as to deduce the parameters of the predistorter. Finally, the obtained predistorter parameters are sent to the ADS to update the corresponding predistorter parameters. The performance of the different predistorters can be evaluated by comparing the output spectra of the transmitter obtained with the various predistorter schemes.

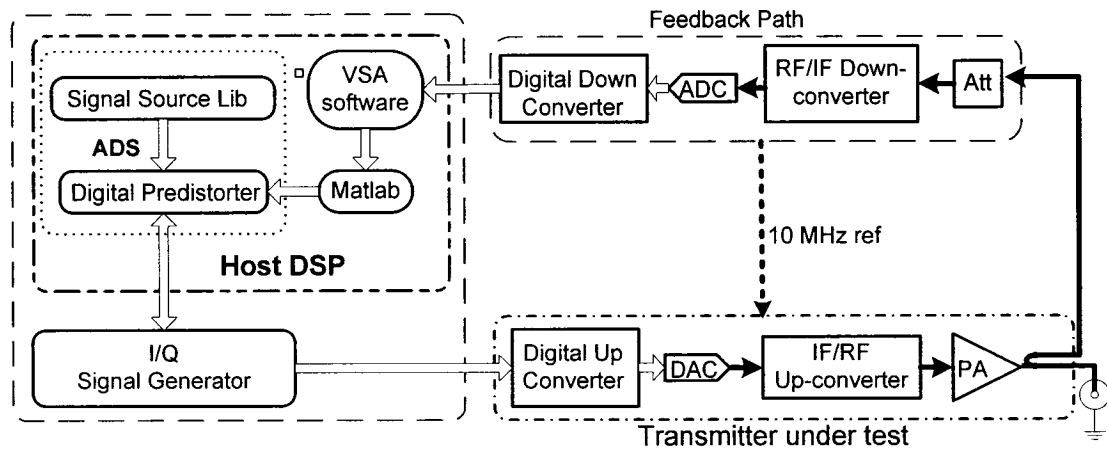


Fig. 3-8 Experimental set-up for verifying digital predistorters.

3.5 VALIDATION RESULTS AND DISCUSSION

To validate the pre-compensation ability of the predistorter, a 1024-entries LUT and the dynamic FIR filter are constructed using the offline training method introduced in the

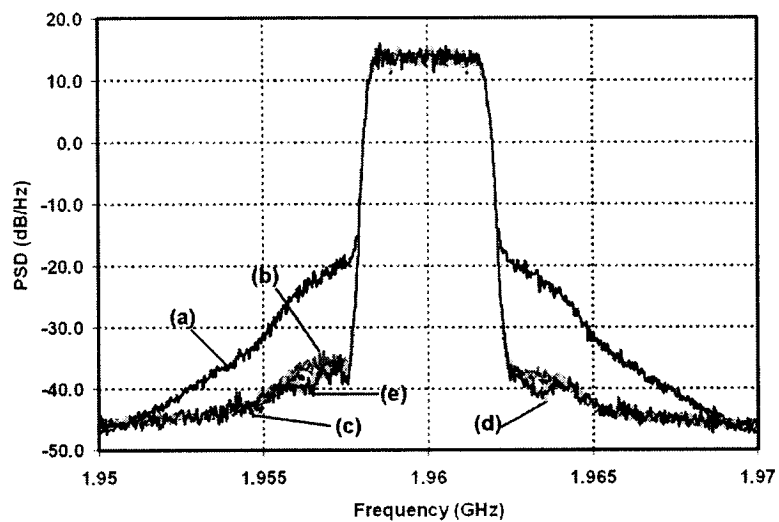
previous section. At first, the LUT is built using the DEWMA method in Matlab[®]. Then, the RLS algorithm is applied to determine the coefficients of the dynamic filter. After that, the constructed predistorter is implemented in ADS to synthesize the predistorted version of the test signal that will be fed to the wideband transmitter. To test the generality of the predistorter, a frame of 3GPP-FDD signal, which is different from the frame used in the predistorter identification stage, is applied to the predistorter during the validation phase.

3.5.1 Hammerstein Predistorter

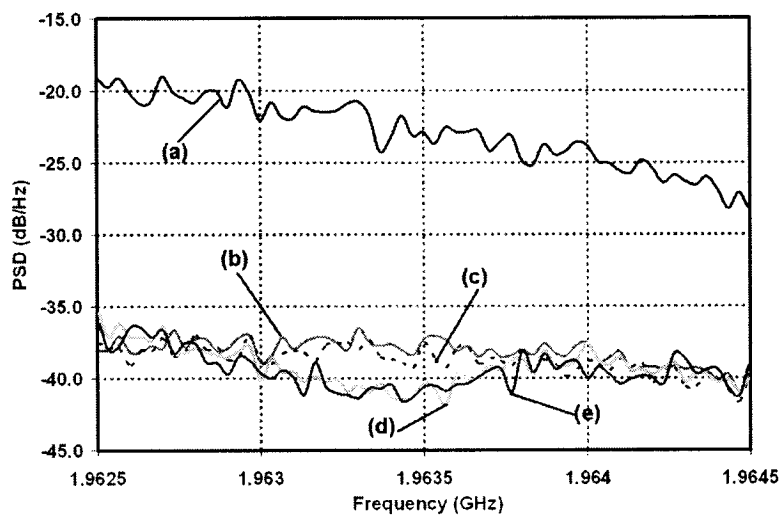
To optimize the Hammerstein predistorter, the dynamic FIR filter is configured with different number of taps so as to evaluate the variation of the residual spectrum regrowth. Fig. 3-9 illustrates the ability of the Hammerstein predistorters with different FIR taps to suppress the output spectrum regrowth of the transmitter while applying the predistorted one-carrier 3GPP-FDD signals. The spectrum of the Hammerstein predistorter having 128-taps FIR filter shows the larger side-lobes suppressing. In comparison to the spectrum of the transmitter obtained using a memoryless predistorter, one can conclude that to some extents all of the different Hammerstein predistorters are able to partially suppress of the spectrum regrowth caused by the memory effects. Fig. 3-10 shows the adjacent channel power ratio (ACPR), at the output of the transmitter for different predistorters, which are assessed at several frequency offsets (-15 MHz, -10 MHz, -5 MHz, 5 MHz, 10 MHz and 15 MHz) from the center frequency within 3.84 MHz bandwidth. The improved ACPR value at 5 MHz offset for the transmitter with the

Hammerstein predistorter having 128-taps FIR filter is as high as 15 dB when compared to the ACPR value of the non-linearized transmitter.

Furthermore, Fig. 3-9 clearly exemplifies all of these Hammerstein predistorters cannot effectively suppress the spectrum regrowth close to the main channel. The best ACPR value at 5 MHz offset for the transmitter with the Hammerstein predistorters is about -55.5 dBc. In comparison to -54.2 dBc of the ACPR obtained with the memoryless predistorter, there is no obvious improvement for further suppressing the spectrum regrowth using these traditional Hammerstein predistorters. Consequently, based on the results obtained, one can conclude that in actual transmitter systems the ability of the Hammerstein predistorter for reducing the transmitter spectrum regrowth caused by the memory effects is limited. This might be due to the fact that real broadband transmitters can not be accurately characterized by and do not obey a Wiener nonlinear model. This is in agreement with the simulation results and conclusion reached in [19] where a perturbed Wiener PA model was simulated and further linearized using a Hammerstein predistorter.



(A) Full spectrum comparison



(B) Zoom-in spectrum comparison

Fig. 3-9 Spectrum comparison of the transmitter with different Hammerstein predistorters. (a) Without predistorter. (b) With memoryless predistorter. (c) Hammerstein predistorter with a 10-tap FIR filter. (d) Hammerstein predistorter with a 64-tap FIR filter. (e) Hammerstein predistorter with a 128-tap FIR filter.

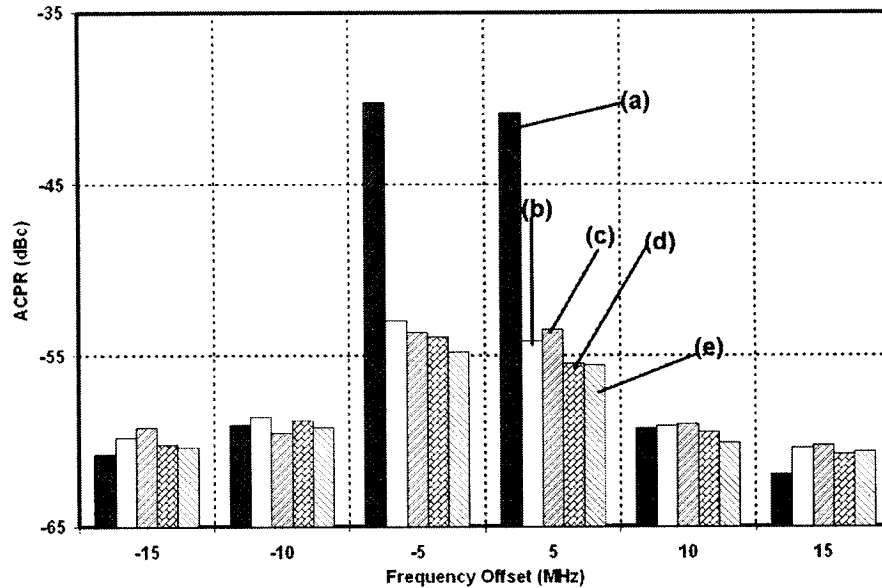


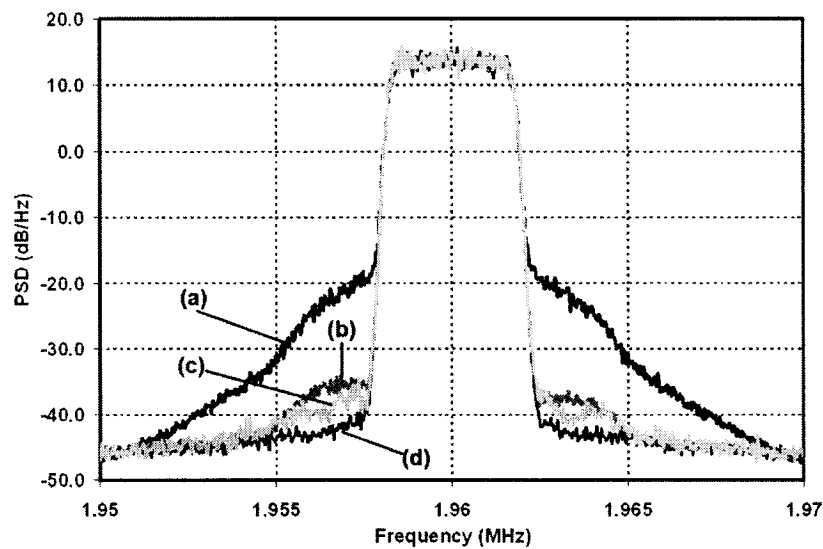
Fig. 3-10 ACPR comparison of the transmitter with different Hammerstein predistorter. (a) Without predistorter. (b) With memoryless predistorter. (c) Hammerstein predistorter with a 10-tap FIR filter. (d) Hammerstein predistorter with a 64-tap FIR filter. (e) Hammerstein predistorter with a 128-tap FIR filter.

3.5.2 Augmented Hammerstein Predistorter

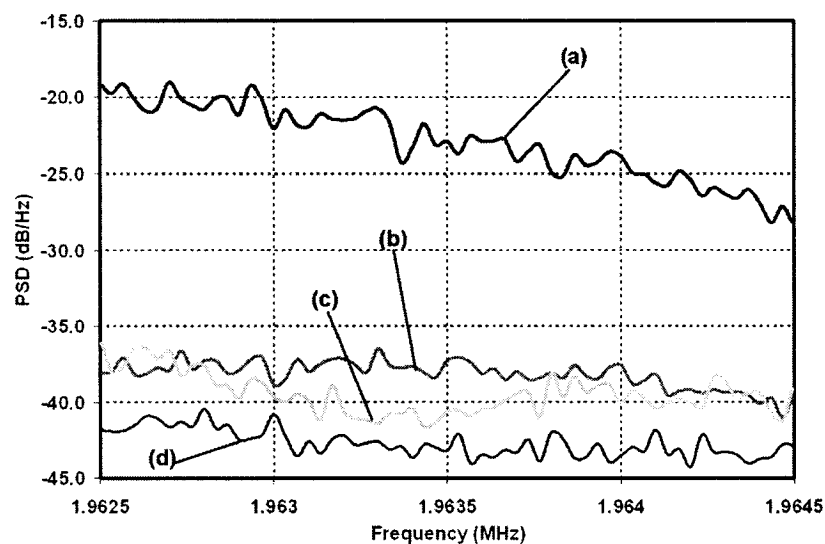
The parameter identification of the augmented Hammerstein predistorter is firstly carried out in terms of the procedure explained in section III. A 1024-entries LUT is constructed and two FIR filters with ten or twenty taps are identified. To illustrate the superior accuracy of this new predistorter scheme, the spectrum and ACPR results obtained while cascading the transmitter with a 128-tap Hammerstein predistorter or a memoryless predistorter are used as references in the validation process. In addition, the spectrum and ACPR of the transmitter without predistorter are also added in the result

comparison to illustrate the performance improvements under the conditions of with and without predistortion. To verify the robustness of the proposed new Hammerstein predistorter, one-carrier and three-carrier 3GPP-FDD signals are chosen as the test signals.

Both the spectrum comparison results shown in Fig. 3-11 and Fig. 3-13, and the ACPR comparison results shown in Fig. 3-12 and Fig. 3-14 for one-carrier and three-carrier 3GPP-FDD signals indicate that the novel augmented Hammerstein predistorter can suppress the memory effects of the transmitter much better than the conventional Hammerstein predistorter. Although the memory effects are not strong for one-carrier 3GPP-FDD signal as shown in Fig. 3-11, the augmented Hammerstein predistorter still provides obvious improvement for suppressing the spectrum regrowth caused by the memory effects. When the transmitter is applied with the three-carrier 3GPP-FDD signal, the transmitter exhibits strong memory effects as illustrated in the curve (b) in Fig. 3-13. The curve (c) in Fig. 3-13 reveals that the traditional Hammerstein predistorter cannot efficiently stifle the spectrum regrowth attributed to the memory effects. Nevertheless, the curve (d) in Fig. 3-13 clearly demonstrates that the new augmented Hammerstein predistorter can successfully compensate for the memory effects.



(A) Full spectrum comparison



(B) Zoom-in spectrum comparison

Fig. 3-11 Spectrum comparison of different predistorters for one-carrier WCDMA signal. (a) Without predistorter. (b) Memoryless predistorter. (c) Hammerstein predistorter with a 128-tap FIR filter. (d) Augmented Hammerstein predistorter with two twenty-tap FIR filter.

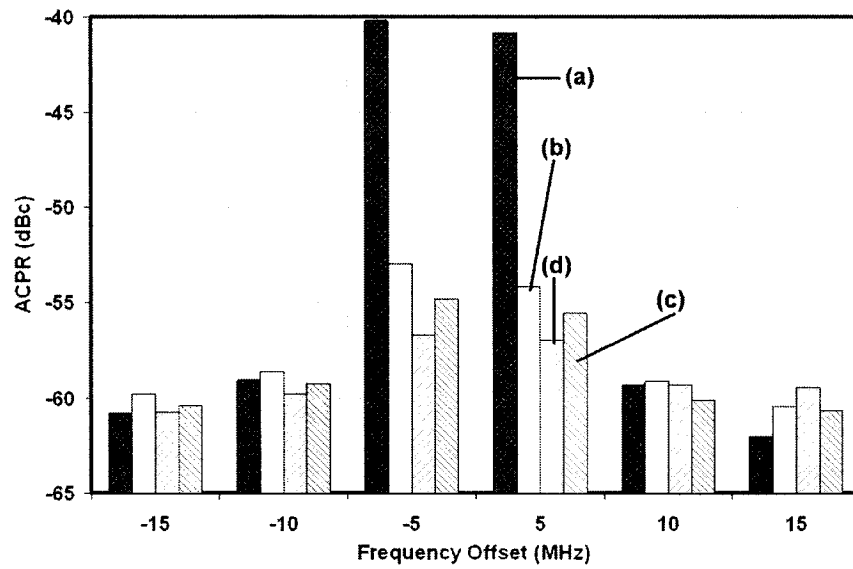
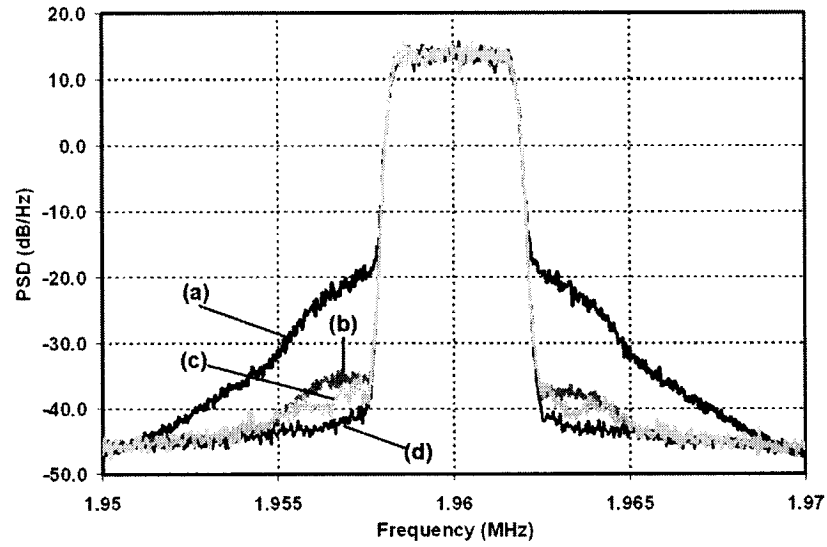
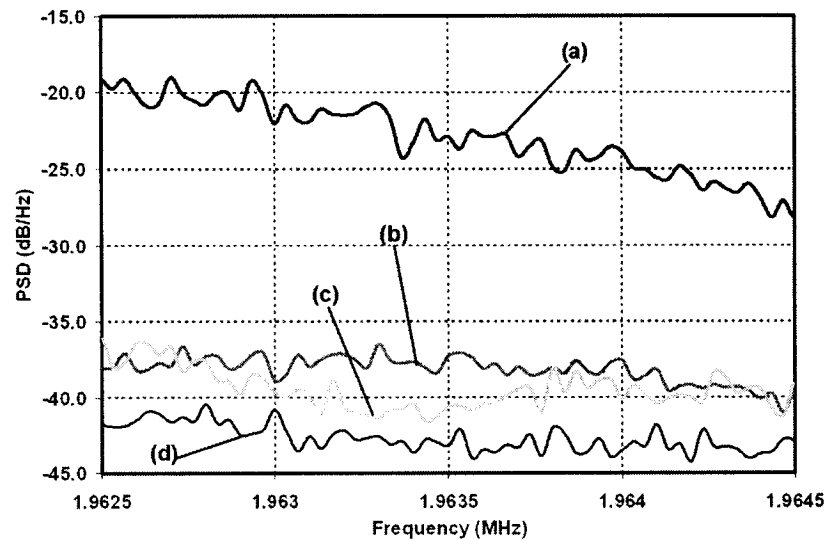


Fig. 3-12 ACPR comparison of different predistorters for one-carrier WCDMA signal. (a) Without predistorter. (b) Memoryless predistorter. (c) Hammerstein predistorter with a 128-tap FIR filter. (d) Augmented Hammerstein predistorter with two twenty-tap FIR filter.



(A) Full spectrum comparison



(B) Zoom-in spectrum comparison

Fig. 3-13 Spectrum comparison of different predistorters for one-carrier WCDMA signal. (a) Without predistorter. (b) Memoryless predistorter. (c) Hammerstein predistorter with a 128-tap FIR filter. (d) Augmented Hammerstein predistorter with two twenty-tap FIR filter.

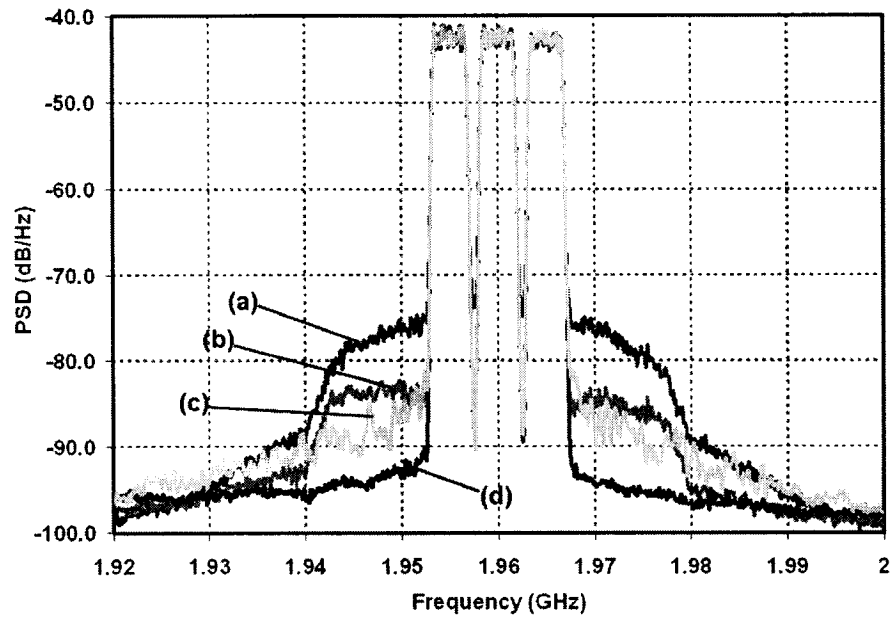
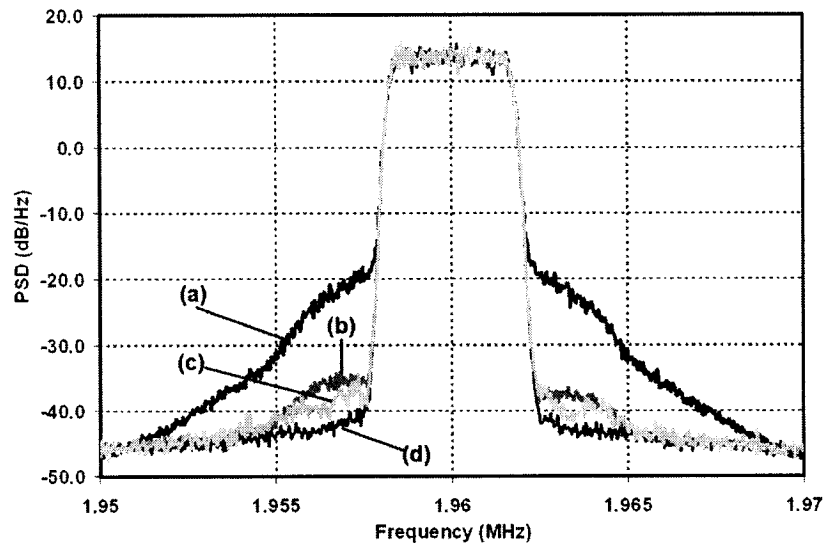
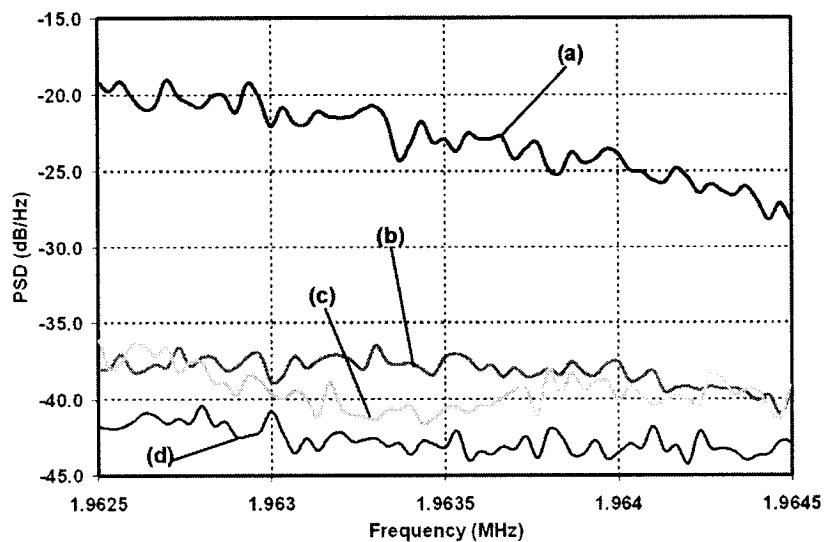


Fig. 3-14 Spectrum comparison of different predistorters for three-carrier WCDMA signal. (a) Without predistorter. (b) Memoryless predistorter. (c) Hammerstein predistorter with a 128-tap FIR filter. (d) Augmented Hammerstein predistorter with two ten-tap FIR filter.



(A) Full spectrum comparison



(B) Zoom-in spectrum comparison

Fig. 3-15 Spectrum comparison of different predistorters for one-carrier WCDMA signal. (a) Without predistorter. (b) Memoryless predistorter. (c) Hammerstein predistorter with a 128-tap FIR filter. (d) Augmented Hammerstein predistorter with two twenty-tap FIR filter.

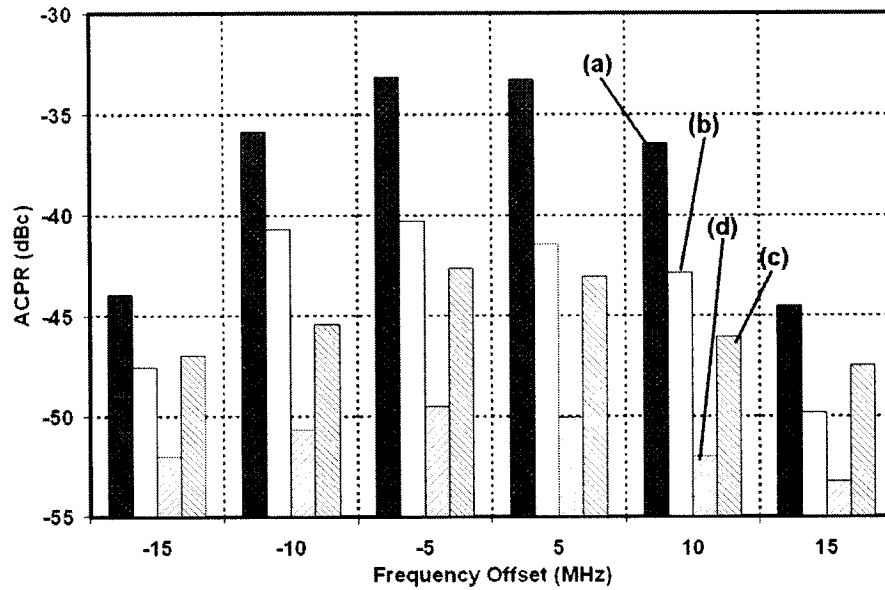


Fig. 3-16 ACPR comparison of different predistorters for three-carrier WCDMA signal. (a) Without predistorter. (b) Memoryless predistorter. (c) Hammerstein predistorter with a 128-tap FIR filter. (d) Augmented Hammerstein predistorter with two ten-tap FIR filter.

3.6 CONCLUSION

In this chapter, a LUT-based Hammerstein predistorter is employed to suppress the spectrum regrowth caused by the nonlinearity and the memory effects in a wideband wireless transmitter. The identification procedure of this predistorter is discussed in details. Consider the limitation of the traditional Hammerstein predistorter in pre-compensating for entire memory effects, an augmented LUT-based Hammerstein predistorter is proposed. In this augmented Hammerstein predistorter, a weak nonlinear FIR-based dynamic filter is utilized to compensate for the memory effects of the

transmitter instead of a linear FIR filter as in the conventional Hammerstein predistorter. To the best of the authors' knowledge, this is the first time such a dynamic nonlinear predistorter is proposed and implemented to compensate for the dynamic nonlinearity existing in a broadband wireless transmitter. Finally, the LUT-based Hammerstein predistorter and the new augmented LUT-based Hammerstein predistorter are tested using a 60-Watt PEP GaAs FET push-pull amplifier based transmitter prototype driven by a one-carrier and a three-carrier 3GPP-FDD signals. Both the linearized output spectrum and the ACPR comparison results demonstrate that the proposed augmented LUT-based Hammerstein predistorter outperforms the conventional LUT-based Hammerstein predistorter in suppressing the spectrum regrowth caused by the memory effects of the broadband wireless transmitter.

REFERENCES

- [1] M. R. Moazzam and C. S. Aitchison, "A low third order intermodulation amplifier with harmonic feedback circuitry," *IEEE MTT-S Int. Microwave Symp. Dig.*, vol. 2, pp. 827-830, June 1996.
- [2] E. Eid, F. M. Ghannouchi, and F. Beaugard, "Optimal feedforward linearization system design," *Microwave Journal*, pp. 78-86, Nov. 1995.
- [3] N. Imai, T. Nojima, and T. Murase, "Novel linearizer using balanced circulators and its application to multilevel digital radio systems," *IEEE Trans. Microwave Theory Tech.*, vol. 37, pp. 1237-1243, Aug. 1989.
- [4] E. G. Jeckeln, F. M. Ghannouchi, and M. A. Sawan, "An L band adaptive digital predistorter for power amplifiers using direct I-Q modem," in *Proc. IEEE MTT-S Int. Microwave Symp. Dig.*, vol. 2, pp. 719-722, June 1998.
- [5] S. Boumaiza, J. Li, and F.M. Ghannouchi, "Adaptive digital/RF predistortion using a nonuniform LUT indexing function with built-in dependence on the amplifier nonlinearity," *IEEE Trans. Microwave Theory Tech.*, vol. 52, pp. 2670-2677, Dec. 2004.
- [6] J. K. Cavers, "Optimum indexing in predistorting amplifier linearizers," in *Proc. IEEE 47th Vehicular Tech. Conf.*, vol. 2, pp. 676-680, May 1997.
- [7] Q. Ren and I. Wolff, "Improvement of digital mapping predistorters for linearising transmitters," in *Proc. IEEE MTT-S Int. Microwave Symp. Dig.*, vol. 3, pp. 1691-1694, June 1997.
- [8] K. J. Muhonen, M. Kavehrad, and R. Krishnamoorthy, "Look-up table techniques for adaptive digital predistortion: a development and comparison," *IEEE Trans. Vehicular Tech.*, vol. 49, pp. 1995-2002, Sept. 2000.
- [9] J. S. Kenney, W. Woo, L. Ding, R. Raich, H. Ku, and G. T. Zhou, "The impact of memory effects on predistortion linearization of RF power amplifiers," in *Proc. 8th Intl. Symposium on Microwave and Optic Technology*, pp. 189-193, June 2001.
- [10] J. H. K. Vuolevi, T. Rahkonen, and J. P. A. Manninen, "Measurement technique for characterizing memory effects in RF power amplifiers", *IEEE Trans. Microwave Theory Tech.*, vol. 49, pp. 1383-1389, Dec. 2001.

- [11] H. Ku and J. S. Kenney, "Behavioral modeling of nonlinear RF power amplifiers considering memory effects", *IEEE Trans. Microwave Theory Tech.*, vol. 51, pp. 2495-2504, Dec. 2003.
- [12] S. Boumaiza and F. M. Ghannouchi, "Thermal memory effects modeling and compensation in RF power amplifiers and predistortion linearizers", *IEEE Trans. Microwave Theory Tech.*, vol. 51, pp. 2427-2433, Dec. 2003.
- [13] J. Kim and K. Konstantinou, "Digital predistortion of wideband signals based on power amplifier model with memory," *Electronics Letters*, vol. 37, pp.1417-1418, Nov. 2001.
- [14] L. Ding, G. T. Zhou, D. R. Morgan, Z. Ma, J. S. Kenney, J. Kim, and C. R. Giardina, "A robust digital baseband predistorter constructed using memory polynomials," *IEEE Trans. Comm.*, vol. 52, pp. 159-165, Jan. 2004.
- [15] A. Ahmed, S. M. Endalkachew, and G. Kompa, "Power amplifier linearization using memory polynomial predistorter with non-uniform delay taps," in *Proc. IEEE MTT-S Int. Microwave Symp. Dig.*, vol.3, pp. 1871-1874, June 2004.
- [16] A. B. J. Kokkeler, "A crosscorrelation predistorter using memory polynomials," in *Proc. Int. Symp. on Circuits and Systems*, vol. 3, pp. 23-26, May 2004.
- [17] R. Raich, H. Qian, and G. T. Zhou, "Orthogonal polynomials for power amplifier modeling and predistorter design," *IEEE Trans. Vehicular Tech.*, vol. 53, pp. 1468-1479, Sept. 2004.
- [18] H. W. Kang, Y. S. Cho, and D. H. Youn, "On compensating nonlinear distortions of an OFDM system using an efficient adaptive predistorter," *IEEE Trans. Comm.*, vol. 47, pp. 522-526, April 1999.
- [19] L. Ding, R. Raich, and G. T. Zhou, "A Hammerstein predistortion linearization design based on the indirect learning architecture," in *Proc. IEEE Intl. Conf. on Acoustics, Speech, and Signal Processing*, vol. 3, pp. 2689-2692, May 2002.
- [20] T. Wang and J. Ilow, "Compensation of nonlinear distortions with memory effects in OFDM transmitters," in *Proc. IEEE Global Telecomm. Conf.*, vol. 4, pp. 2398-2403, Nov. 2004.
- [21] T. Liu, S. Boumaiza, M. Helaoui, H. Ben Nasr and F. M. Ghannouchi, "Behavior modeling procedure of wideband RF transmitters exhibiting memory effects," in *Proc. IEEE MTT-S Int. Microwave Symposium Digest*, June 2005. (accepted)

- [22] E. W. Bai, "An optimal two stage identification algorithm for Hammerstein-Wiener nonlinear systems", *Proc. American Contr. Conf.*, vol. 5, pp. 2756-2760, June 1998.
- [23] L. Ding and G. T. Zhou, "Effects of even-order nonlinear terms on power amplifier modeling and predistortion linearization", *IEEE Trans. Vehicular Tech.*, vol.53, pp. 156-162, Jan. 2004.
- [24] 3GPP specifications: TS 25.104 v4.2.0, TS 25.141 v4.2.0, 2002.
- [25] S. Haykin, *Adaptive filter theory*, 3rd Edition, Prentice Hall, 1996.

CHAPTER 4

DYNAMIC BEHAVIORAL MODELING OF 3G POWER AMPLIFIERS USING REAL-VALUED TIME DELAY NEURAL NETWORKS

In this chapter, we propose a novel Real-Valued Time Delay Neural Network (RVTDNN) suitable for dynamic modeling of the baseband non-linear behaviors of 3G base station Power Amplifiers (PA). Parameters (weights and biases) of the proposed model are identified using the back-propagation algorithm, which is applied to the input and output waveforms of the power amplifier recorded under real operation conditions. Time and frequency domain simulation of a 90-Watt LDMOS PA output using this novel neural network model exhibit a good agreement between the RVTDNN behavioral model's predicted results and measured ones along with a good generality. Moreover, dynamic AM/AM and AM/PM characteristics obtained using the proposed model demonstrated that the RVTDNN can track and account for the memory effects of the PAs well. These characteristics also point out that the small signal response of the LDMOS PA is more affected by the memory effects than the PA's large signal response when it is driven by 3G signals. This RVTDNN model acquires a significantly reduced complexity and shorter processing time in the analysis and training procedures, when driven with complex modulated and highly varying envelope signals such as 3G signals, than previously published neural network based PA models.

4.1. INTRODUCTION

System-level behavioral modeling consists of constructing a black-box analytic function that admits alike responses to those obtained at the output of a real device or a sub-system driven by the same input signal. Such models are of great help for designers of communication systems, in particular, transmitters and Power Amplifiers (PAs), since they provide them with greatly reduced complexity and time-consuming design and optimization procedures. However, these advantages could be achieved providing the capacity of the model to predict the PA output under realistic conditions.

In the literature [1] the non-linear behavioral models were classified as three categories: memoryless, quasi-memoryless behavioral models and those with memory. Polynomial and Saleh [2] functions for a long while have been involved for respectively solid state and traveling wave PAs modeling that admit AM/AM and AM/PM conversion characteristics and belong to the first two categories. However, the continuously growing modulation bandwidth of the new communication multi-carrier signals has triggered new challenging issues in the design of PAs due, namely, to memory effects. These effects are commonly defined as the frequency dependency of inter-modulation distortion levels at the output of PAs on the modulation frequency bandwidth [3]. In time domain, memory effects cause the outputs of the small signals of the power amplifier deviate from the linear output when the signal changes. This results in the deterioration of the whole system signal to noise ratio since the linearity of the PA at small signals is compromised.

Modeling of PAs with memory is the research focus of many authors in last few years that yields to various model topologies. As an example, authors in [4] employed Volterra

series for modeling non-linear PAs with memory effects. However, the use of such series based models is restricted to weak non-linear devices. Solid State power amplifiers (SSPAs) used in the 3G base station transceivers require high order Volterra kernels. In spite of the fact that truncated Volterra series were pursued as a good means of getting rid of the computational complexity [5] of high order Volterra kernels, this model still suffers from the difficulty of its real-time implementation. Authors in [6] reported a cascade of linear ARMA filter and a conventional polynomial memoryless function in order to take into account the frequency dependent distortion at the output of the PA.

Traditionally, the extraction of the behavioral model parameters of power amplifiers was performed with fitting the measured static AM/AM and AM/PM characteristics obtained using power sweep continuous wave at the operation center frequency [2]. In order to handle the frequency response of the amplifier, authors in [7] proposed to extract the behavioral model parameters by fitting static AM/AM and AM/PM characteristics at several carrier frequencies that fall within the signal bandwidth. This method was pursued as a solution to the modeling of PA driven with wideband signals. However, this latter approach still suffers from the lack of accuracy since the static PA characterization technique was performed at each carrier frequency. Thus, researchers in [8]–[10] have chosen to extract model parameters while fitting concurrently measured amplitude and phase of the spectrum components at the PA output such as: fundamentals, third order inter-modulation (IMD3) and fifth order inter-modulation (IMD5) obtained under two-tone excitation signal with varying power and frequency-spacing.

In the last decade, artificial neural network (ANN) technology has been successfully

applied to RF and microwave applications [11] since they can approximate any continuous function arbitrarily well [12]. By profiting from their potential to learn the circuit behavior based on simulated or measured records of its input and output signals, they were used in non-linear transient modeling and digital high-speed interconnects for computer-aided design (CAD) of VLSI modules [13]. They were employed also for the modeling, simulation and design of microwave circuits [14]–[16]. Hence, the ANN based models are seen as a potential alternative to model RF PAs having medium to strong memory effects along with high order non-linearity. This chapter represents an attempt to extend further the use of neural network technology to the dynamic modeling of RF PAs of wireless communication transmitters operating under wideband modulation and highly varying envelope signals such as CDMA 2000, W-CDMA, TD-SCDMA, and WLAN802.11x.

4.2. RVTDNN BEHAVIOR MODEL OF POWER AMPLIFIERS

Many topologies of ANNs were reported in the literature for the modeling of different types of circuits and systems that exhibit different kinds of linear and nonlinear behaviors. In conventional artificial neural network model development procedures, complex input-output measured signals are initially converted to either polar representation (magnitude and phase) or rectangular one (in-phase I and quadrature Q components). Then, two separate and uncoupled real-valued neural networks are used to model the output amplitude and phase (or the output I and Q components) variations as a function of the input power amplitude (or the input I and Q components), as shown in

Fig. 4-1 [17]. The real coefficients of the two networks are identified during a training procedure using the measured amplitude and phase (or I and Q components) of the input and output. This topology suffers from the convergence problems of the training procedure since the two networks are trained separately. Furthermore, authors in [18], [19] proposed applying a complex value based neural network to the complex signal directly, as shown in Fig. 4-2. In such case, both the weights and the activation functions of the network are complex. This type of ANN necessitates a cumbersome complex training algorithm such as the complex back-propagation training algorithm [20]. Thus, the two neural networks topologies described above lead to a lengthy training time and elevated computation resources.

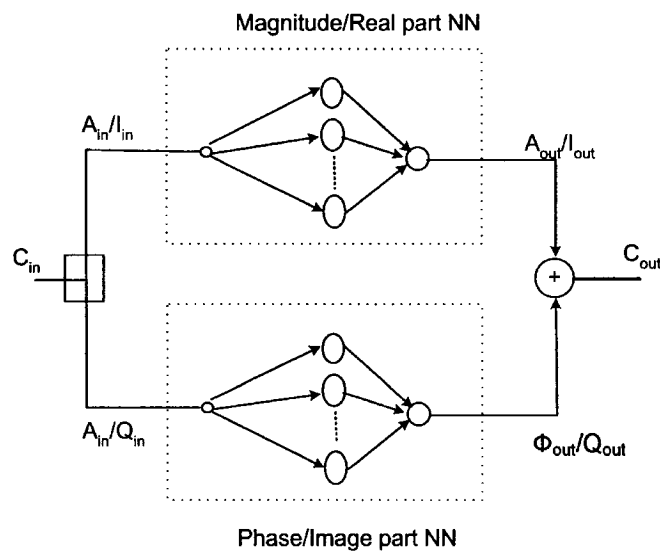


Fig. 4-1 Complex signal processing models of the conventional real-valued neural network.

As a specific ANN, Time Delay Neural Network (TDNN) has been used to learn and represent dynamic systems. It was successfully utilized in the signal processing, speech recognition, system identification and control to solve the temporal processing problems[12], [21]. However, in the case of complex input signals the TDNN was implemented according to Fig. 4-1 or Fig. 4-2 topologies. Therefore, it suffers from the limitations mentioned earlier. In this chapter, we propose a novel Real-Valued Time Delay Neural Network (RVTDNN) to construct a dynamic behavioral model suitable for 3G PAs in real operation conditions. Contrary to previous presented methods, this approach uses only one real valued neural network instead of two separate networks. The newly proposed RVTDNN, which is made up of two-layers, uses real-valued parameters (weights and biases) along with the real components of the input and output signals. As shown in Fig. 4-3, the RVTDNN model utilizes the two components of the input signal (I_{in}, Q_{in}) in order to predict the correspondent two components (I_{out}, Q_{out}) of the output signal. The proposed RVTDNN is based on the FeedForward Neural Network (FFNN) [22], with the addition of two Tapped Delay Lines (TDLs) in its two baseband inputs. TDLs are used so as to consider the history of the input signal, which is needed for memory effects modeling. Thus, the FFNN entries include not only the current value of the input signal but also its previous ones. The memory depth of the Device-Under-Test (DUT) will be reflected on the length of the TDL taps. Consequently, the TDL structure, included in the RVTDNN, leads to the modeling of the short-term memory effects exhibited by the power amplifier. However, the long-term memory is built into the RVTDNN through a

supervised learning. This kind of long-term memory can be used to simulate the slow dynamic changes of non-linear characteristics of the PA over time.

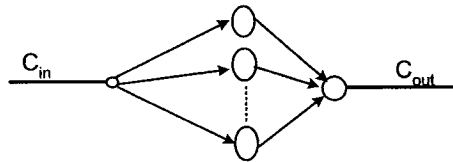


Fig. 4-2 Complex signal processing models of the complex-valued neural network.

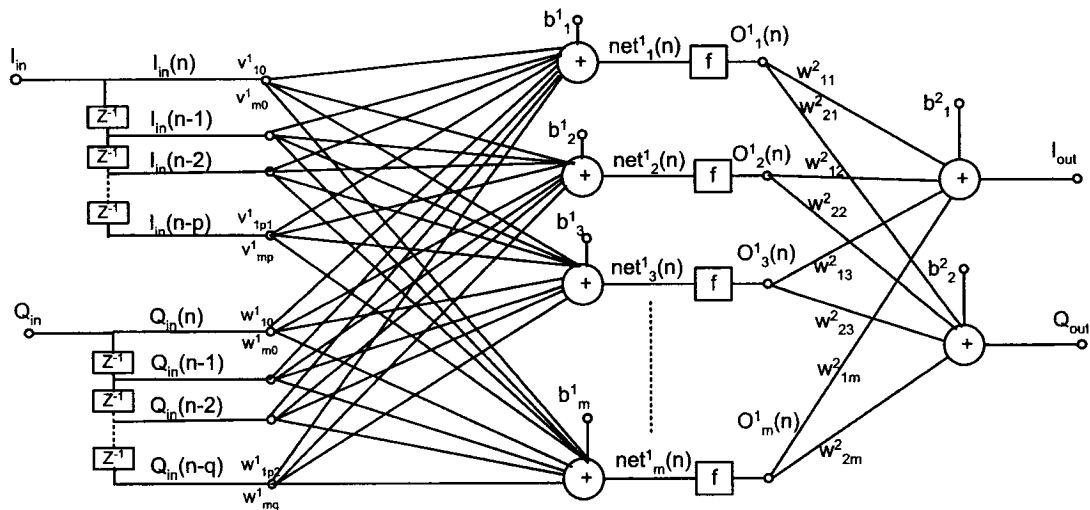


Fig. 4-3 Block diagram of new two-layers RVT-DNN PA behavioral model.

Considering the memory effects of the PA, the baseband output I_{out} and Q_{out}

components of the PA at instant n are a function of P past value of the baseband input I_{in} and q past values of the baseband input Q_{in} according to (1) and (2).

$$I_{out}(n) = f_I [I_{in}(n), I_{in}(n-1), \dots, I_{in}(n-p), Q_{in}(n), Q_{in}(n-1), \dots, Q_{in}(n-q)] \quad (1)$$

$$Q_{out}(n) = f_Q [I_{in}(n), I_{in}(n-1), \dots, I_{in}(n-p), Q_{in}(n), Q_{in}(n-1), \dots, Q_{in}(n-q)] \quad (2)$$

Based on the RVTDNN shown in Fig. 4-3, (1) and (2) can be rewritten as follow:

$$I_{out}(n) = \sum_{k=1}^m w_{1k}^2 O_k^1(n) + b_1^2 \quad (3)$$

$$Q_{out}(n) = \sum_{k=1}^m w_{2k}^2 O_k^1(n) + b_2^2 \quad (4)$$

Where

$$O_k^1(n) = f(net_k^1(n)) \quad (5)$$

$$net_k^1(n) = \sum_{i=0}^p v_{ki}^1 I_{in}(n-i) + \sum_{i=0}^q w_{ki}^1 Q_{in}(n-i) + b_k^1 \quad (6)$$

$k = 1, 2, \dots, m$, and $f(x) = \tanh(x) = \frac{(1 - e^{-2x})}{(1 + e^{-2x})}$ is the activation function.

When $p = q = 0$, i.e., the length of TDL is zero. Then the RVTDDNN regresses to a Real-Valued FeedForward Neural Network (RVFFNN) and hence it will be limited to a memoryless or quasi-memoryless model.

4.3. EXTRACTION OF RVTDDNN BEHAVIORAL MODEL PARAMETERS

Parameter extraction of the RVTDDNN model commonly denoted as learning procedure is performed with fitting the measured input and output i and o components. Furthermore, as one observes in Fig. 4-3 the RVTDDNN model can be converted to a common Feed-Forward Neural Network (FFNN) or Multi-Layer Perceptron (MLP) with $p+q+2$ inputs and two outputs. Thus, the dynamic problem becomes a static problem and the standard back-propagation training algorithm [12] can be employed to train it. The algorithm adjusts the network parameters so as to minimize the cost function E , over an epoch, defined below:

$$E = \sum_{n=1}^N E_n = \frac{1}{2N} \sum_{n=1}^N \left[\left(I_{out}(n) - \hat{I}_{out}(n) \right)^2 + \left(Q_{out}(n) - \hat{Q}_{out}(n) \right)^2 \right] \quad (7)$$

where E_n is the instantaneous error. $I_{out}(n)$ and $Q_{out}(n)$ represent the outputs of RVTDDNN at instant n , $\hat{I}_{out}(n)$ and $\hat{Q}_{out}(n)$ are the desired outputs at instant n . N denotes the length of the training sequence.

In this work, the training procedure of the real-valued neural network is performed based on a realistic dynamic characterization of an amplifier under test fed with a modulated input signal instead of one-tone or two-tone signals. Thus, the characterization of the PA is made without any induction of self-heating effects due to signal excitation as the case of continuous wave based measurement techniques. Moreover, the behavioral model will yield to enhanced prediction accuracy since its parameters are identified using characterization data captured when the DUT is fed with a modulated input signal that implies a real operation condition. Experiments conducted for the training and validation of the neural network used a real time two-channel time domain sampling system. I_{in} and Q_{in} components of the equivalent complex baseband input signal of the PA are used as two independent inputs of the RVDNN. The RVDNN also has two outputs corresponding to I_{out} and Q_{out} components of the equivalent complex baseband output signal respectively. In such a way, measured i and q components of the complex baseband input and output signals are directly exploited to train the RVDNN.

The initialization of the network is an important issue for training the RVDNN with the back-propagation algorithm. The initial weights were chosen randomly from a suitable range, such as (-0.8, 0.8). They were uniformly distributed inside this range and symmetric around zero. After the RVDNN training procedure converges, the RVDNN model parameters are found. Since the model is derived directly from the time domain sampled data emerging for the PA driven by the real signal, it is possible to update the model parameters when the performance of the PA changes due to any internal or

external factors or important changes in the nature and/or statistics of the driving signal.

Once the RVTDNN is trained, all of the model parameters are known and it becomes the dynamic behavioral model of the power amplifier. The generality is an important specification to evaluate the performance of the trained neural network model. Good generality requires that the neural network must perform well on new test data set distinct from the one used in the training sequence. Thus, a very small value of the cost function reached by the trained network does not imply that a good model is obtained and it can generalize well to new inputs. Moreover, it has been observed, during this work, that excessive training on the training sequence decreases occasionally the performance on the test data. This phenomenon, called over fitting, could be avoided through a constant evaluation of the network using a set of test data, i.e. making cross-validation, as learning proceeds. If there is a succession of training epoch in which performance improves only for the training data and not for the test data, over fitting is considered to have occurred and the training process should be terminated. Hence, the learning process should be controlled carefully so as to obtain good performance neural network behavioral models of PAs.

4.4. MEASUREMENTS OF BASEBAND DATA OF A 3G PA

The baseband I and Q waveforms at the input and the output of the DUT needed in the different steps of this work were captured using the complex behavior PA instantaneous characterization test bed shown in Fig. 4-4 [23], [24]. For that, the vector signal generator (SMIQ) in combination with the (I/Q) arbitrary waveform generator (AMIQ) was used for

generating test signals. These signals are synthesized using the software WinIQSIM (version 3.6) from Rohde and Schwarz and Advanced Design System from Agilent Technologies. RF signals at the input and output of the DUT are first translated, in the frequency domain, to an intermediate frequency using a double channel down-converter. The IF1 and IF2 outputs of the down-converter feed the two channels of the baseband vector signal analyzer (VSA) 89610B. The dynamic range of this dual-channel receiver is better than 70 dB. A laptop in this test bed is used to run the vector signal analysis software for the acquisition of the two-channel waveform signals. The delay calibration function of the VSA is exploited to compensate for the time delay lag between the receiver's two channels caused by the group delay of the DUT.

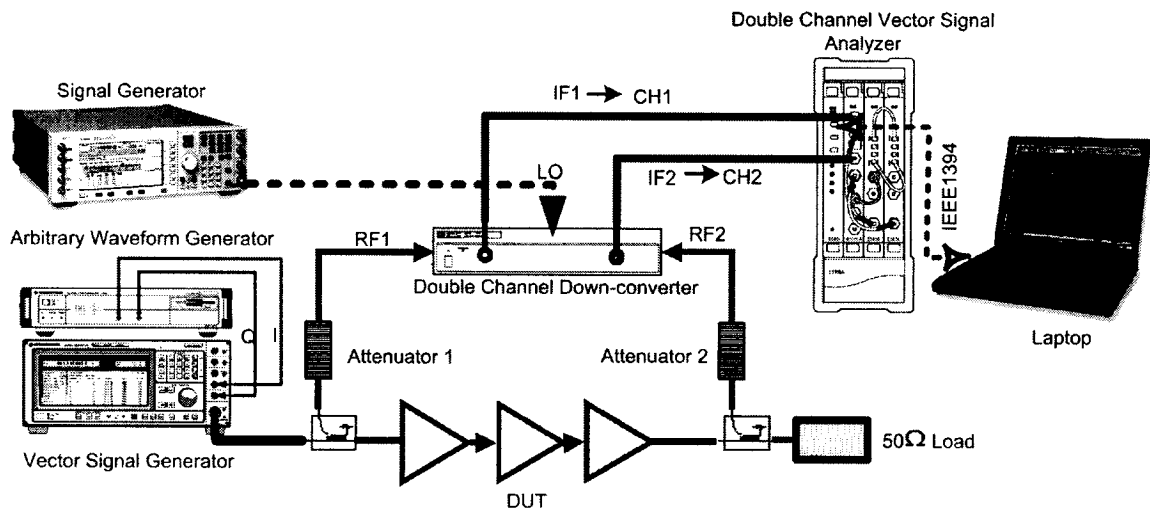


Fig. 4-4 An accurate complex behavioral test-bed block diagram.

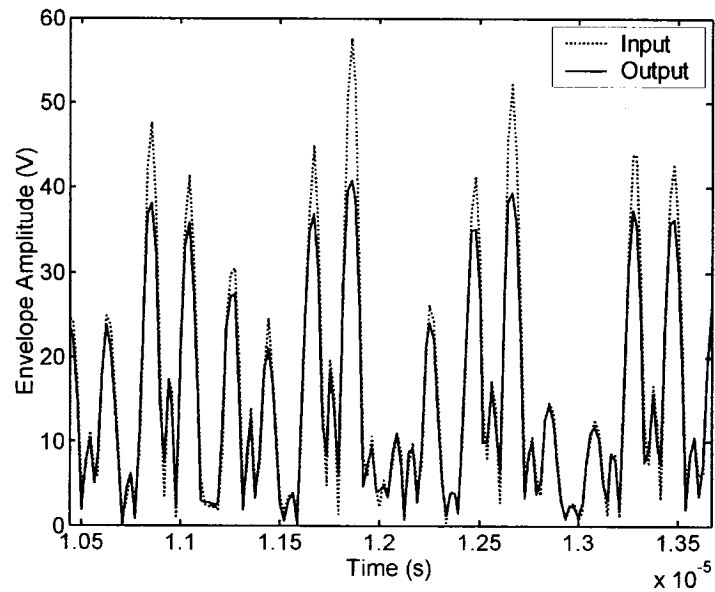
4.5. RVTDNN MODEL: TRAINING AND VALIDATION RESULTS (I)

A 90-Watt peak class AB LDMOS PA [23] was used at first for model validation purposes. It is a three-stage PA suitable for 3G wireless base station transmitter operating at the band of 1930–1990 MHz. The overall small-signal gain of the lineup is 58 dB. The PA peak output power at 1dB gain compression is approximately 49 dBm.

The system described above was used to collect the instantaneous baseband input and output signals for training and validation purposes of the RVTDNN. Three tests signals were used for validation purposes of the RVTDNN model: (i) an IS 95 signal, (ii) a one-carrier CDMA-2000-SR3 signal, and (iii) a three-carrier CDMA-2000-SR3 signal. All these signals have been synthesized with the ADS CDMA2000 library. TABLE 4-1 gives the main characteristics of these signals. The crest factors of the synthesized signals are defined at 0.001% of the Complementary Cumulative Probability Density Function (CCPDF). Fig. 4-5 shows the envelope waveforms of the three-carrier CDMA2000-SR3 signal at the input and the output of the PA, where the input signal was multiplied by the small signal gain of the PA. The gain compression can be easily seen in Fig. 4-5a. The variation of small signal gain due to memory effects can be illustrated as shown in Fig. 4-5b.

TABLE 4-1 TRAINING AND VALIDATION SIGNAL CHARACTERISTICS

| Signal | IS95 | CDMA2000-SR3 | Three-Carrier CDMA2000-SR3 |
|------------------------|------------|--------------|-------------------------------|
| Frequency Bandwidth | 1.2288 MHz | 3.6864 MHz | 13.6864 MHz |
| Crest Factor | 10.73 dB | 9.70 dB | 12.75 dB |



(a)

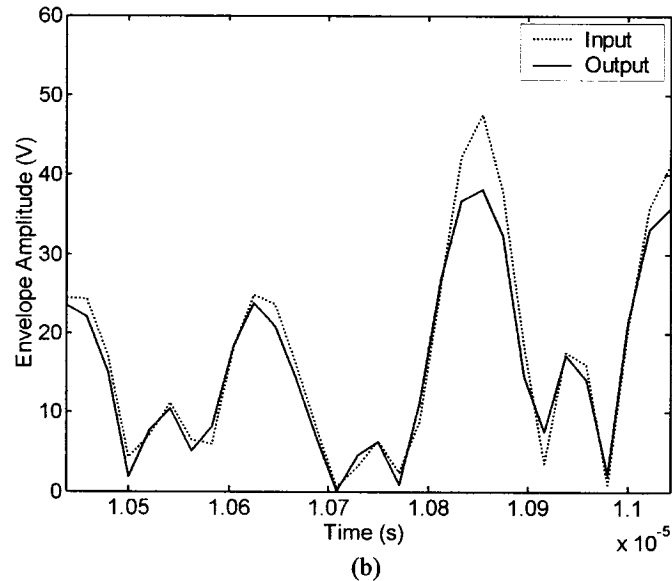


Fig. 4-5 Envelope waveforms of the three-carrier CDMA2000 signal. (a) Normalized input and output signals magnitude vs. time. (b) Zoom-in of the input and output waveforms.

4.5.1. *Training and validation of the RVTDNN Model with three-carrier CDMA2000-SR3 signal*

A two-layer RVTDNN, as shown in Fig. 4-3, was used to illustrate the performance of this behavioral model. It contained two neurons in the input layer and output layer respectively. The number of the neurons in the hide layer and the number of taps in the two input tapped delay lines were determined by an optimization program. A RVTDNN model having fifteen neurons and five taps was found, through optimization procedure, to be appropriate for the LDMOS PA driven by 3G signals.

Ten thousand (10K) sample data from the three-carrier CDMA-2000-SR3

measurements were used to train the RVTDNN. Five thousand (5K) sample data from measurements at another period of time were used to make cross-validation during the training process to ensure the generality of the model. Thirty thousand (30K) sample data from other period of measurements were used to test the behavioral model trained.

Fig. 4-6 shows a typical convergence curve of the RVTDNN training process using a three-carrier CDMA-2000-SR3 signal. The test set of the validation data (30k data), which had never been used during training process, was used to validate the model obtained. Fig. 4-7 and Fig. 4-8 show the time domain validation results of ι and ϱ components of the neural behavioral model for a three-carrier CDMA-2000-SR3 signal. The behavioral model matches the measurement data well even though the validation data have never been used in training. Therefore one can state that the extracted RVTDNN model exhibits good generality for the three-carrier CDMA2000 signal. The Power Spectral Density (PSD) comparison between the results of the RVTDNN behavioral model and the measurement results is shown in Fig. 4-9. It demonstrates that the RVTDNN behavioral model also has good performance in frequency domain.

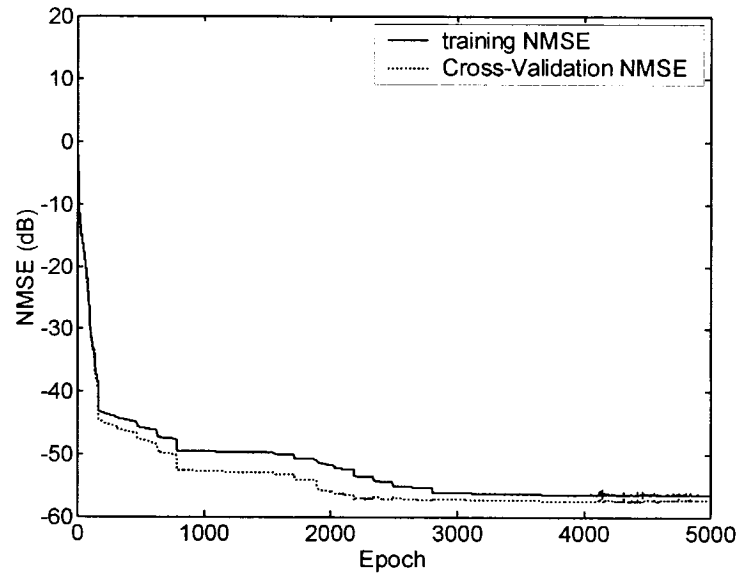


Fig. 4-6 A typical convergence curve of the training process.

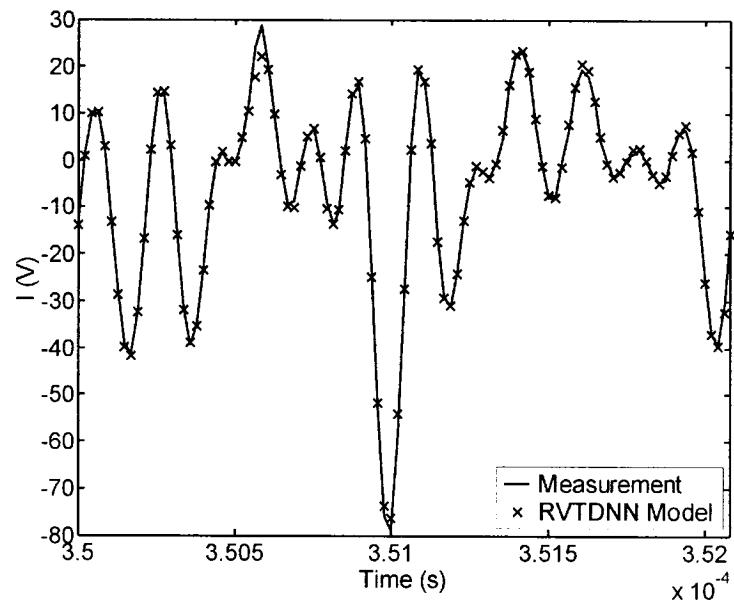


Fig. 4-7 Validation results of I component in time domain.

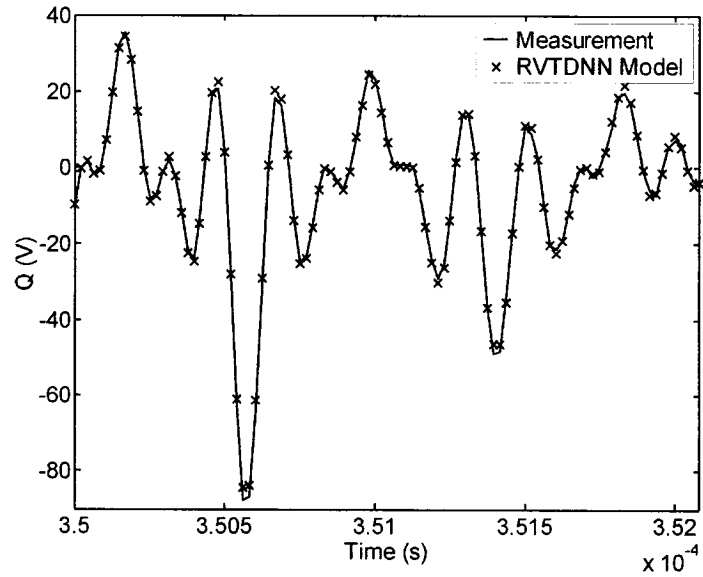


Fig. 4-8 Validation results of Q component in time domain.

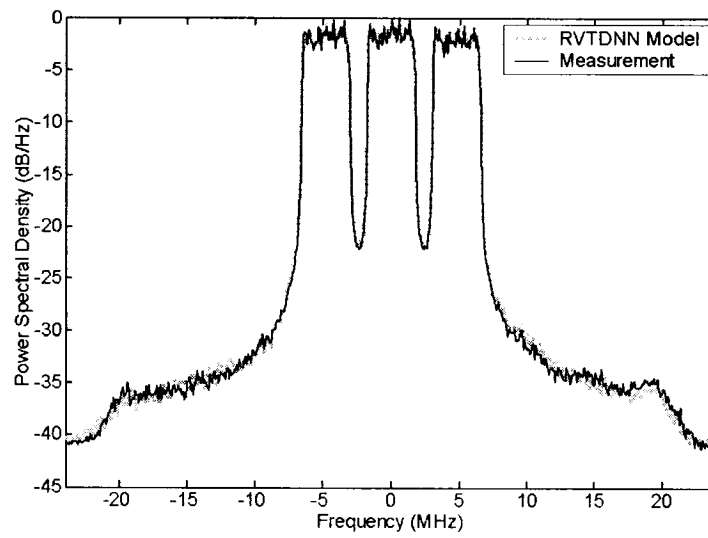


Fig. 4-9 PSD comparison between the RVDNN behavioral model and the measurement data of the three-carrier CDMA2000 signal.

4.5.2. *Dynamic AM/AM and AM/PM Curves for RVDNN and RVFFNN Models*

In order to demonstrate the merit of the proposed RVDNN model, a conventional Real-Valued FeedForward Neural Network (RVFFNN) model is utilized to characterize the equivalent baseband behavior of the power amplifier. The output of a RVFFNN is dependent only on the inputs at the same instantaneous. The RVFFNN has two layers, in which there are fifteen neurons in the hidden layer and two neurons in the input and the output layer. These two models were trained using a three-carrier CDMA-2000-SR3 signal. The training performance for RVFFNN and RVDNN models are listed in TABLE 4-2. MSE, NMSE and R represent the mean square error, the normalized mean square error and the correlation coefficient [25] respectively. Based on this table, both of the correlation coefficient R obtained for the two kinds of neural network models are higher than 0.997 ($\cong 1$). This suggests that outputs of these two models almost covary with the measurement data, which means that they vary nearly by the same amount with the measurement data for both networks. However, one can clearly observe that the proposed RVDNN model offers better accuracy than the RVFFNN one since it allows a lower value of the MSE and NMSE in the prediction of the PA output.

With the time domain validation results of the RVFFNN and RVDNN behavioral models, the comparison between the dynamic AM/AM and AM/PM characterizations of the behavioral models and those of the measurement data can easily be given, as shown in Fig. 4-10 and Fig. 4-11 respectively. Herein, the measured dynamic AM/AM and AM/PM conversion characteristics are no longer smooth curves as those we see generally for a

memoryless/quasi-memoryless PA. These kinds of deviation reveal the time dependent relations of the outputs to the inputs of 3G PAs. It is this time dependent relation that stands for the memory effects of 3G PAs. The outputs of the 3G PAs, corresponding to the inputs with same amplitudes, will vary at different instantaneous. As we anticipated, the RVTDDN behavioral model represents the memory effects (time-dependent effects) of the power amplifier. However, the RVFFNN model cannot express this kind of time-dependent effects of the power amplifier and it is only a statistical mean result because RVFFNN's structure determines RVFFNN will try to learn the average between different outputs when the current inputs are the same.

TABLE 4-2 COMPARISON OF TRAINING PERFORMANCES FOR RVFFNN AND RVTDDN

| Model | RVFFNN | | RVTDDN | |
|---------------|-----------------------|-------------------------|-----------------------|-------------------------|
| Method | Training | Cross-Validation | Training | Cross-Validation |
| MSE | 5.01×10^{-4} | 4.64×10^{-4} | 1.39×10^{-4} | 1.14×10^{-4} |
| NMSE | 1.81×10^{-2} | 1.71×10^{-2} | 5.03×10^{-3} | 3.98×10^{-3} |

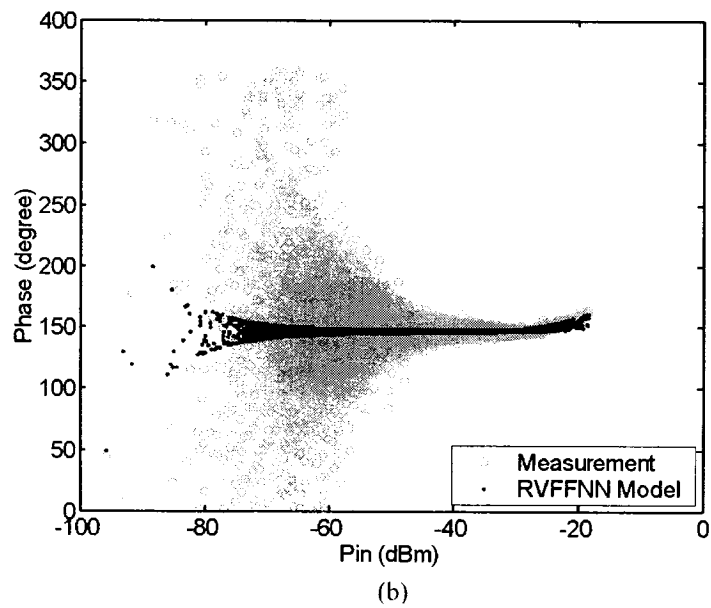
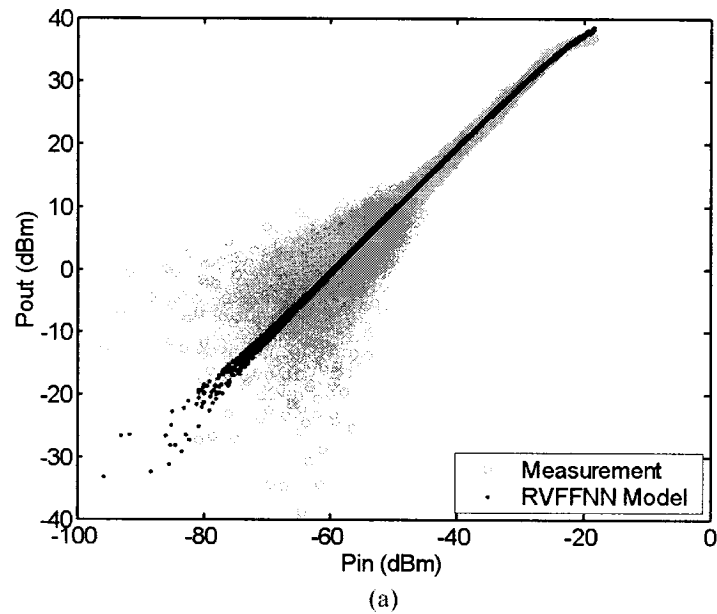


Fig. 4-10 Dynamic AM/AM and AM/PM characteristic comparison between the RVFFNN behavioral model and the measurement data. (a) Dynamic AM/AM characteristics. (b) Dynamic AM/PM characteristics.

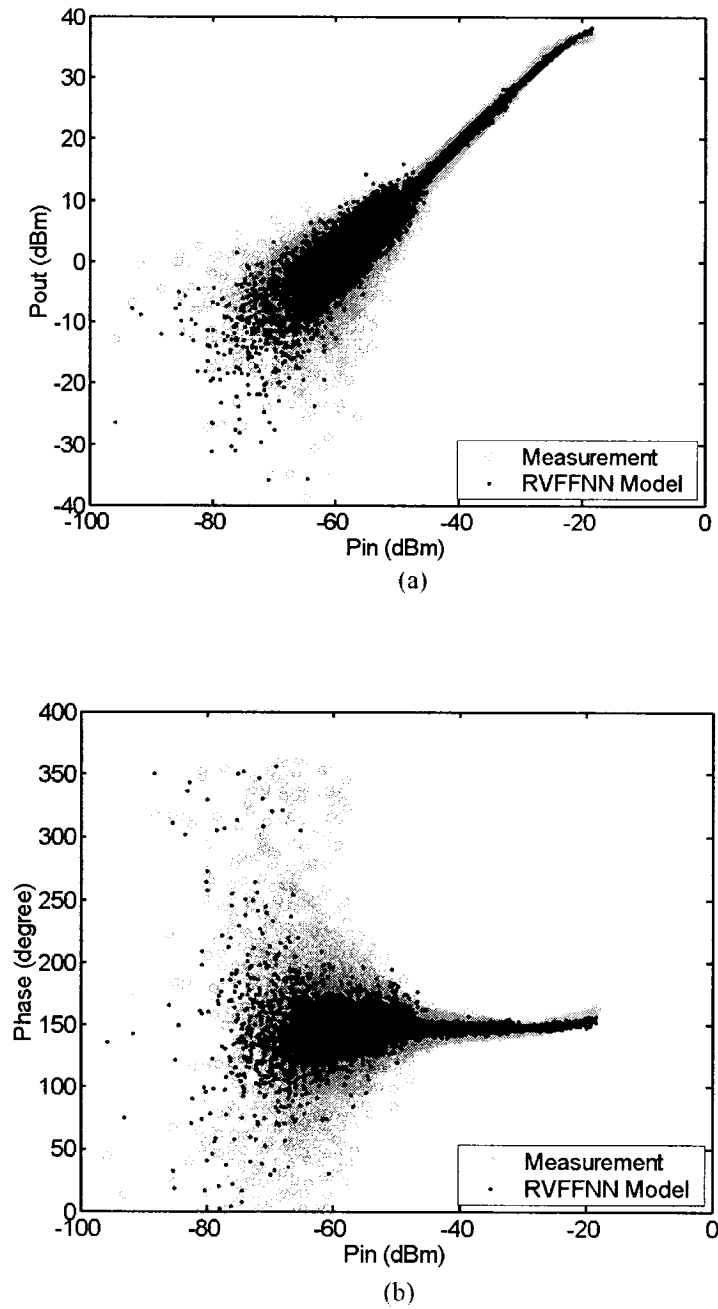


Fig. 4-11 Dynamic AM/AM and AM/PM characteristic comparison between the RVTDNN behavioral model and the measurement data. (a) Dynamic AM/AM characteristics. (b) Dynamic AM/PM characteristics.

The dynamic AM/AM and AM/PM characteristics also suggest that the small signal response of the PA is strongly affected by the memory effects for 3G applications contrary to the PA's large signal response, which is caused by the high peak-to-average ratio of 3G signals. At first view this looks like strange since the traditional narrow band system with constant envelope signals should present linear properties for small signals, i.e., there is no AM/AM and AM/PM conversion for small signals. But for 3G power amplifiers the output of a small signal will be strongly affected by the nearby previous large signals because of the memory effects when the signal. The relative variation (scattering) range of the small signals is larger than that of the large signal. It is easy to see that this kind of relative variation becomes larger and larger with the signal becoming smaller and smaller from the measured AM/AM and AM/PM conversion characteristics. This is in agreement with the results previously published in [6].

4.5.3. Validation with IS95 and CDMA-2000-SR3 signals

With the purpose of proving the effectiveness of the RVTDNN model for other signals, a one-carrier CDMA2000 signal was used to train the same RVTDNN as described above. A different set of data of the one-carrier CDMA2000 signal and a new set of data of the IS95 signal, which was never used before, were applied to the RVTDNN model obtained. Fig. 4-12 and Fig. 4-13 show the Power Spectral Density (PSD) comparison between the results predicted by the RVTDNN model and the measurement results for both signals. Even though IS95 signal was not used to train the RVTDNN, the validation still gave satisfactory results. Hence the RVTDNN model does have good

generality for similar signals having close statistical characteristics and it is back compatible with signals having a smaller bandwidth.

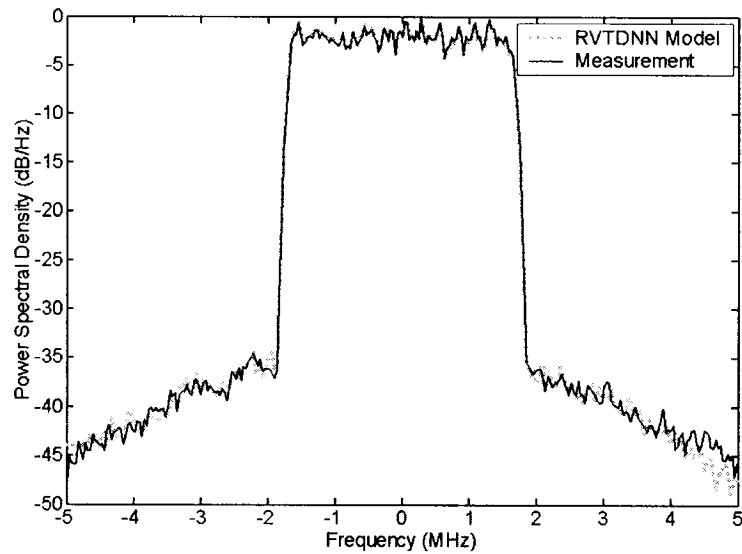


Fig. 4-12 PSD comparison between the RVT DNN behavioral model and the measurement data of the one-carrier CDMA2000 signal.

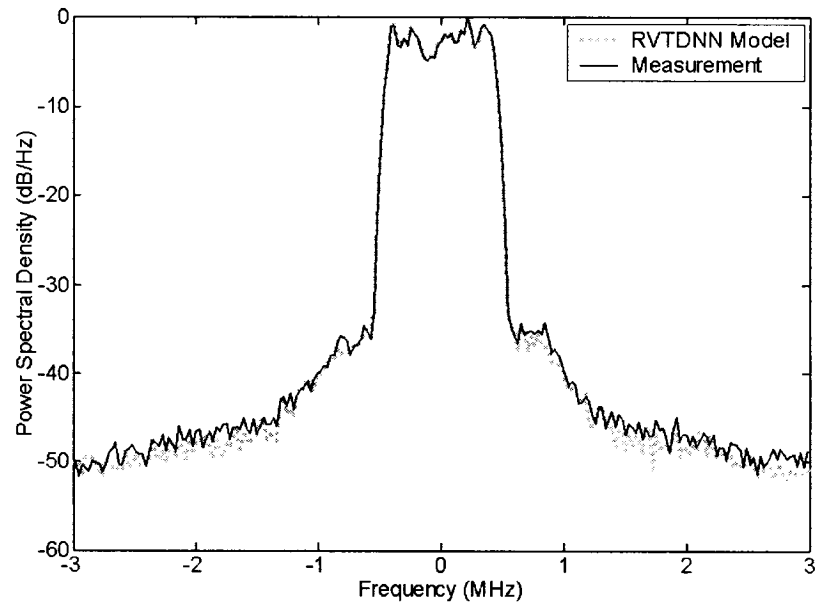


Fig. 4-13 PSD comparison between the RVTDNN behavioral model and the measurement data of IS95 signal.

4.6. RVTDNN MODEL: TRAINING AND VALIDATION RESULTS (II)

The second PA used for experiment in this work is built for 3G wireless base station transmitters operating at the band of 2110–2170 MHz. It has a small signal gain and a saturated power equal to 51 dB and 49 dBm respectively. The whole line-up of the PA includes three stages that use three Laterally Diffused Metal-Oxide-Semiconductor (LDMOS) transistors operating in Class-AB. The test signal has two neighboring 3GPP-FDD carriers (carrier spacing 5MHz). Each carrier is configured according to 3GPP test model 3 with a 32 code channels [26]. The test signal synthesized using the Agilent Advanced Design System (ADS) 3GPP library has a crest factor of 9.4 dB.

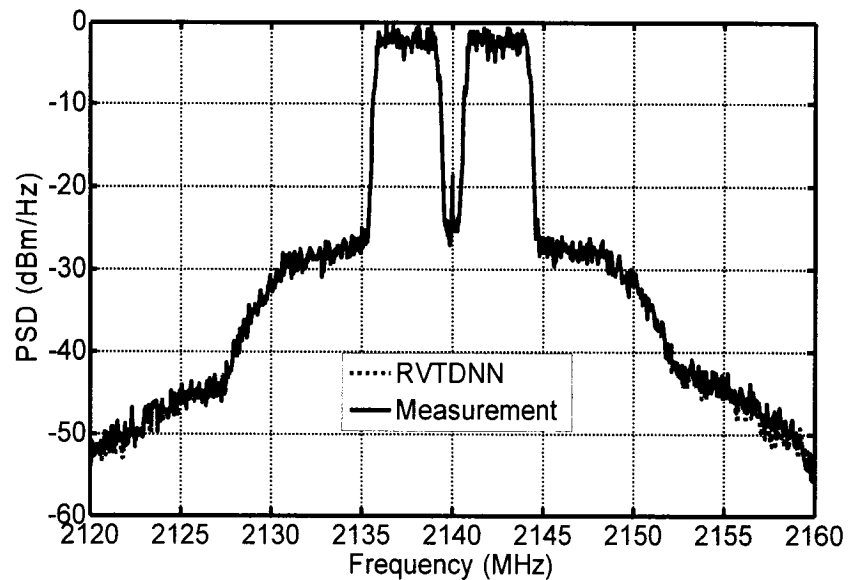
A three-layer RVTDNN is used to illustrate the performance of this behavioral model.

It contains two neurons with a pure linear activation function in the output layer. A RVTDNN model, having six neurons in the two hidden layers and three taps in the two input TDLs, is chosen according to the optimization procedure as mentioned early.

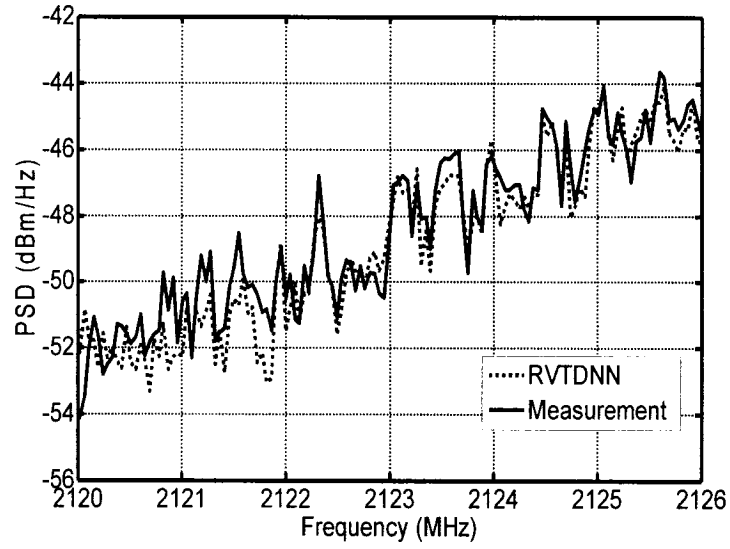
The lengths of both of the training sequence and the validation sequence for training the RVTDNN are 2560. Both of them are extracted at different period of a record of the envelope of the input and output of the DUT driven with a modulated signal. The application of the SCGM algorithm implemented in Matlab (MathWorks Inc.) permits the determination of the model parameters. Finally, the identified RVTDNN model is implemented in ADS and the synthesized two-carrier 3GPP signal is applied to this model to test its accuracy by comparing the output of the RVTDNN model with the output of the PA prototype.

The demonstration of the accuracy of the RVTDNN behavioral model for predicting the output signal of the DUT is carried out through several stages. First, the simulated output spectrum of the trained model is compared to the output spectrum of the power amplifier. Based on Fig. 4-14, a very good agreement between the predicted Power Spectral Density (PSD) and the one measured at the output of the power amplifier is achieved. Then, based on the baseband components of the output of DUT captured via the VSA, the accuracy of the model is proven both in time and power domain. Fig. 4-15 and Fig. 4-16 confirm the excellent agreement between the measured and the simulated in-phase and quadrature components obtained at the output of the DUT and RVTDNN model, respectively. This demonstrates the good generality of the extracted RVTDNN model. Based on the time domain capture of the input and output envelopes of both of the

trained RVDNN model and the DUT, a power domain validation is completed by comparing the dynamic Amplitude Modulation–Amplitude Modulation (AM/AM) and Amplitude Modulation–Phase Modulation (AM/PM) characteristics. Fig. 4-17 and Fig. 4-18 corroborate the ability of the RVDNN to reproduce the dispersive dynamic AM/AM and AM/PM conversion characteristics of the DUT and consequently to predict the memory effects (time-dependent effects) of the 3G power amplifier.



(a) Original size spectrum



(b) Spectrum zoomed-in

Fig. 4-14 Spectrum comparison of the test results

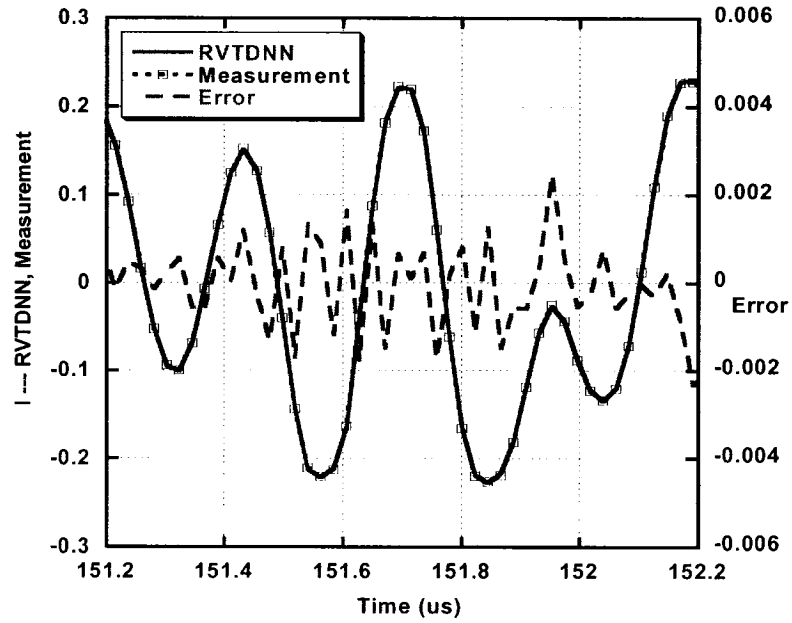


Fig. 4-15 I component (in-phase) comparison of the test results

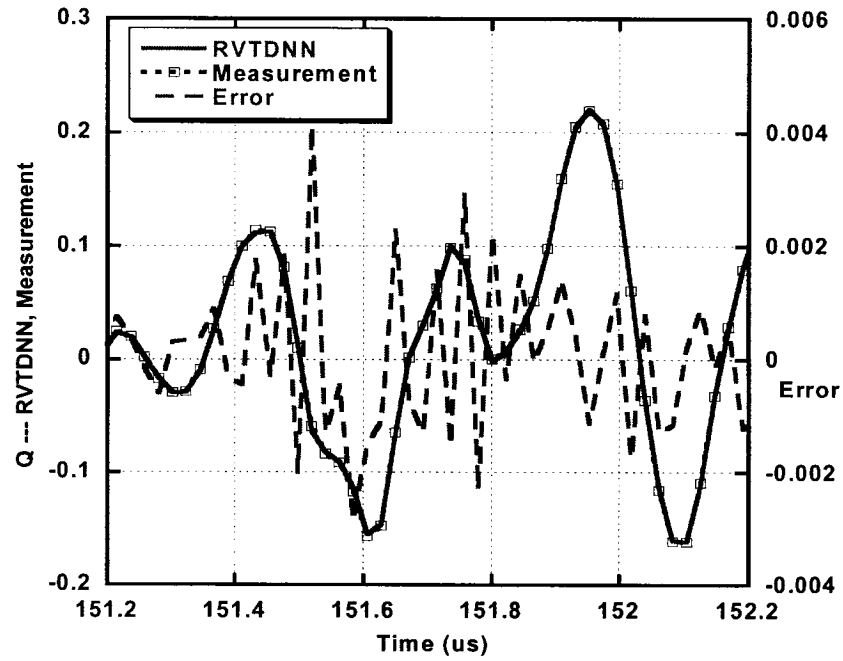


Fig. 4-16 Q component (quadrature) comparison of the test results

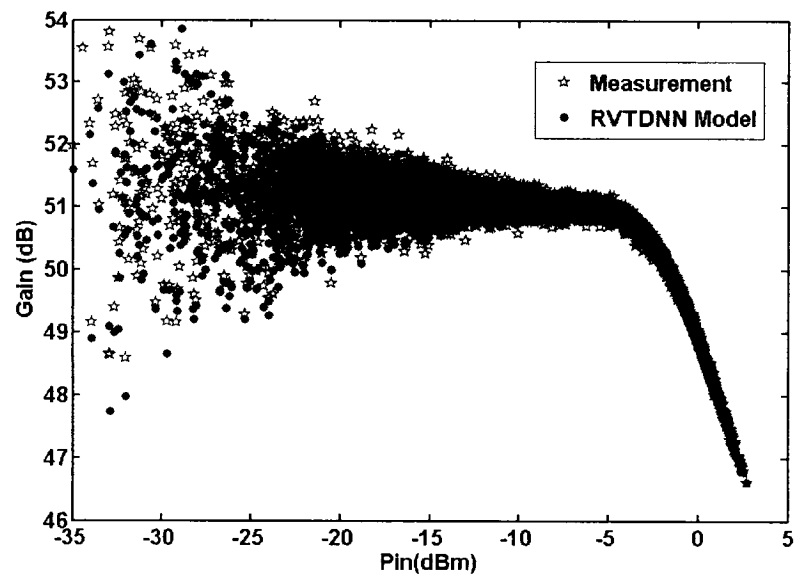


Fig. 4-17 AM/AM characteristics comparison of the test results

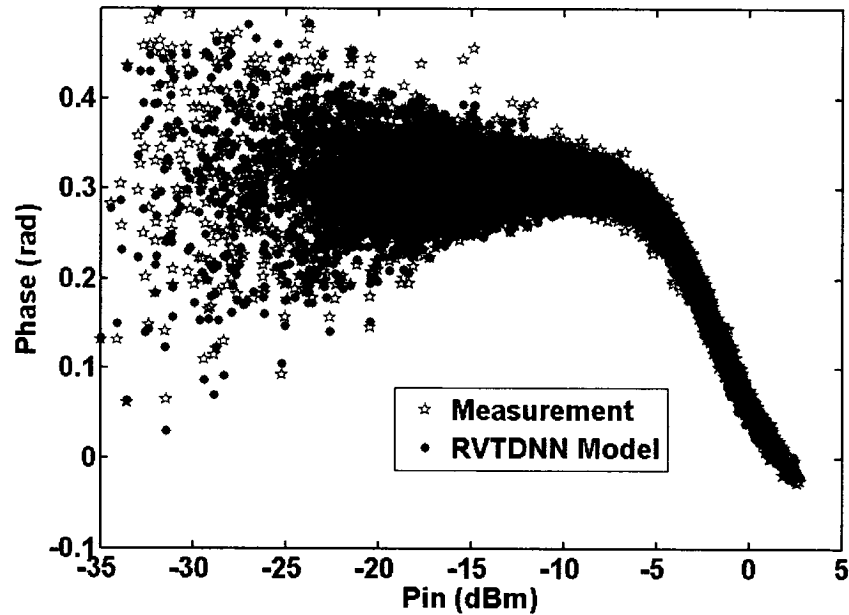


Fig. 4-18 AM/PM characteristics comparison of the test results

4.7. CONCLUSION

In this chapter a RVTDNN that has the capability to learn and to predict the dynamic behavior of non-linear PAs is proposed. This real-valued neural network model largely reduces the complexity of the neural network in the presence of complex modulated signals having highly time varying envelopes. The back-propagation algorithm is used to train the neural network so as to extract the model parameters. Validation and accuracy assessment of the developed RVTDNN model in time domain showed an agreement between the RVTDNN behavioral model output data and measurement ones for 3G signals. The frequency domain validation of the model also showed a good agreement between the PA's output spectrum calculated using the RVTDNN model predicted

waveforms and the measured spectrum for IS 95, one-carrier CDMA2000-SR3 and three-carrier CDMA2000-SR3 signals.

The dynamic AM/AM and AM/PM simulation results point out that the RVTDNN can account for the memory effects (time-dependent effects) of the LDMOS PA very well. Moreover, the dynamic AM/AM and AM/PM characteristics also suggest that the small signal response of the LDMOS PA is strongly affected by the memory effects for 3G applications. The satisfactory validation results of IS95 signal, which was applied to a RVTDNN model trained by a one-carrier CDMA2000-SR3 signal, proved that the RVTDNN model obtained does have good generality for similar signals having close statistical characteristics and crest factors. In such a case the RVTDNN model shows it is back compatible and can be used to predict the response of the PA with signals having smaller modulation bandwidth.

Moreover, a three-layer RVTDNN is also utilized to build a dynamic nonlinear behavioral model, which is able to predict the response of a wideband 3G power amplifier in better accuracy. Another 90-Watt LDMOS power amplifier operated at 2110-2170 GHz is used as a device-under-test. Time-domain, power-domain and spectral domain test results illustrate the excellent prediction accuracy of the baseband dynamic behavior of the power amplifier driven with a two-carrier 3GPP signal.

REFERENCES

- [1] K. Hyunchui, M. D. Mckinley, and J. S. Kenney, "Extraction of accurate behavioral models for power amplifiers with memory effects using two-tone measurements", *IEEE MTT-S Int. Microwave Symp. Digest*, vol.1, pp.139-142, June 2002.
- [2] M. C. Jeruchim, P. Balaban, and K. S. Shanmugan, *Simulation of communication systems: modeling, methodology, and techniques*, New York : Kluwer Academic/Plenum Publishers, 2000.
- [3] J. H. K Vuolevi, T. Rahkonen, and J. P. A. Manninen, "Measurement technique for characterizing memory effects in RF power amplifiers", *IEEE Trans. Microwave Theory Tech.*, vol.49, pp.1383 –1389, Aug. 2001.
- [4] M. Schetzen, *The Volterra and Wiener Theories Nonlinear Systems*, New York:Wiley, 1980.
- [5] A. Zhu, M. Wren and T. J. Brazil, "An Efficient Volterra-Based Behavioral Model for Wideband RF Power Amplifiers", *IEEE MTT-S Int. Microwave Symp. Digest*, vol.2, pp.787-790, June 2003.
- [6] E. G. Jeckeln, S. Huei-Yuan, E. Martony, and M. Eron, "Method for modeling amplitude and bandwidth dependent distortion in nonlinear RF devices", *IEEE MTT-S Int. Microwave Symp. Digest*, vol.3, pp.1733-1736, June 2003.
- [7] F. Launay, Y. Wang, S. Toutain, S. T. D. Barataud, J. M. Nebus, and R. Quere, "Nonlinear amplifier modeling taking into account HF memory frequency", *IEEE MTT-S Int. Microwave Symp. Digest*, vol.2, pp.865-868, June 2002.
- [8] A. A. Moulthrop, C. J. Clark, C. P. Silva, and M. S. Muha, "A dynamic AM/AM and AM/PM measurement technique", *IEEE MTT-S Int. Microwave Symp. Digest*, pp.1455-1458, June 1997.
- [9] H. Ku, M. D. McKinley, and J. S. Kenney, "Quantifying memory effects in RF power amplifiers", *IEEE Trans. Microwave Theory Tech.*, vol.50, pp.2843 –2849, Dec. 2002.
- [10] Y. Yang, J. Yi, J. Nam, and B. Kim, "Behavioral modeling of high power amplifiers based on measured two-tone transfer characteristics", *Microwave Journal, Euro-Global Edition*, vol.43, pp. 90-104, Dec. 2000.
- [11] Q. J. Zhang and K. C. Gupta, *Neural networks for RF and microwave design*, Artech House, 2000.
- [12] S. Haykin, *Neural networks: a comprehensive foundation*, Prentice-Hall, 1999.

- [13] Y. Cao, J. J. Xu, V.K. Devabhaktuni, R.T. Ding, and Q. J. Zhang, "An adjoint dynamic neural network technique for exact sensitivities in nonlinear transient modeling and high-speed interconnect design", *IEEE MTT-S Int. Microwave Symp. Digest*, vol.1, pp.165-168, June 2003.
- [14] J. J. Xu, M. C. E. Yagoub, R. T. Ding, and Q. J. Zhang, "Neural-based dynamic modeling of nonlinear microwave circuits", *IEEE Trans. Microwave Theory Tech.*, vol.50, pp.2769-2780, Dec. 2002.
- [15] Y. H. Fang, M. C. E. Yagoub, F. Wang, and Q. J. Zhang, "A new macromodeling approach for nonlinear microwave circuits based on recurrent neural networks", *IEEE Trans. Microwave Theory Tech.*, vol.48, pp.2335-2344, Dec. 2000.
- [16] J. W. Nandler, M. A. Ismail, J. E. Rayas-Sanchez, and Q. J. Zhang, "New directions in model development for RF/microwave components utilizing artificial neural networks and space mapping", *IEEE MTT-S Int. Antennas and Propagation Symp. Digest*, vol.4, pp.2572-2575, 1999.
- [17] M. Ibnkahla, J. Sombrin, F. Castanie, and N.J. Bershad, "Neural networks for modeling nonlinear memoryless communication channels", *IEEE Transactions on Communications*, vol.45, pp. 768-771, July 1997.
- [18] N. Benvenuto, F. Piazza, and A. Uncini, "A neural network approach to data predistortion with memory in digital radio systems", *Proceedings of ICC '93 - IEEE International Conference on Communications*, Singapore, vol.1, pp.152-156, Nov. 1995.
- [19] M. Ibnkahla and F. Castanie, "Vector neural networks for digital satellite communications", *IEEE International Conference Communications*, Seattle, vol.3, pp.1865-1869, June 1995.
- [20] H. Leung and S. Haykin, "The complex backpropagation algorithm", *IEEE Transactions on Signal Processing*, vol.39, pp.2101-2104, Sept. 1991.
- [21] Y. Bengio, *Neural networks for speech and sequence recognition*, ITC Press, 1995.
- [22] I.W. Sandberg, *Nonlinear dynamical systems: feedforward neural network perspectives*, New York: Wiley, 2001.
- [23] S. Boumaiza and F. M. Ghannouchi, "An accurate complex behavior test bed suitable for 3G power amplifiers characterization", *IEEE MTT-S Int. Microwave Symp. Digest*, vol.3, pp.2241-2244, June 2002.

- [24] S. Boumaiza and F. M. Ghannouchi, "Realistic power-amplifiers characterization with application to baseband digital predistortion for 3G base stations", *IEEE Trans. Microwave Theory Tech.*, vol.50, pp.3016-3021, Dec. 2002.
- [25] J. C. Principe, N. R. Euliano, and W. C. Lefebvre, *Neural and Adaptive Systems: Fundamentals through Simulations*, John Wiley & Sons, 2000.
- [26] *3GPP specifications: TS 25.104 v4.2.0*, *TS 25.141 v4.2.0*, 2002.

CHAPTER 5

CONCLUSIONS AND FUTUTRE WORKS

This dissertation introduced a novel two-box model, where a dynamic weakly nonlinear filter was proposed for the first time to replace the linear filter in the conventional two-box model to characterize the memory effects in the broadband transmitter. The dynamic weakly nonlinear filter is constructed by adding a new parallel branch to the linear FIR filter. In this new parallel branch, the input signal is multiplied by its magnitude and applied to another FIR filter. This new weakly nonlinear filter can characterize the memory effects more accurate than a linear filter. Hence this novel two-box model can be used to accurately simulate or pre-compensate the dynamic nonlinearity of the transmitter without changing anything in the model topology.

Based on the novel two-box model, an augmented Wiener model was proposed to mimic the dynamic behaviors of a wideband transmitter, which consists of two digital-to-analog converters (DAC), an RF vector modulator and a power amplifier. The power amplifier (last stage) used in this work is based on an FLL600IQ-2 FET transistor, which is of a dual transistor push-pull configuration. The validation results with a two-carrier WCDMA signal reveal that the new proposed model can mimic the out-of-band emission caused by the memory effects more accurately than the conventional two-box model.

Similarly, an augmented Hammerstein predistorter was presented to pre-correct the dynamic nonlinearities of the wideband transmitter mentioned above. The superiority of

this augmented Hammerstein predistorter to the conventional Hammerstein predistorter in pre-compensating the dynamic nonlinearity of the transmitter is also demonstrated by the spectrum and ACPR comparison results while applying a one-carrier and a three-carrier 3GPP-FDD signals to the transmitter.

For the two-box model involved in this work, a Look-Up-Table (LUT), which is based on the baseband AM/AM and AM/PM curves of the transmitter, is employed to take into account for the memoryless nonlinearity. The two blocks are obtained directly from the real-time measurement data in a real work conditions by initially de-embedding the nonlinearity via a new dynamic exponential weighted moving average (DEWMA) and identifying the memory effects afterward. This parameter extraction method allows us to alleviate the burden of the identification procedure of the analytical model's parameters, such as the high-order (even and odd) polynomial function's coefficients and the Bessel series model's coefficients, particularly when the power amplifier (PA) operates in Class AB. Therefore, this technique is inherently so robust that it can be used for any type of RF transmitters exhibiting any complex gain shape variations. Both of the augmented Wiener model and the augmented Hammerstein predistorter exhibit much better numerical stability than the memory polynomial model and the corresponding predistorter.

The time delay that exists between the input and the output baseband data waveforms of the transmitter has to be accurately estimated so as to align input and output I - Q streams prior to identifying the transmitter behavioral model. In fact, the time-delay estimation becomes more critical when wideband transmitters are concerned, since any time-delay misalignment induces an extra dispersion of AM/AM and AM/PM

characteristics of the transmitter. To identify the memory effects accurately, a time-delay estimation algorithm based on Lagrange interpolation and cross-covariance calculation was developed to align the input and output raw baseband data captured beforehand.

In order to evaluate the accuracy and robustness of the different Weiner models, a novel validation method was proposed in this work. This method is based on annulling the spectrum regrowth that is caused by the static nonlinearity, with the help of cascading the inverse of the complex memoryless model. In this way, the spectrum regrowth produced by the static nonlinearity is numerically removed from the output spectrum of the transmitter. As a result, the output spectrum observed in the spectrum analyzer is strongly dominated by the memory effects of the wideband RF transmitter.

In addition, in this dissertation, a RVTDNN that has the capability to learn and to predict the dynamic behavior of non-linear PAs is proposed. This real-valued neural network model largely reduces the complexity of the neural network in the presence of complex modulated signals having highly time varying envelopes. In this way, the general back-propagation algorithm can be used to train the neural network so as to extract the model parameters. Validation and accuracy assessment of the developed RVTDNN model in time domain showed an agreement between the RVTDNN behavioral model output data and measurement ones for 3G signals. The frequency domain validation of the model also showed a good agreement between the PA's output spectrum calculated using the RVTDNN model predicted waveforms and the measured spectrum for IS 95, one-carrier CDMA2000-SR3 and three-carrier CDMA2000-SR3 signals.

The dynamic AM/AM and AM/PM simulation results point out that the RVTDNN can

account for the memory effects (time-dependent effects) of the LDMOS PA very well. Moreover, the dynamic AM/AM and AM/PM characteristics also suggest that the small signal response of the LDMOS PA is strongly affected by the memory effects for 3G applications. The satisfactory validation results of IS95 signal, which was applied to a RVTDNN model trained by a one-carrier CDMA2000-SR3 signal, proved that the RVTDNN model obtained does have good generality for similar signals having close statistical characteristics and crest factors. In such a case the RVTDNN model shows it is back compatible and can be used to predict the response of the PA with signals having smaller modulation bandwidth.

5.1 CONTRIBUTIONS

The major contributions of this dissertation are summarized as follows:

- Proposed an augmented Wiener behavioral model along with its parameter-identification procedure;
- Proposed an augmented Hammerstein predistorter as well as the predistortion estimation procedure;
- Presented a new dynamic exponential weighted moving average algorithm to remove the dispersion in the AM/AM and AM/PM characteristics of the wideband transmitter so as to get the memoryless LUT model of the transmitter;
- Developed a robust modeling technique for wideband RF transmitters based on de-embedding the strong memoryless nonlinearity first and identifying the parameters of the memory subsystem afterwards;

- Introduced a memoryless pre-compensator based model validation method to easily identify the capabilities of the different behavioral models in predicting the memory effects;
- Implemented a time-delay estimation algorithm based on Langle interpolation and cross-covariance calculation to accurately calculate the time delay between the input and the output baseband data waveforms of the transmitter;
- Proposed a novel real-valued time-delay neural network to establish a dynamic behavioral model for characterizing the baseband nonlinear behaviors of 3G base station power amplifiers.

5.2 FUTURE WORKS

In the dissertation, the augmented Wiener model and the augmented Hammerstein predistorter was proved to be an accurate model for characterizing the memory effects and an effective baseband predistortion architecture to pre-compensate for the dynamic nonlinearities of a wideband transmitter, respectively. The validation was carried out in a wideband transmitter prototype, which consists of two digital-to-analog converters (DAC), an RF vector modulator and a power amplifier. The transmitter prototype is physically constructed by an ESG and a power amplifier. The augmented Wiener model and the augmented Hammerstein predistorter were built in ADS and then downloaded to the ESG to synthesize the wanted signals. Therefore, the next step for this research work is to implement the augmented Wiener model in DSP to demonstrate the model accuracy

of this new model and the numerical stability of the parameter identification procedure when the fixed-point number is adopted during the calculation process. Then the augmented Hammerstein predistorter will be implemented in a Field Programmable Gate Array (FPGA) to test the pre-compensation performance for the dynamic nonlinearity of a wideband transmitter. The parameters of the augmented Hammerstein predistorter will be extracted in DSP and uploaded to FPGA to update the parameters of the predistorter in FPGA accordingly.

Moreover, the RVTDNN has been demonstrated that it can accurately simulate the dynamic behaviors of a 3G power amplifier. Therefore, a predistorter based on RVTDNN is expected to be able to suppress the dynamic nonlinearity of the broadband transmitter as well. In the next step, such a predistorter should be constructed with the experimental set-up used in this work and the future DSP-FPGA platform.

APPENDIX A

PUBLICATION LIST

JOURNAL PAPERS:

1. T. Liu, S. Boumaiza, and F. M. Ghannouchi, "Dynamic behavioral modeling of 3G power amplifiers using real-valued time-delay neural networks," *IEEE Trans. Microwave Theory Tech.*, vol. 52, no. 3, pp. 1025-1033, Mar. 2004.
2. T. Liu, S. Boumaiza, and F. M. Ghannouchi, "De-embedding Static Nonlinearities and Accurately Identifying and Modeling Memory Effects in Wideband RF Transmitters," *IEEE Trans. Microwave Theory Tech.*, vol.53, no.11, pp. 3578-3587, Nov. 2005.
3. T. Liu, S. Boumaiza, and F. M. Ghannouchi, "Augmented Hammerstein Predistorter for Linearization of Broadband Wireless Transmitters," *IEEE Trans. Microwave Theory Tech.* (Accepted).
4. T. Liu, S. Boumaiza, and F. M. Ghannouchi, "A New Class of Two-box Behavior Models Suitable for Broadband Wireless Transmitter Distortion Compensation," *IEEE Trans. Microwave Theory Tech.* . (Submitted in Dec. 2005)
5. S. Boumaiza, T. Liu, M. Helaoui, O. Hammi, and F. M. Ghannouchi, "Systematic and Adaptive Characterization Approach for Behavior Modeling of Nonlinear Transmitters Driven by Modulated Signals," *IEEE Trans.*

Microwave Theory Tech. . (Submitted in Dec. 2005)

CONFERENCE PAPERS:

1. T. Liu, S. Boumaiza, M. Helaoui, H. Ben Nasr and F. M. Ghannouchi, "Behavior modeling procedure of wideband RF transmitters exhibiting memory effects," in 2005 IEEE MTT-S Int. Microwave Symp. Dig., Long Beach, CA, USA, Jun. 12-17, 2005, pp. 1983-1986.
2. T. Liu, S. Boumaiza, and F. M. Ghannouchi, "Application of Neural Networks to 3G Power Amplifier Modeling," in Proc. of Int. Joint Conf. on Neural Networks, Montreal, Canada, Jul. 31- Aug. 4, 2005, pp. 2378-2382.
3. T. Liu, S. Boumaiza, and F. M. Ghannouchi, "Pre-compensation for the Dynamic Nonlinearity of Wideband Wireless Transmitters Using Augmented Wiener Predistorters," Asia-Pacific Microwave Conf., Suzhou, China, Dec. 4 - 7, 2005.
4. T. Liu, S. Boumaiza, and F. M. Ghannouchi, "Identification and Pre-compensation of the Electrical Memory Effects in Wireless Transceivers," in 2006 IEEE Radio and Wireless Symp. Dig., San Diego, CA, USA, Jan. 17- 19, 2006. (Accepted)
5. S. Boumaiza, T. Liu, F. M. Ghannouchi, " Pre-compensation for the long and short-term memory effects in RF transmitters," IEEE Topical Workshop on Power Amplifiers for Wireless Communications, January, 2006, San Diego, USA. . (Accepted)

6. Dong-Ya Shen, Yihuai Yang, Taijun Liu, "Physical-statistical Propagation Model for the Land Mobile Communication," Asia-Pacific Microwave Conf., Suzhou, China, Dec. 4 - 7, 2005.